INAUGURAL – DISSERTATION

zur

Erlangung der Doktorwürde

der

Naturwissenschaftlich - Mathematischen Gesamtfakultät

der

Ruprecht - Karls - Universität

Heidelberg

vorgelegt von

M.Sc. (Molekulare Medizin) Tina Ruckdeschel

aus: Lichtenfels

Tag der mündlichen Prüfung: 4. Oktober 2017

Characterization of the novel pericyte receptors S1PR3 and PTGER2

Gutachter:

Prof. Dr. Ursula Klingmüller

Prof. Dr. Hellmut Augustin

Die vorliegende Arbeit wurde in der Abteilung „Vaskuläre Onkologie und Metastasierung“ am Deutschen Krebsforschungszentrum (DKFZ) in Heidelberg zwischen Oktober 2012 und Oktober 2017 durchgeführt.

Acknowledgement – Danksagung

Schreiben musste ich diese Arbeit zwar allein – aber ohne die Unterstützung jeder Menge Menschen, wäre die Fertigstellung dieser Arbeit nicht gelungen. Daher möchte ich mich bei allen bedanken, die mich während meiner Promotion begleitet haben.

Besonderem Dank gilt meinem Doktorvater Prof. Dr. Hellmut G. Augustin für die Betreuung meiner Dissertation in der Abteilung Vaskuläre Onkologie und Metastasierung am Deutschen Krebsforschungszentrum in Heidelberg. Durch dich habe ich gelernt selbstständig zu arbeiten, mich durchzusetzen und vor allem durchzuhalten.
Prof. Dr. Ursula Klingmüller danke ich, dass sie mir die Möglichkeit gegeben hat, meine Doktorarbeit an der Mathematisch-Naturwissenschaftlichen Gesamtfakultät der Ruprecht-Karls-Universität und dem DKFZ in Heidelberg durchzuführen. Vielen Dank an Sie und Guillem Genové für die wissenschaftlichen Diskussionen und Ratschläge zu meinem Projekt während der Thesis Advisory Committee Treffen.
Ebenfalls möchte ich mich bei Prof. Dr. Bartenschlager und Prof. Dr. Amir Abdollahi für die Teilnahme an meinem Prüfungskommitee bedanken.

Frank van der Hoeven und Ulrich Kloz gilt ein großer Dank. Ihr ward beide an dem mühsamsten und problematischsten Teil meiner Doktorarbeit beteiligt und ich bin euch für eure Unterstützung und eurem Optimismus sehr dankbar!

Speziell bedanken möchte ich mich bei der ´Pericyte for president` Gruppe: Laura Milde, Katharina Schlereth, Stella Hertel, Lena Vogelbacher, Stephanie Kapel und unser ehemaliges Mitglied Martin ´El Sabotage´ Teichert. Unsere regelmäßigen Meetings, die uneingeschränkte Hilfsbereitschaft in schwierigen Phasen und die gemeinsame ´Hass-Liebe´ zu Perizyten haben mich immer wieder motiviert und ihr seid mir wirklich sehr ans Perizyten-Herz gewachsen. Großer Dank geht auch an Karin Laaber, die ihre Masterarbeit den Perizyten gewidmet hat. Wir hatten eine tolle Zeit und du hast mich wirklich sehr unterstützt! Ich wünsche dir viel Erfolg in deiner weiteren Karriere!

Katharina Schlereth und Laura Milde möchte ich für die intensive Korrektur meiner Dissertation danken. Und einen großen Dank an Courtney König für die Unterstützung bei der Formatierung der finalen Version.

Ein besonderer Dank geht an alle Augustiner: ein kunterbunter, verrückter Haufen, in dem es nie langweilig wurde und in dem jeder immer ein offenes Ohr hatte. Die Arbeit mit euch allen hat es um vieles leichter und vor allem lustiger gemacht! Ein großes Dankeschön geht speziell an meine Bay (die coole 4. Bay): Anja Runge, Courtney König, Maria Riedel, Lise Roth und Moritz Jakab. Ihr habt mehr als alle anderen meine Launen über gute als auch vor allem schlechte Ergebnisse zwangsläufig mit mir geteilt. Ich danke euch für die wirklich sehr ungezwungene und abwechslungsreiche Atmosphäre im Laboralltag!

Weiterhin möchte ich mich wirklich sehr bei den „Mädels“ bedanken: Anja Runge, Courtney Barbie König, Lise Postdoc Roth, Stephanie Hüribert Kapel, Katharina Mutti Schlereth, Soniya Christian Savant, Laura Milde, Silvia Sonsilvia La Porta, Eva Giannakouri, Claudia Fatty Korn, Beate Motzi Scholz, Chefsekretärin Maike Deckers, Aida Monster Freire. Ihr seid alle wirklich echte Freunde geworden, habt mich in Krisen unterstützt und auch meine kleinen Erfolge mit mir ausgiebig gefeiert. Frei nach dem Motto „What happened in/at Barcelona, Vasto, Stockholm, Cambridge, Europapark, Karneval, Kopenhagen stays in/at Barcelona, Vasto, Stockholm, Cambridge, Europapark, Karneval, Kopenhagen” haben wir viele Ausflüge ausserhalb des Labors unternommen. Es war eine super Zeit mit Euch und ich werde mich immer an diese Zeit erinnern!

Ein besonderer Dank geht auch an die „technischen“ helfenden Hände: Maria Riedel, Eva Besemfelder, Jessica Wojtarowicz, Benni Schieb, Carleen Spegg, Doro Terhardt, Lukas Schmitt und Stella Hertel. Ihr habt so einiges ermöglicht und habt mich immer unterstützt, wenn Not an der Bench war.

Mein größter Dank geht an die Menschen, die mich am besten kennen und in jeder Situation meines Lebens unterstützt und bestärkt haben. Besonderer Dank geht hierbei vor allem an meine Eltern, meine Schwester Sandra, meinen Schwager Michi, meine Großeltern und auch meine Nichten Mia und Leana, die mir mit ihrem Kinderlachen so einiges leichter gemacht haben. Ihr alle habt mir immer einen Rückzugsort geboten und neue Motivation gegeben, so dass ich mit neuer Energie weiterkämpfen konnte. Alles, was ich bisher erreicht habe, habe ich Eurer Unterstützung zu verdanken.

Ein großes DANGE geht an Marc. Ich weiss, dass du den größten Unmut und die Frustration abbekommen hast und viele Stunden im Auto auf mich warten musstest. Umso mehr danke ich Dir, dass du wie kein anderer geduldig und verständnisvoll warst. Auch wenn ich oft verzweifelt war, hast du mich immer wieder angespornt und hast die schwere Zeit mit mir ausgesessen. Danke, dass du einfach immer da bist!

Table of Contents

List of Figures

List of Tables

Zusammenfassung

Perizyten sind murale Zellen des mikrovaskulären Systems. Sie entstehen aus dem Mesenchym und ummanteln kapilläre Endothelzellen auf der abluminalen Seite. Sie spielen eine zentrale Rolle in der Ausreifung von neu gebildeten Gefäßen und stellen ein Charakteristikum des ruhenden Endothels in den meisten mikrovaskulären Systemen dar. Die Perizytenforschung ist durch die begrenzte Verfügbarkeit an stabilen Perizyten-spezifischen Markern aufgrund von überlappender Markerexpression in unterschiedlichen mesenchymalen Zellen eingeschränkt. Um neue und funktionell relevante Perizytenmarker zu identifizieren, wurde eine Expressionsanalyse von fünf unterschiedlichen humanen primären Perizyten und anderen mesenchymalen Zellen (Endothelzellen, Adipozyten, Fibroblasten, mesenchymale Stammzellen) durchgeführt. Diese Transkriptomanalyse identifizierte unter anderem die zwei G-Protein gekoppelten Rezeptoren, Prostaglandin-E Rezeptor 2 (*PTGER2*) und Sphingosin-1 Phosphat Rezeptor 3 (*S1PR3*), als neue Perizyten-angereicherte Transkripte. Nur vaskuläre glatte Muskelzellen wiesen vergleichbare Expressionslevel an *S1PR3* auf.

Anschließende zelluläre Studien zeigten erstmalig, dass S1PR3 in Perizyten $G\alpha_i$ und $G\alpha_q$ aktiviert und die Phosphorylierung der leichten Myosin-Kette reguliert. Um die Rolle von S1PR3 in Perizyten in physiologischem Kontext zu untersuchen, wurden Co-Kultur Experimente mit Endothelzellen und Perizyten mit *S1PR3* Herunterregulierung durchgeführt und transkriptomische Veränderungen beider Zelltypen verfolgt. Die Expression von *S1PR3* in Perizyten ergab subtile aber klare Veränderungen in der Expression von Zell-Zell und Zell-Extrazellulärer Matrix Molekülen. MPRIP, ein Regulator von RhoA und der leichten Myosin-Kette, wurde als eines der physiologisch vielversprechendsten regulierten Gene identifiziert. Funktionelle *in vitro* Analysen von Perizyten mit einer *S1PR3* Herunterregulierung resultierten ebenso in einer verringerten Transmigration und zunehmender Zellgröße.

Bemerkenswerterweise war *PTGER2* ausschließlich in Perizyten exprimiert. Eine transkriptomische Analyse von co-kultivierten Perizyten mit *PTGER2* Herunterregulierung und Endothelzellen zeigte Veränderungen in der Expression von zellteilungsassoziierten Genen (Herunterregulierung von Proliferationsinhibitoren). Funktionelle *in vitro* Analysen von Perizyten mit einer *PTGER2* Herunterregulierung hatten dementsprechend eine gesteigerte Zellteilung zur Folge.

Um die Validierung der Expression von *S1PR3* und *PTGER2* in Perizyten und funktionelle Studien *in vivo* zu ermöglichen, sind Mausmodelle mit konditionaler Deletion dieser Gene erforderlich. Auf Grundlage der Expressionsdaten und der zellulären Studien, und dem Fehlen von *S1pr3* floxed Mauslinien wurden Experimente für die Generierung von konditionalen *S1pr3* Mäusen vorgenommen. Hierzu wurde die aufeinanderfolgende Integration von zwei LoxP Sequenzen mittels CRISPR/Cas Technologie (Cas9 Wildtyp) durchgeführt.

Zusammenfassend hat diese Studie PTGER2 als neuen Perizytenmarker und S1PR3 als neuen muralen Zellmarker in der mesenchymalen Zelllinie identifiziert. Beide Rezeptoren kontrollieren wichtige Funktionen der Perizyten. Darüber hinaus erwies sich CRISPR/Cas als eine geeignete Methode, um konditionale *S1pr3* knockout Mäuse zu generieren.

Summary

Pericytes are mural cells of the microvascular system of mesenchymal origin, which abluminally ensheath capillary endothelial cells (EC). Pericytes play a pivotal role in the maturation of newly formed vessels and are a hallmark of the quiescent endothelium in most microvascular beds. Pericyte-based research is hampered by the limited availability of robust pan-pericyte markers due to their overlapping marker expression with various cells of mesenchymal origin. In order to identify novel functionally relevant pericyte markers, an expression profiling of five different human primary pericyte populations and other mesenchymal cell populations (EC, adipocytes, fibroblasts, mesenchymal stem cells [MSC]) was performed. Among others, this screen identified Prostaglandin E receptor 2 (PTGER2) and Sphingosine-1-phosphate receptor 3 (S1PR3), two G-protein-coupled receptors (GPCRs), as novel, highly pericyte-enriched transcripts. Only *S1PR3* showed comparable expression levels also in smooth muscle cells (SMC).

Subsequent cellular studies demonstrated for the first time that S1PR3 signals via $G\alpha_i$ and $G\alpha_q$ in pericytes and regulates myosin light chain (MLC) phosphorylation. To study the role of pericyte-expressed *S1PR3* in a physiological setting, comparative co-culture experiments of EC with *S1PR3*-silenced pericytes were performed and transcriptomic profiles were traced. The expression of *S1PR3* by pericytes resulted in subtle, but distinct transcriptomic changes, including changes in cell-cell as well as cell-extracellular matrix interaction molecules. MPRIP, a regulator of RhoA and MLC phosphorylation, was identified as one of the most promising candidate genes. Functional *in vitro* assays of *S1PR3* silenced pericytes resulted in reduced transmigration capacity and increased cell size.

Notably, *PTGER2* was exclusively expressed by pericytes. Transcriptomic analyses of co-cultured pericytes silenced for *PTGER2* revealed expression changes of proliferation-associated genes (downregulation of negative regulators). Correspondingly, functional *in vitro* assays of *PTGER2* silenced pericytes resulted in enhanced proliferation.

To enable the validation of pericyte-expressed *S1pr3* and *Ptger2* and further functional studies *in vivo*, mouse models for the conditional deletion of these genes are required. Based on the expression profiling and cellular screening experiments and the fact that conditional mice for *S1pr3* are not available, experiments were set out with the aim to generate *S1pr3* floxed mice by CRISPR/Cas technology. Sequential integration of two LoxP sites using Cas9 wildtype was successfully used to generate conditional *S1pr3* mice.

Taken together, the experiments identified PTGER2 as novel pericyte marker and S1PR3 as novel mural cell marker within the mesenchymal cell lineage that both control important pericyte functions. Furthermore, CRISPR/Cas technology proved as a suitable approach to generate conditional *S1pr3* knockout mice.

1. Introduction

1.1 The vascular system

The vascular system of vertebrates consists of two highly branched tubular networks: the blood and the lymphatic vascular system. The heart and the following network of hierarchically structured tissue including afferent arteries and arterioles, capillaries (exchange vessels) and heart afferent venules and veins, are building the blood vascular system (Adams and Alitalo, 2007). *For it is by the heart's vigorous beat that the blood is moved, perfected, activated, and protected from injury and coagulation. The heart is the tutelary deity of the body, the basis of life, the source of all things, carrying out its function of nourishing, warming, and activating body as a whole* (William Harvey, De Motu Cordis, 1628). Indeed, the heart pumps O_2- and nutrient-rich blood to the tissues and deoxygenated CO_2-rich blood back to the lung circulation. Thereby gases, liquids, nutrients, warmth and signaling molecules are transported through the organized and specialized blood vessels between different organs and tissues, regulating tissue fluid homeostasis (Herbert and Stainier, 2011). The lymphatic vascular system is an unidirectional blind-ended network. It drains interstitial fluid through a conduit system of collecting vessels, lymph nodes, lymphatic trunks and ducts and returns the fluid back into the venous system. Lymphatic vessels thereby control macromolecule and protein drainage, as well as immune cell trafficking (Adams and Alitalo, 2007; Alitalo, 2011). About 75 % of all deaths are correlated with structural changes and dysfunctions (atherosclerosis, diabetes, stroke, aneurysms, myocardial infarction, neurodegenerative disorders and cancer) of the vascular system emphasizing its importance (Carmeliet, 2003; Folkman, 2007).

1.1.1 Vessel architecture and function

The inner layer of a vessel wall, termed tunica intima, consists of a single cobble-stone-like layer of endothelial cells (EC) covered by a basement membrane (BM) (Neufeld et al., 2014). EC are very heterogenous depending on the specific needs of certain organs (Potente and Mäkinen, 2017). Three EC vessel phenotypes are classified: continuous, fenestrated and discontinuous endothelium. Continuous endothelium can be predominantly found in the brain, where it maintains the blood brain barrier (BBB) through specialized tight junctions and a continuous BM. Fenestrated endothelium is characterized by intercellular gaps and continuous BM to ensure required fluid exchange in organs like intestine and kidney. Organs like liver, spleen and bone marrow require unrestricted cell trafficking and fluid exchange. In these organs the endothelium is discontinuous with even larger gaps and a discontinuous BM (Cleaver and Melton, 2003).

EC of the microvasculature (capillaries, small arterioles and venules) are more or less covered with pericytes. Pericytes are mural cells that are embedded in the BM to directly interact with EC. The tunica intima in large caliber vessels is enveloped by two additional layers, named tunica media and tunica externa/adventitia. The tunica media consists of a smooth muscle cell (SMC) layer, proteoglycans, elastin and collagen, whereas the tunica adventitia is composed of elastic and collagenous fibers (Cleaver and Melton, 2003; Neufeld et al., 2014).

1.1.2 Developmental blood vessel formation

The first functional organ in the vertebrate embryo is the cardiovascular system and it is essential for O_2 and nutrient supply of the embryo (Jin and Patterson, 2009). During development, blood vessels develop by *de novo* formation of a primitive vascular plexus from angioblasts, called vasculogenesis. Early in embryonic development mesodermal stem cells differentiate into hemangioblasts, which can give rise to the hematopoietic lineage and the endothelial cell lineage. On embryonic day 7.0, hemangioblast-derived cells called angioblasts (endothelial precursor cells) and hematopoietic precursor cells migrate out of the mesoderm and form blood islands, in which the angioblasts surround hematopoietic precursors. The blood islands fuse to a cord-like structure and give rise to a primitive luminized vascular plexus (Risau, 1997; 1995). The first major embryonic vessels formed by this process are the dorsal aorta and the cardinal vein. Arterial and venous specification follows EC differentiation (Swift and Weinstein, 2009). The remodeling of the primitive vascular plexus to a mature vascular network involves a second process termed angiogenesis.

1.1.3 Physiological angiogenesis

Angiogenesis is defined as the growth of blood vessels from pre-existing vessels (Carmeliet, 2005; Risau, 1997) and can be divided into sprouting angiogenesis and intussusception (non-sprouting angiogenesis) (Djonov et al., 2000; Potente et al., 2011; Risau, 1997). After birth, angiogenesis contributes to the growth of organs, however, in adulthood the vasculature is quiescent except during the progress of the cycling ovary, pregnancy and wound healing (Carmeliet, 2005; Risau, 1997). Inadequate or excessive vessel growth contribute to diseases such as myocardial infarction, stroke, obesity-associated disorders, cancer and eye disease (Folkman, 2006; Potente et al., 2011). Therefore, the formation of new blood vessels needs to be tightly regulated (Potente et al., 2011).

1.1.3.1 Phases of angiogenesis

Nutrient and O_2 deprivation initiate proangiogenic stimuli leading to the recruitment of new blood vessels (angiogenic switch). Initially, hypoxia inducible-factor α (HIF1α) is stabilized and activates the transcription of vascular endothelial growth factor A (VEGFA) (Fraisl et al., 2009). Upon VEGF stimulation, EC get activated and particular EC are selected to become a tip cell. VEGF further loosens EC junctions and matrix metalloproteases (MMPs) degrade the BM, shared by EC and pericytes. Tip cells develop filopodia leading to a coordinated tissue invasion towards the angiogenic stimulus and vessel sprouting into avascular areas (Adams and Alitalo, 2007; Distler et al., 2003; Gerhardt et al., 2003; Potente et al., 2011). Following stalk cells are less motile, produce BM and associate with mural cells. Stalk cells form EC junctions and the vessel lumen. After lumen formation, the new vessel is perfused, which is a key inducer of vascular quiescence (vessel maturation) (Potente et al., 2011). Junctions of the quiescent EC (phalanx cells) are further strengthened and mural cells (pericytes, SMC) are recruited (Dejana, 2004; Potente et al., 2011). Pericytes, integrated into the BM, wrap around the EC and stabilize the new blood vessel. This

mature primitive plexus undergoes vascular remodeling upon changes in metabolic demands such as the lactating breast and tumor growth. Finally, a hierarchically structured vascular network is formed by regulating vessel density, either through new vessel sprouts or selective regression of redundant branches (Baffert et al., 2006; Wacker and Gerhardt, 2011).

1.1.3.2 Signaling pathways in EC

VEGF is the most intensely investigated regulator of angiogenesis. The VEGF family consists of the vertebrate VEGF-A to VEGF-D, placenta growth factor (PIGF), parapoxvirus VEGF-E and snake venom VEGF-F. Deletion of just one copy of *Vegfa* results in embryonic lethality demonstrating the importance of VEGF-A in vascular development (Carmeliet et al., 1996; Ferrara et al., 1996). VEGF-A was first described as vascular permeability factor due to its permeability-inducing property (Keck et al., 1989; Senger et al., 1983; Sun et al., 2012b). Furthermore, VEGF-A promotes survival, proliferation and migration (Bernatchez et al., 1999; dela Paz et al., 2012; Simons et al., 2016). However, alternative splicing variants of VEGF-A trigger different effects. VEGF165 binds to heparin-sulfate proteoglycans (HSPG) resulting in a gradient of VEGF signaling, which is important for vessel outgrowth. VEGF121 instead, is freely diffusible and does not bind HSPG (Cohen et al., 1995; Koch et al., 2011). All VEGF bind with high affinity to the three receptor tyrosine kinases VEGFR1-3, of which VEGFR2 is the main signaling receptor in EC (Simons et al., 2016). Upon VEGF-A binding, VEGFR2 dimerizes, autophosphorylates and activates downstream signaling pathways like phospholipase Cy (PLCy), focal adhesion kinase (FAK), Src, mitogen-activated kinase (MAPK) and phosphatidylinositol 3-kinase (PI3K) signaling (Koch and Claesson-Welsh, 2012). Neuropilin-1 (NRP1) and Neuropilin-2 (NRP2) are known co-receptors for VEGFR2 enhancing its signaling (Ferrara et al., 2003; Neufeld et al., 2002). However, NRP1 can also signal independently of VEGFR2 (Roth et al., 2016). VEGF-A binds with higher affinity to VEGFR1 than to VEGFR2. VEGFR1 is described to have a weak kinase activity. Therefore, VEGFR1 as well as its alternative splicing variant VEGFR1 (soluble) act as VEGF-A trap antagonizing VEGFR2 signaling (Chappell et al., 2009; Hiratsuka et al., 1998). Whereas VEGFR1 and VEGFR2 are predominantly expressed in vascular endothelial cells, lymphangiogenesis is primarily regulated by VEGF-C binding to VEGFR3, mainly expressed by lymphatic EC (Kaipainen et al., 1995, 1995).

Together with VEGFR2/VEGF-A signaling, the Notch pathway plays a major role in controlling angiogenesis. As mentioned above, VEGF/VEGFR2 stimulates tip cell and filopodia formation (Gerhardt et al., 2003). Notch signaling in contrast inhibits tip cell formation in neighboring stalk cells (Phng and Gerhardt, 2009; Roca and Adams, 2007). Endothelial cells express Notch receptors NOTCH1/NOTCH4 (Roca and Adams, 2007; Wu et al., 2005) and corresponding Notch ligands Jagged1, Jagged2, Dll1 and Dll4 (Beckers et al., 1999; Villa et al., 2001). During sprouting angiogenesis, tip cells express high levels of Dll4, which in turn activates Notch signaling in NOTCH1 expressing stalk cells (Hellström et al., 2007; Leslie et al., 2007; Lobov et al., 2007). VEGFR2/VEGF-A signaling induces Dll4 expression in tip cells and conversely activation of Notch signaling in the stalk cells downregulates VEGFR2 and upregulates VEGFR1 (Funahashi et al., 2010; Suchting et al., 2007). This feedback mechanism (lateral inhibition) of VEGF and Notch signaling

selects the tip cell and is substantial for controlled branching of blood vessels into a hierarchically ordered vascular network.

1.2 Pericytes

Endothelial cells are the active center in the formation of new blood vessels and angiogenesis research in the 1990´s mainly focused on EC. However, this research ignored that maturation of the newly formed vascular network is dependent on mural cells (pericytes and SMC). This changed upon gain of interest in the maturation processes of angiogenesis.

Already in 1871, Eberth described the presence of pericytes (Stricker et al., 1872). Yet, the discovery of pericytes is assigned to the French scientist Charles-Marie Benjamin Rouget describing contractile cells surrounding small blood vessels (Rouget, 1873). Since its discovery, the definitions of a pericyte, found in the literature, are still conflicting and confusing. Pericytes are described as: i) contractile and motile cells as described by Rouget (Rouget, 1873), ii) contractile cells, covering capillaries outside of the BM (Blood, 1988), iii) undifferentiated adventitial cells (Stedman, 1995), iv) SMC/pericytes of the capillaries (Fabry et al., 1993), v) stem or mesenchymal cells that can differentiate into fibroblasts or SMC (Ding et al., 2004; Dore-Duffy et al., 2006). The currently accepted definition of a mature pericyte is a cell that is associated to microvessels within the BM. However, more practical criteria like location, gene expression pattern and morphology are nowadays used to identify pericytes (Armulik et al., 2011). Still, the differentiation between pericytes and SMC, surrounding larger vessels, is challenging.

1.2.1 Morphology

Pericytes are located on the abluminal side of blood microvessels, but not on lymphatic capillaries (Armulik et al., 2011; Marchetti and Piacentini, 1990). Predominantly, pericytes wrap the endothelial layer in capillaries, whereas in terminal precapillary arterioles and venules a transition to SMC occurs (Díaz-Flores et al., 1991). The morphology of pericytes is heterogeneous and depends on the location and type of vessel (Joyce et al., 1984). Mostly, pericytes appear as stellate-shaped cells with a sophisticated network of branches surrounding EC (Weibel, 1974). The cell body is round and primary processes running parallel to the length of the capillary. Primary processes give rise to secondary perpendicular processes that attach to EC (Armulik et al., 2011). Covering of EC by pericyte cytoplasmic processes is incomplete, but the processes can span more than one EC suggesting a role of pericytes in integrating EC functions (Gerhardt and Betsholtz, 2003). In contrast, pericytes in the kidney glomerulus, named mesangial cells, are round, compact and show less contact to the vessel surface (Armulik et al., 2005).

Pericyte density and the proportion of the covered EC surface vary depending on organ, species and physiological/pathological conditions. The covered vessel area ranges from 10-50%, whereas the ratio pericytes to EC varies from 1:100 (skeletal muscle) to 1:1 (retina, brain). These differences are organ- and function-dependent, since pericyte density and coverage positively correlate with permeability of certain vessel beds. The high pericyte coverage in the central

nervous system indicates their important role in contributing to the blood-brain barrier (Shepro and Morel, 1993).

1.2.2 Origin

Vessel development in the embryo occurs via *de novo* formation of a primitive vascular plexus (vasculogenesis). Mesodermal stem cells give rise to so called angioblasts, which further differentiate into EC. EC and pericytes probably share a common progenitor cell. Depending on their location, pericytes originate from mesenchymal stem cells (mesodermal origin) or the neural crest during vasculogenesis. The majority of the pericytes in the head and neck region, as well as the thymus, arise from the neural crest (Bergwerff et al., 1998; Etchevers et al., 2001; Müller et al., 2008). Pericytes from gut (Wilm et al., 2005), liver (Asahina et al., 2011) and lung (Que et al., 2008) instead derive from the pleural and peritoneal mesothelium (mesodermal origin). Here, mesothelial cells undergo endothelial to mesenchymal transition (EndMT), migrate into the organ and transdifferentiate into pericytes, but also SMC or fibroblasts (Hall, 2006). This indicates a close ontogenic relationship between EC, mural cells (pericytes and SMC) and fibroblasts. Yamashita *et al.* showed that VEGFR2 expressing mesoderm cells differentiate upon VEGF stimulation into endothelial cells, whereas PDGF-B stimulation gives rise to mural cells (Yamashita et al., 2000). Moreover, transdifferentiation of embryonic EC into mesenchymal cells, expressing smooth muscle actins, should be taken into consideration (DeRuiter et al., 1997).

The origin of pericytes during developmental and adult angiogenesis is not fully explored. Mainly three different scenarios are discussed in the literature: i) Pericytes proliferate and develop out of pre-extisting ones (primarily in the CNS) (Armulik et al., 2011; Rajantie et al., 2004), ii) pericytes derive from blood pluripotent stem cells (described also in tumors) (Yamashita et al., 2000 Bababeygy et al., 2008), and iii) pericytes derive from tissue progenitor stem cells (pericytes themselves, myofibroblasts, EC) (Birbrair et al., 2014; Diaz-Flores et al., 1992; Hall, 2006). EC can give rise to perivascular cells via EndMT (Zeisberg et al., 2007, 2008). During EndMT, EC lose their adhesion properties and cell polarity and transform to motile mesenchymal cells. Concurrently, these cells were shown to express mesenchymal markers like PDGFRβ, migrate perivascular and differentiate (Chen et al., 2016). Pericytes themselves are described to represent a perivascular stem cell niche providing a source of mesenchymal stem cells (MSC) (da Silva Meirelles et al., 2008). They can transdifferentiate into osteocytes, chondrocytes and adipocytes (Crisan et al., 2008a).

1.2.3 Molecular signature of pericytes

The morphological diversity and the close ontogenic relationship to other cell types mirrors the diversity on the molecular level of pericytes. In addition to morphological and structural criteria, the expression of well-established markers is used to identify pericytes. Well-established markers are Desmin, Neural/glial antigen 2 (NG2/CSPG4), platelet-derived growth factor receptor beta (PDGFRβ), alpha smooth muscle actin (αSMA), Endosialin (CD248) and regulator of G-protein signaling 5 (RGS5) (Díaz-Flores et al., 2009). These markers are described in section 1.2.3.1 to

1.2.3.4. Other markers, described in the literature (Table 1) include CD13 (alanyl aminopeptidase), SUR2 (ATP-binding cassette), Kir6.1 (potassium inwardly rectifying channel), DLK1 (delta-like 1 homolog) (Armulik et al., 2011). Common transgenic markers for murine studies are XlacZ4 (Tidhar et al., 2001), *Ng2*-dsRED (He et al., 2016; Zhu et al., 2008), *Pdgfrβ*-eGFP (He et al., 2016). However, none of the markers is a pan-pericyte marker (Díaz-Flores et al., 2009). Pericyte marker expression is strongly dependent on species, vessel type, organ, pathological condition and activation state of the vessel. Whereas progenitor cells are positive for Pdgfrβ, but negative for Ng2, αSMA and Desmin, intermediate pericytes express all four makers. Mature pericytes instead lose the expression of Pdgfrβ (Song et al., 2005). Consequently, next to morphology, a combination of several pericyte markers is state-of-the-art to identify pericytes (Díaz-Flores et al., 2009; Gerhardt and Betsholtz, 2003).

1.2.3.1 PDGFRβ

The tyrosine kinase receptor PDGFRβ is one of the most important molecules expressed by pericytes. The PDGF-B/PDGFRβ signaling axis between EC and pericytes is substantial for the recruitment of mural cells during angiogenesis (chapter 1.2.4). PDGFB- and PDGFRβ-deficient mice die around birth with severe vascular defects (Levéen et al., 1994; Lindahl et al., 1997; Soriano, 1994). PDGFRβ is expressed by mesenchymal cells, myofibroblasts, smooth muscle cells and neuronal progenitor cells (Lindahl et al., 1997; Winkler et al., 2010). Despite the fact that PDGFRβ is expressed by other cells, it is considered as the most reliable pericyte marker. Therefore, *Pdgfrβ*-Cre driver mice (Chen et al., 2016; You et al., 2014) as well as *Pdgfrβ*-eGFP reporter mice (He et al., 2016) are widely used in the literature.

1.2.3.2 NG2

NG2 (CSPG4) is a chondroitin sulfate transmembrane proteoglycan. NG2 is expressed on the membrane of several cells including oligodendrocyte progenitors, chondroblasts, smooth muscle cells and pericytes (Goretzki et al., 1999; Murfee et al., 2005). Mainly perivascular cells of the arterioles and capillaries, but not venules, express NG2 (Murfee et al., 2005). Furthermore, tumor pericytes are positive for NG2 (Schlingemann et al., 1991). There has been considerable controversy in NG2 as a marker of mature pericytes (Song et al., 2005) or activated pericytes (Ozerdem et al., 2001, 2002; Schlingemann et al., 1991) in literature. Yet, the majority of published papers suggest that NG2 is a marker of activated pericytes since it is consistently expressed by mural cells in developing vascular structures (angiogenesis or vasculogenesis). However, while NG2 indicates to be a suitable marker for developing pericytes in the microvasculature, smooth muscle cells are positive for NG2 (Ozerdem et al., 2001). Global NG2 knockout mice are viable and without obvious phenotype (Grako et al., 1999). However, upon induction of pathological angiogenesis in the adult mouse retina, neovascularization is significantly reduced (Ozerdem and Stallcup, 2004). Concerning the functional role of NG2, it participates as a co-receptor in angiogenic growth factor signaling and binds basic fibroblast growth factor (bFGF) and PDGF-AA, which might induce proliferation and migration of pericytes

(Goretzki et al., 1999; Ozerdem et al., 2001). It functions as cell surface receptor for extracellular matrix components like Collagen IV, which is a basic component of the BM surrounding EC and pericytes. Binding of Collagen IV induces cytoskeletal reorganization and enhances motility (Ozerdem et al., 2001). NG2-positive pericytes play also a role in the crosstalk of pericytes with EC by binding integrin α3β1 and induction of EC motility and morphogenesis during neovascularization (Fukushi et al., 2004). Pericyte-specific knockout of NG2 in intracranial melanomas results in structural deficits of the vasculature and decreased pericyte coverage, supporting a NG2-dependent mechanism in the crosstalk of pericytes and EC (You et al., 2014). Even though NG2 is not exclusively expressed by pericytes, pericyte-specific deletion of NG2 (*Ng2*-Cre mouse) (Cooke et al., 2012) or transgenic constructs (*Ng2*-dsRED) (He et al., 2016) for isolation of NG2-positive pericytes are well established in literature.

1.2.3.3 αSMA and Desmin

αSMA and Desmin are both contractile proteins of the cell cytoskeleton. αSMA is one member of six different mammalian isoforms of the cytoskeletal protein actin. Whereas β- and γ-actin are ubiquitously expressed, αSMA is mainly expressed in smooth muscle cell lineages and myofibroblasts (Bergers and Song, 2005). Its main function is the regulation of vascular contractility and blood pressure (Schildmeyer et al., 2000). αSMA is a widely used marker to identify pericytes (Herman and D'Amore, 1985; Schlingemann et al., 1990; Verbeek et al., 1994). Albeit, the expression of αSMA is heterogenous and dependent on several conditions. Pericytes from different organs and species show differences in αSMA expression. Brain and retina (rat and bovine) pericytes lack αSMA expression, while pericytes from other organs express αSMA (Nehls and Drenckhahn, 1991; Skalli et al., 1989; Verbeek et al., 1994). In turn, brain pericytes from the chicken do show αSMA expression (Gerhardt et al., 2000). Next, αSMA abundance is related to the localization in the microvasculature. Pre- and post-capillary vessels are positive for αSMA in their microfilament bundles suggesting a role of these cells in the regulation of capillary blood flow. Mid-capillaries instead are negative for αSMA (Nehls and Drenckhahn, 1991). Last, αSMA expression levels differ upon the activation state of pericytes. *In vitro* studies indicate that αSMA may be a marker of dedifferentiation (to a smooth muscle like cell). Cultured pericytes show an upregulation of αSMA upon TGFβ stimulation and downregulation of αSMA after bFGF treatment (Verbeek et al., 1994). Together with *in vivo* studies, the upregulation of αSMA is believed to indicate the transition phase from a quiescent to an activated phenotype, as seen in tumors (Morikawa et al., 2002).

Desmin is a muscle-specific class III intermediate filament and is expressed in mature skeletal, cardiac, smooth muscle cells and pericytes (Herrmann et al., 1989). It is expressed by mature as well as immature pericytes (Nehls et al., 1992; Verhoeven and Buyssens, 1988). Mice deficient for Desmin are viable, but show defects in all muscle tissues due to myocyte cell death and mitochondria defects (Milner et al., 2000). Desmin builds a three dimensional scaffold that connects nucleus, mitochondria, desmosomes and myofibrils to keep cell integrity (Capetanaki et

al., 1997) and is also associated with vessel stability. Coverage with Desmin-positive pericytes is positively correlated with vessel development (Chan-Ling et al., 2004).

1.2.3.4 RGS5 and Endosialin

Regulator of G-protein signaling 5 (RGS5) belongs to a family of about 25 proteins. RGS are described to negatively regulate G-protein coupled receptor (GPCR) signaling (Hollinger and Hepler, 2002). RGS5 is a GTPase activating protein for $G_{\alpha i}$ and $G_{\alpha q}$ and diminishes sphingosine-1-phosphate (S1P), PDGFB, angiotensin II and endothelin-1 signaling (Cho et al., 2003). It was discovered as pericyte- and SMC-specific transcript in PDGFB-deficient mouse embryos, in which developing vessels are almost absent of pericytes. Here, the RGS5 positive signal overlapped with PDGFRβ and NG2 expression (Bondjers et al., 2003). RGS5-deficient mice are viable and have no obvious vascular phenotype (Nisancioglu et al., 2008). However, Berger *et al.* identified RGS5 as the first marker that is specific for activated pericytes as its expression is induced in the vasculature upon physiological (ovulation and wound healing) and pathological (astrocytoma and pancreatic islet carcinoma) angiogenesis (Berger et al., 2005). Furthermore, RGS5 deficiency leads to vascular normalization in pancreatic carcinomas (Hamzah et al., 2008). Yet, RGS5 is not expressed in every tissue and tumor (Bergers and Song, 2005) and under certain pathological conditions (subcutaneous tumor formation/ growth and oxygen-induced retinopathy) no differences in the vasculature were observed in the RGS5-deficient mice (Nisancioglu et al., 2008).
Endosialin (Cd248 or tumor endothelial marker 1 [TEM1]) is one of the four surface C-type lectin domain proteins of the Endosialin family. It was originally discovered as tumor endothelial marker (Christian et al., 2001; Rettig et al., 1992; St Croix et al., 2000). However, subsequent studies identified Endosialin expression restricted to activated stromal pericytes and myofibroblasts (Christian et al., 2008; MacFadyen et al., 2007; Rybinski et al., 2015). Endosialin is an onco-fetal protein, which shows high expression during embryonic development but no or little expression in healthy adult tissues (Lax et al., 2007; MacFadyen et al., 2007; Rupp et al., 2006). In pathological conditions, Endosialin expression is highly associated with multiple cancers and inflammation (Hasanov et al., 2017; Mogler et al., 2015; Viski et al., 2016). Despite several studies of Endosialin expression in physiological and pathological conditions, the mechanism of its action needs further investigation. What ligand binds Endosialin and how it signals, are still not explored. First mechanistic investigations have shown that Endosialin mediates pericyte proliferation by modulating PDGFRβ signaling (Tomkowicz et al., 2010).

Table 1 Pericyte markers

Pericyte Marker	Gene	Expression by other cell types	References
PDGFRβ (Platelet-derived growth factor)	*Pdgfrb*	SMC, neuronal progenitors, myofibroblasts, MSC	(Chen et al., 2011; Farahani and Xaymardan, 2015; Funa and Sasahara, 2014; Lindahl et al., 1997)
NG2 (chondroitin sulfate proteoglycan)	*Cspg4*	Adipocytes, SMC, neuronal progenitors, microglial cells, developing cartilage, bone, muscle	(Chang et al., 2012; Fukushi et al., 2003; Ozerdem et al., 2001; Zhu et al., 2016)
αSMA (alpha-smooth muscle actin)	*Acta2*	SMC, myofibroblasts, myoepithelium, hepatic perisinusoidal cells	(Bergers and Song, 2005; Gugliotta et al., 1988; Rønnov-Jessen and Petersen, 1996; Schmitt-Gräff et al., 1991)
Desmin	*Des*	SMC, MSC	(Liu et al., 2013; Nehls et al., 1992)
RGS5 (regulator of G protein signaling 5)	*Rgs5*	SMC	(Bondjers et al., 2003)
Endosialin	*Cd248*	SMC, myofibroblasts, mesenchymal cells during development	(Christian et al., 2008; MacFadyen et al., 2007; Virgintino et al., 2007)
Angiopoietin 1 (Ang1)	*Angpt1*	SMC	(Wakui et al., 2006)
Sur2 (ATP-binding cassette, subfamily C (CFTR/MRP))	*Abcc9*	SMC, renal tubular epithelium	(Bondjers et al., 2006; Zhou et al., 2008)
Kir6.1 (potassium inwardly rectifying channel, subfamily J)	*Kcnj8*	SMC	(Bondjers et al., 2006)
DLK1 (delta-like 1 homolog)	*Dlk1*	SMC, adipocyte progenitors, hepatoblasts	(Bondjers et al., 2006; Mitterberger et al., 2012; Tanaka et al., 2009)
CD13 (Amino-peptidase N)	*Anpep*	SMC, activated endothelium, renal epithelial cells	(Dermietzel and Krause, 1991; Hauwaert et al., 2013; Mina-Osorio et al., 2008)
Zink finger protein 201	*Zic1*	Neuronal cells	(Daneman et al., 2010; DiPietrantonio and Dymecki, 2009; He et al., 2016)
Vitronectin	*Vtn*	Respiratory epithelial cells, SMC	(Dufourcq et al., 1998; He et al., 2016; Salazar-Peláez et al., 2015)
Interferon induced transmembrane protein 1	*Ifitm1*	Primordial germ cells	(He et al., 2016; Tanaka et al., 2005)

1.2.4 EC-pericyte interactions

Pericytes and EC are anatomically in close contact and both contribute to the BM by which they are separated and embedded (Mandarino et al., 1993). At certain points, pericytes and EC contact each other directly due to fenestrations in the BM. Different types of direct contacts are described: i) Inserted cytoplasmic fingers of pericytes in endothelial invaginations with tight-, gap- and adherence-junctions (peg socket contacts), ii) close contacts of both membranes (occluding contacts), iii) adherens junctions with microfilament bundles of pericytes and fibronectin (adhesion plaques). These junctions are said to be the sites of N-cadherin mediated cell-cell contacts (Armulik et al., 2011; Gerhardt and Betsholtz, 2003). Next to the close anatomical relationship of pericytes and EC, paracrine and juxtacrine communication via diverse signaling pathways, including PDGF-B/PDGFRβ, angiopoietins, sphingosine-1-phosphate and transforming growth factor β (TGFβ) signaling, occurs (Armulik et al., 2011).

PDGF was originally discovered in platelets and serum, *in vitro* acting as mitogen for fibroblasts, glial cells and SMC. The PDGF family consists of four ligands, in which PDGF-A to PDGF-D can form homodimers, and PDGF-A and PDGF-B build heterodimers. The PDGFs bind to two cell-surface receptor tyrosine kinases, PDGFRα and PDGFRβ, where PDGFRβ binds PDGF-B/PDGF-D and PDGFRα binds PDGF-A/PDGF-B/PDGF-C (Betsholtz et al., 2001). Binding of the ligand leads to autophosphorylation and subsequent signal propagation including Ras-MAPK, PI3K, FAK and PLCγ signaling pathways. PDGF-B induces cellular responses like cell growth, motility and differentiation (Heldin et al., 1998) and is a critical factor in the maturation of newly formed blood vessels, since it initiates the recruitment of pericytes. Its expression is mainly induced by hypoxia, thrombin and various growth factors (Heldin and Westermark, 1999). PDGF-B, predominantly expressed by tip cells, binds to HSPG via its C-terminal retention motifs, composed of a stretch of positively charged amino acid residues (Gerhardt and Betsholtz, 2003; Ostman et al., 1991). Consequently, PDGFRβ-positive mural cells (pericytes and SMC) are co-recruited with the angiogenic sprout via a temporal and spatial PDGF-B gradient (Hellström et al., 1999). Deletion of either PDGF-B or PDGFRβ resulted in perinatal lethality with leakage and hemorrhage in the microvasculature (Levéen et al., 1994; Soriano, 1994). Similarly, deletion of the retention motif lead to partial detachment of pericytes (Lindblom et al., 2003). Furthermore, the EC-specific expression of PDGF-B is critical for pericyte coverage of the vasculature, since EC-specific deletion of PDGF-B results in pericyte deficiency (Enge et al., 2002). VEGF signaling interacts with PDGF-B/PDGFRβ signaling via regulation of PDGF-B expression and suppression of PDGFRβ signaling. Interestingly, a positive feedback loop between VEGF-C/VEGFR3 and PDGF-B/PDGFRβ regulates vessel maturation via inducton of PDGF-B (Onimaru et al., 2009). However, VEGF-A is described to be a negative regulator of vessel maturation. VEGFR2 and PDGFRβ assemble a receptor complex in perivascular cells upon VEGF-A stimulation, thereby suppressing PDGFRβ signaling (Greenberg et al., 2008). Additionally, publications show that specific blocking of VEGF-A and PDGF-B in age-regulated macular degeneration suppresses subretinal neovascularization and might be a potential therapeutic approach (Dong et al., 2014).

The Angiopoietin-Tie (Ang-Tie) system is a major signaling pathway of vessel maturation and stability. The Ang-Tie family consists of four Angiopoietins (Ang-1 to Ang-4). While Ang-1 and Ang-2 are the best characterized Angiopoietins. Ang-3 and Ang-4 are orthologues found in mouse and human. All the Angiopoietins are ligands for the receptor Tie-2 (Thomas and Augustin, 2009), whereas the receptor Tie1, exclusively expressed by EC, is an orphan receptor. Tie-1 controls Tie-2 signaling in a context-dependent manner (tip or stalk cell) and is important for controlling angiogenesis and vascular remodeling (Savant et al., 2015). Whereas the PDGF-B/PDGFRβ axis reflects an endothelial-to-pericyte signaling loop, the Ang-Tie axis has reverse orientation since Ang-1 is constitutively expressed by perivascular cells and its main receptor Tie-2 is predominantly expressed by endothelial cells. However, there is evidence that Tie-2 is also expressed by pericytes/SMC (Teichert et al., 2017) and subtypes of monocytes and macrophages (De Palma et al., 2005). Ang-1 is the agonistic ligand of Tie-2. *Ang1*-deficient mice phenocopy the embryonically lethal vascular defects in *Tek* (Tie-2)-deficient mice (Suri et al., 1996; Dumont et al., 1994). Ang-2, only expressed by EC and released upon EC activation from Weibel-Palade bodies (Fiedler et al., 2004), was described as antagonist of Tie-2 (Sato et al., 1995), however, Ang-2 acts as partial agonist in a context-dependent manner (Kim et al., 2016; Korhonen et al., 2016). Taken together, Ang-1 induces vessel quiescence and maturation in a paracrine manner, Ang-2 as autocrine ligand mediates mainly vessel destabilization (Augustin et al., 2009). Interestingly, morphological analysis of Ang-1 or *Tek* null mice demonstrated a lack of mural cells (Suri et al., 1996). A role of Tie-2 in pericyte recruitment was suggested, since various *in vivo* and *in vitro* studies prove that overexpression of Ang-2 results in pericyte loss (Hammes et al., 2004; Stratmann et al., 1998; Zhang et al., 2003). However, mice with signaling-deficient Tie-2 receptors as well as *Tek* null mice showed normal pericyte recruitment to Tie-2-negative vessels (Jones et al., 2001; Tachibana et al., 2005). Recently, Tie2 expression on pericytes was identified. Pericyte-expressed Tie2 mediates vessel maturation by controlling pericyte migration in tumors (Teichert et al., 2017).

In addition to Ang/Tie signaling, sphingosine-1-phosphate (S1P) signaling is indispensable for vascular maturation. This signaling pathway will be discussed in more detail in chapter 1.3.

TGFβ signaling plays a major role in pericyte differentiation. It is involved in the induction of mural cell formation from undifferentiated mesenchymal cells and in the proliferation and differentiation of mural cells and EC. Two distinct type I TGFβ receptors, activin receptor-like kinase (Alk)-1 and -5, and endoglin (Li et al., 1999), a transmembrane accessory receptor for TGFβ, are expressed in pericytes and EC (Armulik et al., 2011). Concurrently, both cell types express the latent pro-form of the ligand TGFβ, which is activated by the cooperation of both cells (Sato and Rifkin, 1989). The active TGFβ is described to inhibit proliferation and migration of EC (Sato and Rifkin, 1989), downregulate VEGFR2 expression in EC (Patterson et al., 1996) and induce differentiation of mural cell precursors to SMC/pericyte fate (Hirschi et al., 1998). In general, the role of TGFβ signaling in vascular development and maintenance is complex. Since both, receptors and ligand, are expressed by pericytes and EC, it is difficult to investigate the primary roles of TGFβ signaling in each cell compartment. For example, TGFβ is described to be pro- and anti-

angiogenic. Indeed, cellular responses differ depending on the TGFβ concentration and the composition of the receptors (Goumans et al., 2003).

1.2.5 Functions of pericytes

Pericytes have multiple functions that depend on developmental stage and organ. However, pericytes do not only play important roles in physiological processes, but are also described in various pathological conditions as fibrosis, cancer and diabetic retinopathy, which will be discussed in the following two chapters.

1.2.5.1 Pericytes in health

Vessel stabilization and regulation of blood flow are the most often associated functions of pericytes. A quiescent, mature vasculature is characterized by an inactive, resting EC layer enveloped by pericytes (Armulik et al., 2005; Hirschi and D'Amore, 1997). Pericytes induce quiescence in a paracrine manner by secreting Ang-1 (Thomas and Augustin, 2009). Further, pericytes mechanically stabilize the vessel wall with their processes incorporated in the BM. The number of pericytes is correlated with the resistance of microvessels to high blood pressure, since pericytes hinder vessels to dilate immoderately (Gerhardt and Betsholtz, 2003; Hellström et al., 2001; Laties et al., 1979). Vasoconstriction and vasodilation for the regulation of capillary blood flow is induced by local compression of EC by pericytes (Nakano et al., 2000). From their discovery on, pericytes are described to be contractile cells (Rouget, 1873). They express contractile proteins (αSMA, tropomyosin and myosin) and cholinergic/adrenergic (α2, β2) receptors, which mediate the contraction or relaxation of pericytes (Ferrari-Dileo et al., 1992). Vasoactive molecules, such as nitric oxide, endothelin-1 and angiotensin II bind to pericytes (Ferrari-Dileo et al., 1996; Haefliger et al., 1994; Lee et al., 1989). Even though most of the studies were performed *in vitro*, pericyte contraction could be shown *in vivo* upon treatment with vasoactive substances (Hirschi and D'Amore, 1996; Tilton et al., 1979). Pericyte contractility and their presence (umbrella-like structure) at endothelial cell-cell junctions modify the intercellular transport. Therefore, vascular permeability positively correlates with pericyte coverage (Rodriguez-Baeza et al., 1998; Sims and Westfall, 1983). The highest pericyte coverage is seen in retina and brain, where the presence of a continuous endothelium is a specific tissue demand of these organs (Armulik et al., 2010). Pericyte contractility is also suggested to play a critical role in neutrophil transmigration. During inflammation, neutrophil activation, rolling and transmigration through the blood vessel wall is an important process, that is well understood. Recent evidence shows that pericytes also play a role in immune cell trafficking across vessel walls. Whereas increased cytoskeletal contractility of EC promotes neutrophil transmigration (Stroka and Aranda-Espinoza, 2011), pericyte relaxation is needed to allow neutrophils to enter in the surrounding tissue (Wang et al., 2012). Furthermore, pericytes secret chemokines (MIF, Interleukin 8) and upregulate adhesion molecules (ICAM-1) to attract immune cells (Pieper et al., 2013; Proebstl et al., 2012; Stark et al., 2013). Pericytes can act as macrophage-like cells with the properties to incorporate macromolecules/soluble and small molecules (Kida et al., 1993; Kristensson and Olsson, 1973;

Mato et al., 1996) and to convert into macrophages (Barón and Gallego, 1972; Maxwell and Kruger, 1965). However, these studies were mainly done in the brain (Balabanov et al., 1996; Thomas, 1999). Pericytes are also involved in adaptive immune responses, since they can act as antigen-presenting cells via expression of major histocompatibility complex (MHC) II (Fujikawa et al., 1989; Hurtado-Alvarado et al., 2014). In summary, pericytes contribute to the immunological defense of the vasculature during inflammation processes (Navarro et al., 2016), complementing with their ability to induce blood coagulation after microvascular injury or rupture (Bouchard et al., 1997; Thomas, 1999).

Pericytes display tissue-specific functions, since they adjust to the special need of each organ. As described above, the ability of pericytes to modify immunological responses are mainly characterized in the brain. Brain pericytes are involved in the formation of the blood brain barrier (BBB) together with EC and astrocytes. The BBB is a continuous endothelium to protect the brain from the invasion of potential toxic factors coming from the blood. Deletion of pericytes leads to increased transcytosis and defects in the polarization of astrocyte endfeet in the brain (Armulik et al., 2010). Hepatic stellate cells (HSC) or Itoh cells are the pericytes of the liver (Sato et al., 2003). The liver endothelium is fenestrated and discontinuous, however HSC and EC have close contact through incomplete BM components and extracellular matrix. HSC represent around 10 to 15 % of the total number of resident cells in physiological condition. Their major roles include regulation of ECM, storage of Vitamin A and recruitment of inflammatory cells during liver diseases (Sato et al., 2003; Sims, 2000). Kidney pericytes are called mesangial cells and represent 30 % of the glomerular cells. Their main function is the contribution to the glomerular basement membrane and splitting of vascular loops, resulting in a large filtration surface. In Pdgfb and Pdgfrβ null mice, mesangial cells are almost completely deleted in severely destructed glomeruli (Betsholtz, 2004).

1.2.5.2 Pericytes in disease

The vasculature is quiescent under physiological conditions. Angiogenesis occurs in rare physiological processes, but is mainly induced under pathological conditions. Therefore, next to EC also pericytes moved into the focus of various pathologies.

Diabetes causes pathological changes of the microvasculature especially in the retina and the kidney. Diabetic retinopathy is accompanied by an early loss of pericytes, named pericyte drop out, caused by chronic hyperglycemia. Acellular-occluded capillaries, microaneuryms and thickening of the vascular basement membrane are following. Further on, an increase of vascular permeability and resulting edema or the formation of new blood vessels via VEGF-A develop. This impaired vascularization leads to blindness in one third of all patients (Hammes et al., 2002). The mechanism of pericyte drop out in diabetic retinopathy is not fully explored. Publications show that a hyperglycemia-induced inhibition of PDGF signaling (Geraldes et al., 2009) or an upregulation of Ang-2 (Hammes et al., 2004) might be the underlying mechanisms. In diabetic nephropathy, massive ECM deposition and thickening of the glomerular basement membrane are hallmarks. Repetitive mechanical stretch of mesangial cells (pericytes of the kidney) induces their

proliferation, increases ECM synthesis and reduces ECM-degrading enzymes during early diabetic nephropathy (Gruden et al., 2000; Kanwar et al., 2008).

Fibrosis is the process of massive ECM deposition and scar formation as a response to chronic injury of a tissue. Mainly inflammatory cells are recruited and myofibroblasts are activated. The origin of myofibroblasts is continuous to be a major challenge in fibrosis research. One hypothesis is that pericytes detach from the EC, migrate and transdifferentiate into collagen-producing myofibroblasts. This hypothesis was proven in lung (Hung et al., 2013), liver (Fabris and Strazzabosco, 2011) and kidney fibrosis (Schrimpf and Duffield, 2011). Even though accumulating evidence indicates that pericytes might be a source of myofibroblasts, the used genetic fate mapping strategies are still no final proof due to overlapping marker expressions of mesenchymal lineages.

Pericytes, together with EC, fibroblasts, leukocytes and the ECM compartment, are part of the tumor stroma. Tumor vessels are highly disorganized, leaky and tortuous. The basement membrane is discontinuous or absent and pericytes are loosely attached to EC. The recruitment of pericytes occurs via PDGF-B/PDGFRβ as in physiological angiogenesis (Abramsson et al., 2002). Pericyte coverage is dependent on the tumor entity and can range from high to no coverage. High pericyte coverage has been associated with poor outcome and increased tumor growth (Gee et al., 2003). In contrast, tumors with low pericyte coverage and compromised vessel structure facilitate blood vessel invasion and metastasis (Cooke et al., 2012). Anti-angiogenic treatment targeting EC seems to eliminate immature, uncovered vessels, whereas mature covered vessels are protected (Ellis and Hicklin, 2008). There is evidence that after stopping anti-angiogenic treatment, pericytes are critical for fast neovascularization (Mancuso et al., 2006). These observations led to the idea to treat EC and pericytes simultaneously with anti-VEGF and anti-PDGF strategies which revealed promising results (Bergers et al., 2003; Erber et al., 2004). However, other publications show no better outcome after depletion of pericytes or inhibition of PDGFRβ signaling (Nisancioglu et al., 2010; Sennino et al., 2007). As mentioned above, pericytes are suggested as negative regulator of metastasis. However, the underlying mechanisms are not fully understood. Pericytes may act as a barrier that hinders tumor cells to intravasate into the circulation. Moreover, it is hypothesized that pericyte-deficient vessels are leaky resulting in interstitial volume and local pressure. This pressure leads to compression of tumor vessels, induction of hypoxia pathways and tumor metastasis through epithelial-mesenchymal transition (EMT) (Cooke et al., 2012). Another study shows that a subset of pericytes (Endosialin-positive pericytes) promote cell-contact dependent tumor cell intravasation (Viski et al., 2016). Different publications also suggest a role of pericytes in the colonization and growth of tumors at distant sites (Kienast et al., 2010; Welti et al., 2012). It has been shown that pericytes modulate the immune response against tumor cells. Mature, RGS5-deficient pericytes and normalized vessels promote immune cell migration into the tumor and lead to prolonged survival (Hamzah et al., 2008). In contrast, RGS5-expressing pericytes are able to inhibit the activity of CD4- and CD8-positive T-cells (Bose et al., 2013; Merelli et al., 2014). In summary, pericytes as part of the tumor microenvironment are crucially involved in tumor development and metastasis.

1.3 Sphingosine-1-phosphate receptor family

Sphingosine, the precursor of sphingosine-1-phosphate (S1P), has already been identified around 1884 (Thudichum and Royal College of Physicians of London, 1884). S1P is a lipid mediator and acts via five isoforms of the S1P receptors (S1PR), a family of G-protein coupled receptors. The pleiotropic effects of S1P on diverse cell types are still not fully unraveled. Extensive research on S1P signaling has revealed its fundamental impact on angiogenesis, cardiogenesis, neurogenesis, limb development and immunity by influencing cell migration, differentiation and survival (Blaho and Hla, 2011; Mendelson et al., 2014).

1.3.1 S1P

S1P is a lysophospholipid, a minor lipid component of the cell membrane. S1P is derived by sequential degradation of sphingomyelin and glycosphingolipids in the cell membrane (Figure 1). The intermediate product ceramide is then further degraded into sphingosine. The majority of sphingosine is produced by degradation in lysosomes (Proia and Hla, 2015). The catabolically generated sphingosine is phosphorylated by one of the sphingosine kinases (SPHK), SPHK1 and SPHK2, to generate S1P. SPHK1 is generally localized in the cytoplasm, but can translocate to the cell membrane upon activation (Pitson et al., 2003). SPHK2 is primarily localized in the nucleus (Igarashi et al., 2003). After formation in the cytoplasm, S1P can follow three pathways: i) S1P is exported to the cell surface by a specific S1P transporter, SPNS2 (Fukuhara et al., 2012), and binds its receptors, ii) S1P is degraded by the S1P lyase (Zhou and Saba, 1998) or iii) S1P is recycled by dephosphorylation through S1P phosphatases, SGPP1 and SGPP2, to produce ceramide (Le Stunff et al., 2007; Proia and Hla, 2015).

The levels of S1P in the cell are tightly regulated by a balance of synthesis and degradation. Sphingolipid metabolism occurs in almost every cell. However, some cell types are metabolically prone to synthesize S1P and whereas other cells are specialized to degrade S1P and keep levels low (Olivera et al., 2013). The association of different cell types with diverging S1P metabolism results in the generation of a S1P concentration gradient between blood (~1 µM S1P)/lymph (~100 nM S1P) and the surrounding tissue (0.5-75 pmol/mg S1P) (Xiong and Hla, 2014). During embryonic development, red blood cells are the main source of plasma S1P (Xiong et al., 2014), whereas postnatally, red blood cells and EC supply the plasma with S1P (Pappu et al., 2007; Venkataraman et al., 2008). EC play an important role in the maintenance of the S1P gradient due to their strategic position between the two compartments (blood and tissue) with very different S1P concentrations. EC express enzymes for the synthesis (SPHK1/2) as well as for the degradation (SGPP and S1P lyase) or export (SPNS2) of S1P, which allows a continuous filtration of S1P across the endothelial membrane (Venkataraman et al., 2008). Conditional deletion of the S1P transporter SPNS2 in EC reduces the level of circulating S1P in the blood by 50% (Fukuhara et al., 2012). However, reduced levels of S1P on the luminal side alone are not able to induce S1P-driven lymphocyte trafficking. This suggests that EC might be able to regulate S1P levels on the abluminal side to induce lymphocyte trafficking by hitherto unknown mechanisms.

S1P is highly hydrophobic and is therefore mainly bound to carrier proteins, such as HDL (60%) and albumin (30 %) (Proia and Hla, 2015). HDL binds S1P via apolipoprotein M (ApoM) that controls S1P level in the blood and binding to its receptors (Christoffersen et al., 2011).

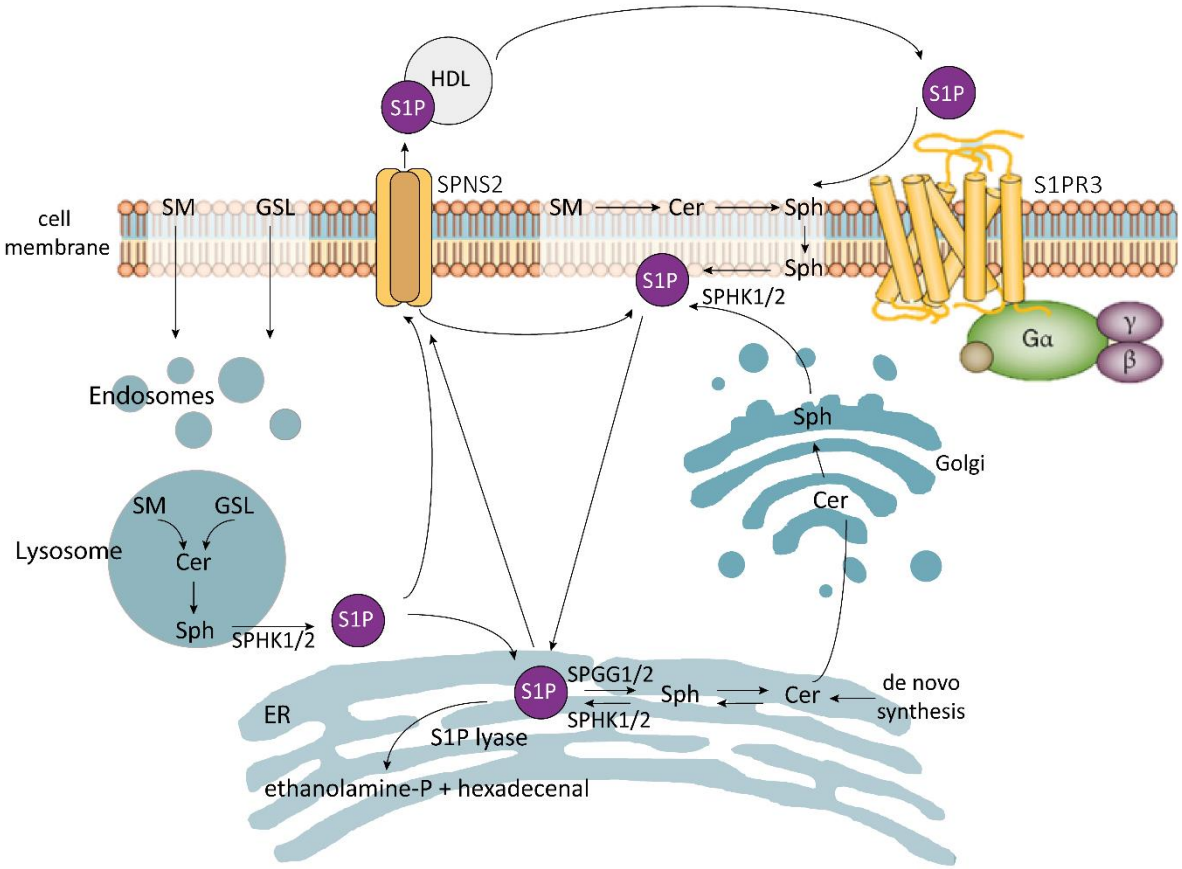

Figure 1: Synthesis, metabolism and export of S1P
Sphingomyelin (SM) and glycosphingolipids (GSL) are localized in the cell membrane. The degradation of sphingolipids to ceramide (cer) and subsequently to sphingosine (sph) occurs in lysosomes and the cell membrane. Sph is phosphorylated by SPHK1/2 to produce S1P. Once produced, S1P can follow three pathways: a) S1P can be irreversibly degraded by S1P lyase, b) S1P can be dephosphorylated and recycled for ceramide (cer) synthesis in the golgi and c) S1P can be transported out of the cell by its transporter SPNS2.

1.3.2 S1P receptors

S1P mainly exerts its effects by interacting with the five high-affinity S1P receptors (S1PR1-5), even though there is evidence that S1P acts as an intracellular (second) messenger (Maceyka et al., 2012; Spiegel and Milstien, 2003). The five G-protein coupled receptors are structurally very similar, but show different expression patterns and distinct coupled signaling pathways.

In 1990, S1PR1 was discovered as endothelial differentiation gene (EDG-1) that is solely expressed in EC (Hla and Maciag, 1990). Further studies revealed that S1PR1 is the most highly expressed receptor of the S1PR family and is ubiquitously expressed in different organs and cell types (Regard et al., 2008). *S1pr1* global knockout mice die around embryonic day (E) 12.5 to 14.5 due to massive hemorrhages with abnormal pericyte and SMC coverage of vessels (Liu et al., 2000). The EC-specific deletion of *S1pr1* in mice mimicks the phenotype seen in the global knockout, indicating the important role of S1PR1 in vascular development (Allende et al., 2003). S1PR1 is exclusively coupled to $G\alpha_i$ mediating Rac activation (Lee et al., 1996) and binding of S1P to S1PR1 has been described to induce vascular barrier integrity (Gaengel et al., 2012). Rac activity is required for S1P-induced endothelial cytoskeleton rearrangement and adherens junctions assembly (Singleton et al., 2005). *In vitro*, S1PR1 signaling induces the migration and proliferation of EC and SMC (Kluk and Hla, 2001; Paik et al., 2001). Furthermore, S1P can transactivate VEGF receptors in the context of migration and proliferation. In detail, S1PR1 induces Src activation resulting in VEGFR2 phoshorylation. This transactivation leads to the activation of signaling cascades that induce vascular remodeling and movement. At the same time the activated VEGFR2 receptor stimulates SPHK1 and increases S1P levels. Subsequent ERK/MAPK signaling results in DNA synthesis (Spiegel and Milstien, 2003).

S1PR2 was discovered as a receptor being predominantly expressed in lung and heart (Okazaki et al., 1993). Further studies identified S1PR2 as ubiquitously expressed in different organs and cells (Blaho and Hla, 2014). Global deletion of *S1pr2* in mice did not cause any obvious phenotype except smaller litter sizes (Ishii et al., 2002). Double deletion of *S1pr1* and *S1pr2* resulted in a more severe phenotype than *S1pr1* global knockout with embryos mostly dying before E12.5 (Kono et al., 2004). S1PR2 signals via $G\alpha_i$, $G\alpha_q$ and $G\alpha_{12/13}$. Surprisingly, S1PR2 showed contrast effects on cell migration, proliferation and cytoskeleton reorganization compared to S1PR1 and S1PR3 (Okamoto et al., 2000).

S1PR3 is highly homologous to S1PR1 and is described to be ubiquitously expressed (Yamaguchi et al., 1996). In the vascular system, expression of S1PR3 is mainly indicated in EC and SMC (Lee et al., 1999). Intriguingly, global knockout of *S1pr3* shows no obvious phenotype (Kono et al., 2004), whereas an increased perinatal lethality was observed for the *S1pr2*/*S1pr3* double knockout (Ishii et al., 2002). Double null mice for *S1pr1* and *S1pr3* were mimicking the *S1pr1* knockout phenotype. *S1pr1/S1pr2/S1pr3* triple null embryos display a substantially more severe phenotype with a less developed capillary network compared to *S1pr1* null embryos (Kono et al., 2004). This implies that S1P receptors 1-3 have redundant or cooperative functions during embryonic development. In different cell types, including SMC (Fujii et al., 2014), S1P receptor 3 is described to signal via $G\alpha_i$, $G\alpha_q$ and $G\alpha_{12/13}$ (Figure 2) (An et al., 1998, 1999, 2000; Ancellin and Hla, 1999;

Windh et al., 1999) and it induces migration and adherens junctions formation in endothelial cells *in vitro* (Ancellin and Hla, 1999; Lee et al., 1999). Interestingly, crosstalk of S1PR3 and PDGFRβ signaling concerning cell migration was observed in SMC (Mousseau et al., 2012a). PDGFRβ signaling activates and translocates SPHK1 to the cell membrane, which leads to the formation of S1P that in turn activates S1P receptors after cellular export (Spiegel and Milstien, 2003).
In contrast to the S1P receptors 1-3, the expression of S1PR4 is limited to lymphoid tissues (such as thymus, spleen and bone marrow) (Gräler et al., 1998) and S1PR5 is restricted to brain (Im et al., 2000). The functions of both receptors are still not fully explored.

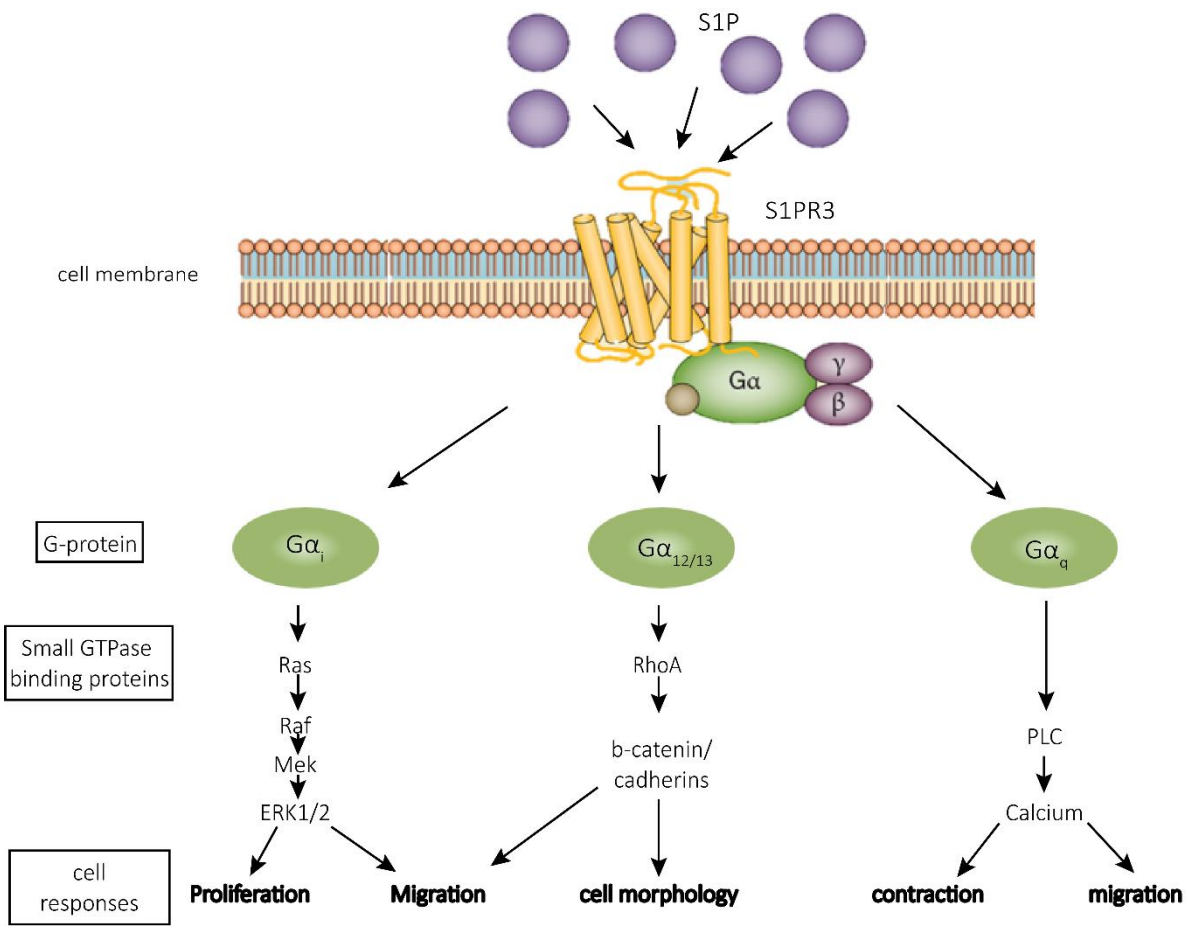

Figure 2: Described downstream signaling pathways activated by S1PR3
S1PR3 signals via Gα$_i$, Ras, Raf and Mek to ERK activation. Phosphorylation (activation) of ERK results in proliferation and migration. S1PR3 activates RhoA resulting in migration and stress fiber formation (cell morphology changes). Calcium release is induced by PLC activation via Gα$_q$ leads to cell migration and contraction.

1.3.3 S1P in health and disease

S1P signaling is an important regulator of vascular development via its S1P receptors 1-3. Especially S1PR1 on endothelial cells is important for embryonic cardiovascular development and the maintenance of vascular integrity. Phenotypic analysis of genetic mouse models deleted for S1PR2 and/or S1PR3 indicate accessory or partially redundant roles for these receptors during vascular development (as described in 1.3.2) (Proia and Hla, 2015). However, S1PR2 and S1PR3 are described to be expressed by mural cells, thereby regulating vascular tone (Bischoff et al., 2000; Murakami et al., 2010; Ohmori et al., 2003; Tosaka et al., 2001). Next to the importance of S1P in embryonic vascular development, it is critical in embryonic neurogenesis (Mizugishi et al., 2005). In the adult nervous system, S1P regulates neurotransmission (Chan et al., 2012). Elevated level of S1P in the blood and lymph nodes, sensed by its receptors, are an important mechanism for trafficking of cells (immune cells, hematopoietic cells). Thereby, S1P regulates the egression of B- and T-cells from lymphoid tissues (Pappu et al., 2007) into the blood or hematopoietic stem cell mobilization from the bone marrow into the circulation (Juarez et al., 2012; Massberg et al., 2007).

S1P and its receptors are expressed in every organ of the body and are involved in many physiological processes as indicated above. Therefore, it is not surprising that the S1P/S1PR axis is implicated in various pathophysiological conditions in almost every organ (Maceyka et al., 2012).

Multiple sclerosis (MS) is a chronic autoimmune disease of the brain characterized by immune cell infiltration, demyelination and neurodegeneration. S1P signaling is substantially involved in the trafficking of auto-reactive adaptive immune cells. Fingolimod (FTY720), a sphingosine analog, is an established treatment for MS. It was approved in 2010 by the US Food and Drug Administration as first-line treatment for relapsing forms of MS. FTY720 acts as a functional antagonist as it is phosphorylated by SPHK2 to produce the potent agonist FTY720-phosphate for S1PR1 and S1PR3-5. Its binding results in internalization and downregulation of the receptors (Brinkmann et al., 2010; Proia and Hla, 2015). Moreover, FTY720 modifies the retention of auto-reactive T-cells in the lymph nodes that are known to damage the nervous system (Proia and Hla, 2015).

Substantial evidence indicates an involvement of S1P in cancer by regulating angiogenesis, tumor cell proliferation and survival, metastasis and immune cell infiltration. Thus, S1P signaling in cancer is complex but opens opportunities for potential therapeutics targeting the S1P/S1PR axis. Elevated mRNA and protein levels of SPHK1 are described in different types of cancer and is correlated with disease progression and reduced patient survival (Johnson et al., 2005; Kohno et al., 2006; Li et al., 2008, 2009). Confirming these observations, inhibition of SPHK1 in xenograft models results in reduced tumor growth, angiogenesis and chemo resistance (Guan et al., 2011; Pyne and Pyne, 2010). In general, S1PR1 and S1PR3 expression in tumors promotes migration, whereas S1PR2 expression inhibits migration (Pyne and Pyne, 2010). Inhibition of the crosstalk of S1PR1/S1PR3 and PDGFRβ signaling by FTY720 and sunitinib malate (VEGFR/PDGFRβ kinase inhibitor) of breast cancer *in vivo* results in reduced tumor angiogenesis and vessel normalization. FTY720 thereby potentiates the effects of sunitinib malate (Mousseau et al., 2012b). Potential

new therapeutics can target S1P signaling on multiple levels including sphingosine kinases, sphingosine lyases, sphingosine phosphatases and S1P receptors. These inhibitors were shown to be effective in many animal models of human diseases (Maceyka et al., 2012).

Atherosclerosis is an inflammatory disease of the wall of large vessels. Atherosclerotic vessels show increased expression of S1PR3. Consistently, *S1pr3* null mice form significantly smaller lesions upon arterial injury response suggesting a role of S1PR3 in the migration of SMC in atherosclerotic conditions and immune cell recruitment (Keul et al., 2011; Shimizu et al., 2012). In addition, *S1pr2* knockout mice exhibit reduced macrophage content and lesion size of atherosclerotic plaques indicating a role of S1PR2 in myeloid cell recruitment (Skoura et al., 2011).

Endothelial barrier disruption and vascular permeability are the hallmarks of acute lung injury, caused by infections (bacterial, viral), sepsis or trauma (Ware and Matthay, 2000). Treatment with FTY720 or S1P reduce vascular permeability in LPS-induced lung injury models (McVerry et al., 2004; Peng et al., 2004). Furthermore, S1PR3 is described to be a novel biomarker in acute lung injury (Sun et al., 2012a). In summary, S1P signaling is complex and plays important roles in physiology and pathology. Further understanding of S1P signaling pathways might improve therapeutic options in pathology.

1.4 Prostaglandin signaling

Prostaglandins are eicosanoid lipid mediators acting on at least nine known prostaglandin receptor variants. Prostaglandins have diverse physiological functions in the CNS, cardiovascular, gastrointestinal, genitourinary, endocrine and respiratory system. However, their function in modulating the immune system is most studied. Extensive research on prostaglandin signaling revealed its implication in many diseases like cancer, inflammation, cardiovascular diseases and hypertension (Hata and Breyer, 2004; Narumiya et al., 1999).

1.4.1 Prostaglandins

Eicosanoids (greek: eicos = twenty) consist of prostanoids (prostaglandins, prostacyclins and thromboxanes), epoxyeicosatrienoic acids and leukotrienes and are produced in every mammalian cell, except erythrocytes. The different eicosanoids are generated by sequential metabolism of arachidonic acid (C20) by individual synthase enzymes (Figure 3). Arachidonic acid is esterified to glycerophospholipids in the cell membrane. Upon release of arachidonic acid by phospholipase A2, it undergoes oxidation by different enzymes (Balsinde et al., 2002). The synthesis of prostanoids is initiated by the conversion of arachidonic acid via an unstable endoperoxide Prostaglandin G2 (PGG_2) to Prostaglandin H2 (PGH_2), which serves as a substrate for the prostaglandin synthase enzymes (Bonvalet et al., 1987; Smith, 1992). This conversion is mediated by two cyclooxygenases, COX-1 and COX-2. COX-1 is constitutively expressed in most tissues, whereas COX-2 is tightly regulated and not expressed under normal physiological conditions. But its expression is induced in various inflammatory settings. Both COX enzymes are located at the endoplasmatic reticulum (ER) and nuclear membrane to uptake released arachidonic acid (Smith et al., 2000).

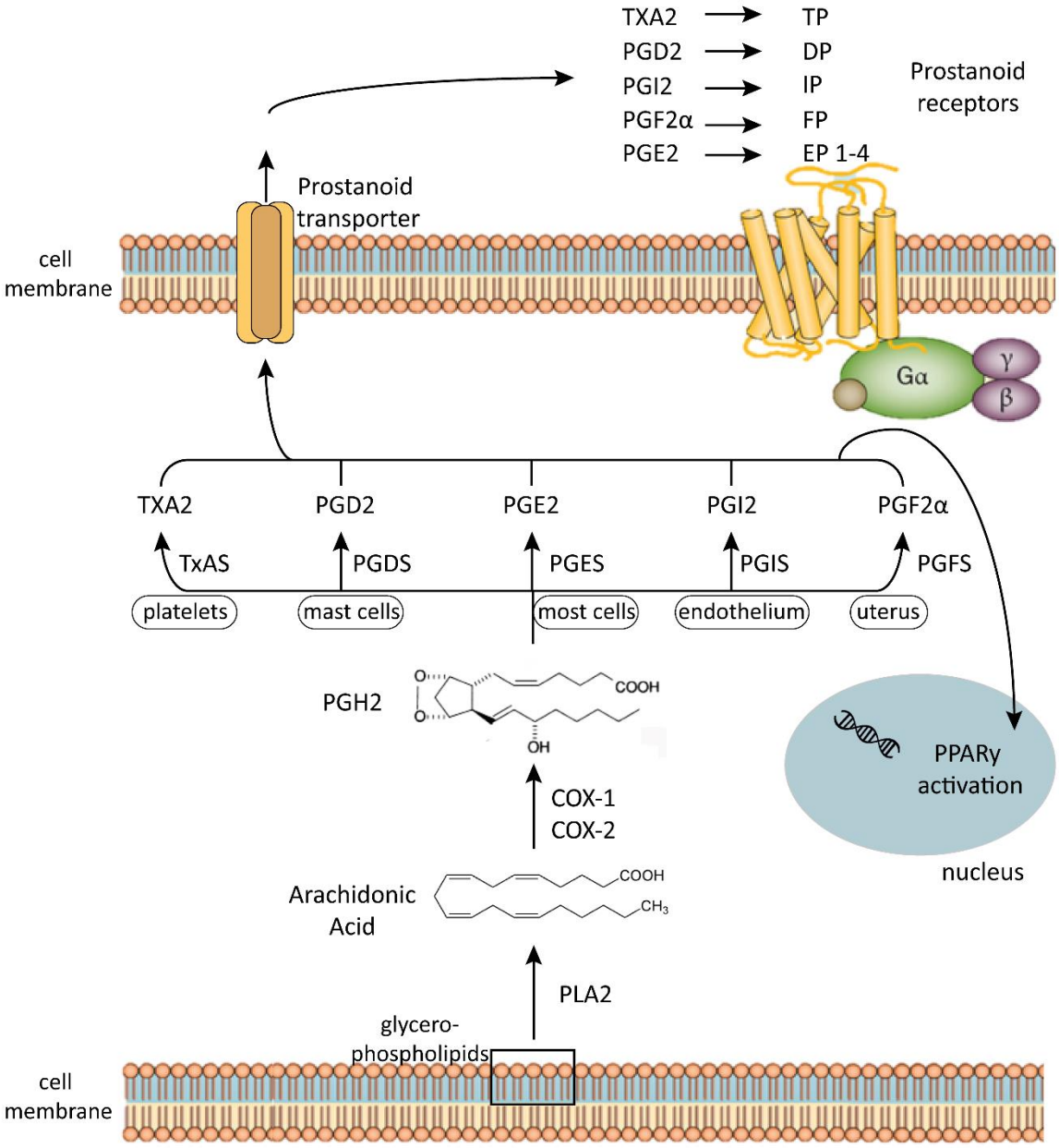

Figure 3: Synthesis and export of prostanoids

Phospholipase A2 (PLA2) initiates the release of arachidonic acid from glycerophospholipids in the cell membrane. Arachidonic acid is metabolized by COX-1 and COX-2 to the intermediate prostaglandin H2 (PGH_2). Cell-type specific expression of prostaglandin synthase enzymes (TxAS, thrombaxansynthase; PGDS, prostaglandin-D synthase; PGES, prostaglandin-E synthase; PGIS, prostaglandin-I synthase; PGFS, prostaglandin -F synthase) generate thromboxane A2 (TXA2), prostacyclin PGI2 and prostaglandins PGE2, PGD2 and PGF2α. These prostanoids are exported by prostanoid transporters to subsequently activate diverse G-protein coupled receptors (TP, thromboxane receptor; DP, prostaglandin D2 receptor, IP, prostaglandin I2 receptor; FP, prostaglandin F2 receptor; EP, prostaglandin E2 receptor). These prostanoids are also able to enter the nucleus and activate peroxisome proliferator-activated receptor γ (PPARγ).

In a cell-dependent mechanism, a heterogeneous family of PGH2 metabolizing enzymes forms five bioactive prostanoids: thromboxane A2 (TXA2), prostacyclin PGI2 and prostaglandins PGE2, PGD2 and PGF2α (Breyer et al., 2001; Funk, 2001). These prostanoids are exported by prostaglandin transporters (PGT) or other transporters to activate cell surface G-protein coupled receptors (TP, DP, PTGER1-4, IP, FP) (Schuster, 1998). Prostanoids are not stored but are synthesized *de novo*. Due to their short half-lives (seconds to minutes), they are considered as local hormones. Therefore, they are not transported to distal sites of the body and have autocrine or paracrine effects on target cells in close proximity. Prostanoids are described to potentially enter the nucleus and activate nuclear hormone receptors as PPARγ (Funk, 2001).

1.4.2 Prostaglandin E receptors and their functional role

PGE2 is the major product in the arachidonic acid metabolism in many physiological settings. PGE2 exerts a variety of partly opposing functional effects on different tissues. These diverse effects of PGE2 are a result of the existence of four G-protein coupled receptors EP1-4 (gene symbol: *PTGER1-4*) and their differential expression in various tissues as well as their distinct coupling to intracellular signaling pathways (Bos et al., 2004). For example, PGE2 can induce smooth muscle relaxation or constriction (Davis et al., 2004; Walch et al., 2001). Thus, investigation of the four prostaglandin receptors is challenging due to their simultaneous expression in tissues/cells and the different binding affinities to PGE2 (EP3/EP4 > EP1/EP2) (Abramovitz et al., 2000). The prostaglandin receptors can be divided in three groups according to the activation of a certain type of heterotrimeric G-protein by each of the receptors: i) relaxant receptors EP2 and EP4 (via G_s), ii) contractile receptor EP1 (via G_q) and iii) inhibitory receptor EP3 (via G_i) (Bos et al., 2004).

In human, EP1 was described to be expressed in the myometrium (Senior et al., 1991), pulmonary veins (Norel et al., 2004), mast cells (Wang and Lau, 2006), colon (Smid and Svensson, 2009) and keratinocytes (Konger et al., 2009). Whereas in mice, EP1 transcription is detectable in lung, stomach and kidney (Watabe et al., 1993). EP1 null mice appeared without any obvious phenotype. However, studies in EP1-deficient mice revealed functions in the context of stress responses, chemical carcinogenesis and inflammatory thermal hyperalgesia (Moriyama et al., 2005; Mutoh et al., 2002; Tanaka et al., 2012). Originally, EP1 as well as EP3 were described to induce smooth muscle constriction (Bos et al., 2004; Coleman et al., 1994). EP3 is widely expressed and is the only receptor in the prostanoid receptor family that has three splice variants arising from alternative splicing of the C-terminal tail. Major research was performed on the receptor splice variants and their signal transduction. However, the physiological relevance of EP3 is still poorly understood. First studies in EP3 null mice suggest a role in fever generation, type I allergy, tumor angiogenesis and pain perception (Amano et al., 2009; Kunikata et al., 2005; Ueno et al., 2001; Ushikubi et al., 1998).

The receptors EP2 and EP4 were first thought to be the same receptor. However, next to the fact that they are both coupled to adenylate cyclase, their pharmacological binding and structure are different (Bos et al., 2004). EP2 is expressed in almost every organ but at much lower levels than

EP4 (Katsuyama et al., 1995). Overall, EP2 is the least abundant prostaglandin receptor (Ricciotti and FitzGerald, 2011). It was originally described to induce smooth muscle relaxation in the cat trachea (Gardiner, 1986) and recent studies further confirmed a role on proliferation of SMC (Yau and Zahradka, 2003). EP2 null mice show impaired ovulation/fertilization and salt-sensitive hypertension (Hizaki et al., 1999; Kennedy et al., 1999). Furthermore, EP2 regulates angiogenesis, gastrointestinal secretion and motility, cellular immune responses and spatial learning (Dey et al., 2006; Kamiyama et al., 2006; Nataraj et al., 2001; Yang et al., 2009). EP4 is the most widely distributed prostaglandin receptor. Even though, EP4 and EP2 signal via G_s, both receptors induce different functional actions. This might arise from the structural differences of the C-terminal tail length which is important for agonist-induced desensitization and internalization (Bastepe and Ashby, 1999; Desai et al., 2000). EP4 null mice on a C57BL/6 background die within three days after birth due to a patent ductus arteriosus (Segi et al., 1998). Breeding of EP4 null mice in a mixed background can improve the survival and allowed the investigation of the functional role of EP4. Physiological functions of EP4 include the closure of the ductus arteriosus, induction of bone formation and Langerhans cell migration/maturation (Kabashima et al., 2003; Segi et al., 1998; Yoshida et al., 2002).

1.4.3 Prostaglandin signaling in health and disease

Prostaglandins are generally considered as pro-inflammatory mediators. During inflammation, induction of COX-2 through inflammatory stimuli and growth factors results in production of prostaglandins. Pharmacological agents, known as nonsteroidal anti-inflammatory drugs (NSAIDs), block prostaglandin synthesis by inhibiting COX-1/-2 and are commonly used as therapeutic for pain, fever and inflammation (Hata and Breyer, 2004). However, inhibition of both COX enzymes leads to gastrointestinal adverse effects based on the blockage of COX-1 derived prostanoids in the gastric epithelium. Therefore, NSAIDs with selective blockage of COX-2 (COXIB) are used for the treatment of arthritis or chronic inflammatory diseases (Ricciotti and FitzGerald, 2011). PGE2 is of particular interest in inflammatory reactions, since it leads to the typical signs of inflammation: redness, swelling and pain. This symptoms are based on increased blood flow, arterial dilatation and increased vascular permeability (Funk, 2001). The membrane associated PGES (mPGES) is described to play an important role in the synthesis of PGE2 in the context of inflammation (Trebino et al., 2003). Dependent on the receptor expression, PGE2 can exert pro- or anti-inflammatory responses. For example, prostaglandin signaling via EP2 and EP4 induces swelling in collagen-induced arthritis and hyperalgesia via EP1 (Honda et al., 2006; Moriyama et al., 2005). In contrary, anti-inflammatory effects are mostly seen in allergy and inflammatory processes (Kunikata et al., 2005; Matsuoka et al., 2000). Additionally, PGE2 binding of different prostaglandin receptors on immune cells (B- and T-cells, dendritic cells and macrophages) regulates cytokine expression profiles and differentiation of these cells (Egan et al., 2004; Johansson et al., 2013; Yao et al., 2009). This leads to the induction of pro- or anti-inflammatory effects (Ricciotti and FitzGerald, 2011).

Many human cancers are described to have elevated levels of COX and PGE2. PGE2 is considered as a tumor-promoting factor. Clinical studies and epidemiological studies indicate that long term (10-15 years) use of NSAIDs reduces the risk of colon and rectal cancers of about 50% (Rosenberg et al., 1991). Furthermore, strong evidence for the effects of NSAIDs on cancer risk is given by several rodent and clinical studies, in which different kind of cancers were treated with NSAIDs (Fischer et al., 2011b). These effects of NSAIDs on cancer risk might be explained by the regulation of COX-dependent (anti-inflammatory effects) and COX-independent (anti-tumor effects) targets (Wang and DuBois, 2006). Chronic inflammation is associated with an increased cancer risk, for example in hepatocellular carcinoma or gastric cancer (Alison et al., 2011; Uemura et al., 2001). Here, NSAIDs reduce the risk of cancer by their anti-inflammatory and analgesic effects via the inhibition of COX. At the same time, high doses of NSAIDs inhibit tumor cell growth and induce apoptosis by the regulation of different targets (NFκB, Par-4, Bcl-X_L) in a COX-independent manner (Kashfi and Rigas, 2005; Zhang and DuBois, 2000; Zhang et al., 2000). PGE2 and its receptors are the major prostaglandin players in cancer. Elevated levels of COX-2 and higher catalytic activity of mPGES are the main drivers of increased PGE2 levels in cancer (Nakanishi and Rosenberg, 2013). Next to its pro-inflammatory and pro-tumorigenic effects, PGE2 signaling influences the tumor microenvironment by the induction of tumor angiogenesis through the expression of pro-angiogenic factors (VEGF and bFGF) and by shifting the cytokine expression to a more immunosuppressive pro-tumorigenic environment (Hernández et al., 2001; Huang et al., 1998; Tsujii et al., 1998; Yang et al., 2003). Complementary, deletion of prostaglandin receptors (EP1-4) confirmed the tumorigenic role of PGE2. Here, specific EP receptor profiles in different cancers affected cancer incidence. Deletion of EP1 and EP4 lead to a decrease of preneoplastic lesions in the intestine (Mutoh et al., 2002; Watanabe et al., 1999), whereas EP3 deletion contributes to squamous cell carcinoma in the skin (Shoji et al., 2005). EP2 accelerates the number and size of intestinal polyps in a mouse model of human familial adenomatous polyposis (Sonoshita et al., 2001). Blockage of EP1 with a receptor antagonist reduced tumor burden in a carcinogen-induced breast cancer model (Kawamori et al., 2001). COX inhibitors, targeting the PGE2/EP axis, are promising drugs for the prevention or treatment of cancer. However, mPGES- or EP-inhibitors may offer an alternative to NSAIDs (Wang and DuBois, 2006).

1.5 Aim of the study

So far, pericytes, the mural cells of the microvasculature, have been identified by using a mixture of different criteria including morphology, location and gene/protein expression pattern. Until now, the recognition by using pericyte markers is the most convenient method from a practical perspective (Armulik et al., 2011). However, the definition of pericytes by this approach faces some challenges: i) Pericytes are a heterogenous cell population within the mural cells and none of the established markers recognizes all pericyte phenotypes since their expression is highly dynamic and dependent on the tissue and activation state (Bergers and Song, 2005; Díaz-Flores et al., 2009). ii) Pericytes are cells of mesenchymal origin and the expression of the established pericyte markers are overlapping with various mesenchymal cells (SMC, adipocytes, fibroblasts, MSC) (Armulik et al., 2011; Díaz-Flores et al., 2009).

Therefore, the aim of the present study was the identification of unique pericyte-specific markers in the vascular niche and their potential functional role in pericytes *in vitro* and *in vivo*. Expression profiling by microarray analysis of different pericyte populations and various mesenchymal cell populations was performed to discover novel pericyte markers. The role of the detected pericyte-specific transcripts in a physiological setting was investigated by comparative co-culture experiments of EC with pericytes silenced for the novel markers and subsequent transcriptomic profiling. These transcriptomic analyses were combined with functional *in vitro* studies to relate gene expression changes with functional phenotypes. In addition, mouse models with targeting the identified genes should be generated to extend the understanding of the role of the novel pericyte markers *in vivo*.

2 Results

2.1 Pericyte-specific expression of *S1PR3* and *PTGER2*

Distinct molecular markers are currently used for pericyte detection. However, their expression is dynamic due to the diverse characteristics, functions and locations of pericytes. Moreover, among these markers is no single entirely pericyte-specific marker (Armulik et al., 2011; Bergers and Song, 2005). Therefore, a microarray-based expression screening of primary human muscle pericytes (MP), lung pericytes (LP), pancreas pericytes (PancP), brain pericytes (BP) and placenta pericytes (PlaP) compared to other cells of mesenchymal origin (human umbilical arterial endothelial cells [HUAEC], human umbilical venous endothelial cells [HUVEC], human saphenous vein endothelial cells [HSAVEC], adipocytes [Adi], mesenchymal stem cells [MSC], fibroblasts [Fib]) was performed in biological replicates (n>3) to identify pericyte-specific transcripts. Pericytes, adipocytes, fibroblasts and MSC used for microarray analysis showed typical morphological features (elongated cell shape and long cell processes) of mesenchymal cells compared to EC (Figure 4). Additionally, pericytes displayed tissue-specific cell morphology.

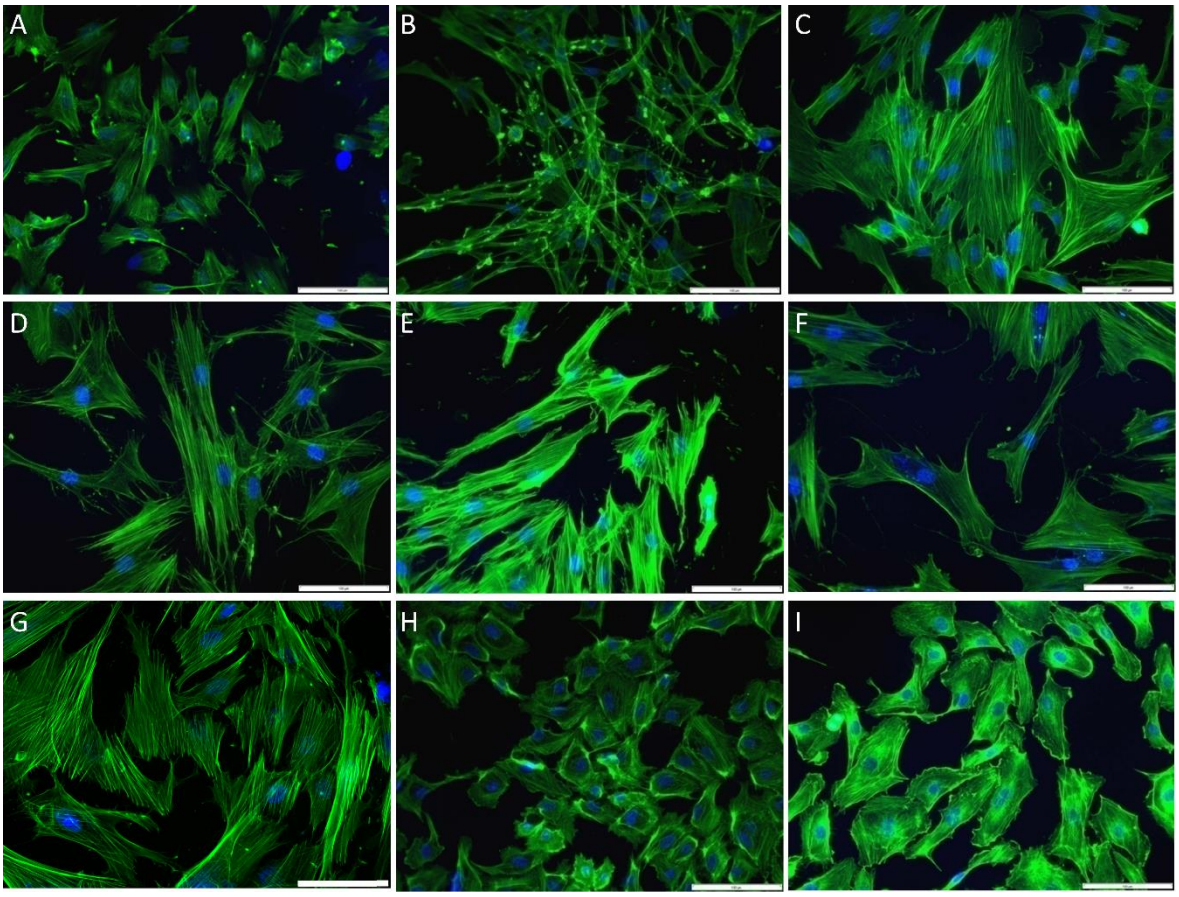

Figure 4: Cell morphologies of human pericytes and other mesenchymal cells
(A-C) Phalloidin stained human primary pericytes, (D-G) other mesenchymal cells and (H-I) EC. (A-C) Primary human pericytes are shown: (A) Brain pericytes, BP; (B) Lung pericytes, LP; (C) Placenta pericytes (PlaP). (D-G) Other primary human mesenchymal cells are shown: (D) adipocytes, Adi; (E) fibroblasts, Fib; (F) mesenchymal stem cells, MSC; (G) umbilical artery smooth muscle cells, HUASMC; (H, I) Human primary endothelial cells are shown: (H) umbilical vein endothelial cells, HUVEC; (I) saphenous vein endothelial cells, HSAVEC. Scale bars: 100 µm.

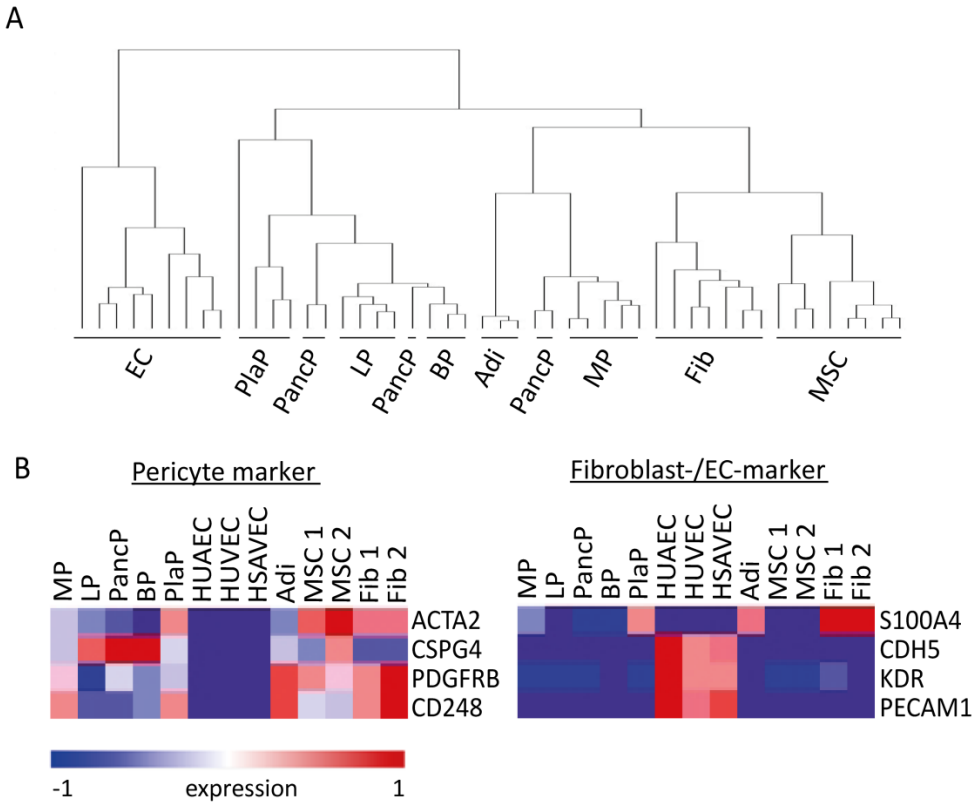

Figure 5: Human primary cells show lineage-specific expression pattern
(A) Clustering tree of the microarray analysis performed with primary human pericytes, endothelial cells and different mesenchymal cells (B) Heatmap depicting the expression pattern of pericyte-specific, fibroblast- and EC-specific genes (n=3-6). High expression is marked in red and low expression in blue. MP – muscle pericytes, LP – lung pericytes, PancP – pancreas pericytes, BP – brain pericytes, PlaP – placenta pericytes, HUAEC – human umbilical arterial endothelial cells, HUVEC – human umbilical venous endothelial cells, HSAVEC – human saphenous vein endothelial cells, Adi - adipocytes, MSC – mesenchymal stem cells, Fib – fibroblasts, EC – endothelial cells. n= number of independent experiments.

To analyze different gene expression profiles, a clustering of the microarray data was created (Figure 5A). The gene expression profiles of the different endothelial cells (EC) clustered and showed the most different gene expression compared to the other mesenchymal cells. Pericytes revealed organ-specific gene expression profiles, except for PancP. All mesenchymal lineages, except for EC, expressed the well-established pericyte markers described in literature (Figure 5B, left) (Armulik et al., 2005). Whereas all EC lack pericyte marker expression, *CSPG4* (*NG2*) seemed to be the most abundantly expressed gene in pericytes compared to Adi, MSC and Fib. In contrast, endothelial-specific (*CDH5, KDR, PECAM1*) and fibroblast-specific (*S100A4*) genes were almost exclusively expressed in the corresponding cells (Figure 5B, right). Altogether, this quality control analysis verified the microarray data to use it for novel pericyte marker identification.

In total, 13 genes were identified to be differentially expressed in pericytes compared to the other mesenchymal lineages (Figure 6A, B). Among them, five transcripts are only marginally described (C20orf127, LOC441019, LOC100130835, LOC100131866, C14orf149, CCDC34). Other transcripts were described to be involved in translation (ELOF1, MRPL55), cell division (PIGU), post-translational modification (DPH3) and extracellular matrix (Col7A1). Pathway analysis using Ingenuity Software and Gene Set Enrichment Analysis did not unveil any pathways, which could have gained further knowledge. However, *S1PR3* and *PTGER2*, coding for two G-protein coupled receptors, were identified as the most promising genes for further analysis.

For validation, microarray samples (Figure 7A) and biological replicates (Figure 7B) were investigated for *S1PR3* and *PTGER2* expression. The expression of both genes was not only significantly higher in all pericyte populations compared to the other mesenchymal cells but also almost exclusively restricted to pericytes. Since pericytes are mural cells of the microvasculature and pericytes are discussed as phenotypic variants of vascular SMC, human dermal blood endothelial cells (HDBEC), human brain microvascular endothelial cells (HBMEC) and smooth muscle cells (SMC) were included in the validation (Figure 7B). Whereas *PTGER2* expression was absent in these cells, *S1PR3* expression was detected in SMC.

A

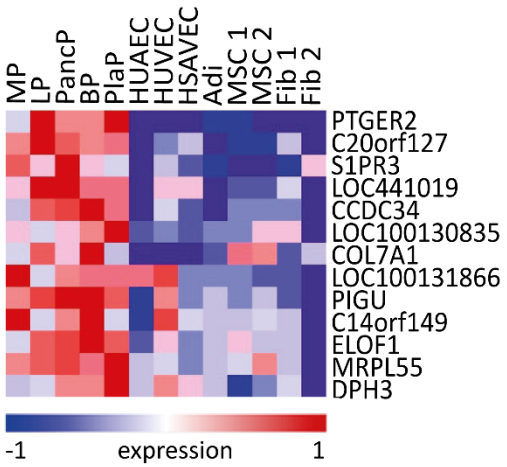

B

GENE	log2FC
PTGER2	2.93
C20orf127	2.23
S1PR3	2.17
LOC441019	1.57
CCDC34	1.41
LOC100130835	0.81
COL7A1	0.79
LOC100131866	0.77
PIGU	0.64
C14orf149	0.59
ELOF1	0.49
MRPL55	0.49
DPH3	0.48

Figure 6: Primary human pericytes show distinct gene expression compared to other mesenchymal cells
(A) Heatmap and (B) list showing the expression changes of the differentially expressed genes in pericytes compared to other mesenchymal lineages (n=3-6). High expression is marked in red and low expression in blue. MP – muscle pericytes, LP – lung pericytes, PancP – pancreas pericytes, BP – brain pericytes, PlaP – placenta pericytes, HUAEC – human umbilical arterial endothelial cells, HUVEC – human umbilical venous endothelial cells, HSAVEC – human saphenous vein endothelial cells, Adi – adipocytes, MSC – mesenchymal stem cells, Fib – fibroblasts. n= number of independent experiments.

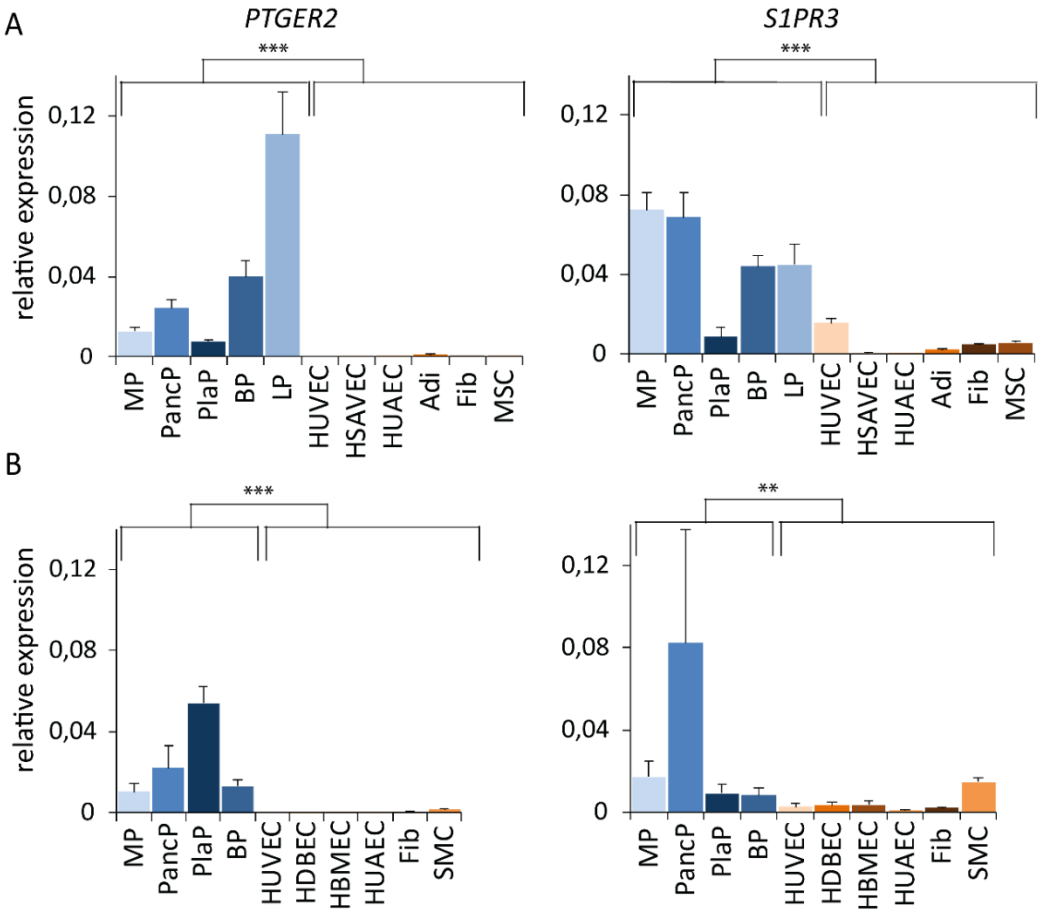

Figure 7: S1PR3 and PTGER2 are specifically expressed by pericytes
(A) Quantification of *S1PR3* and *PTGER2* gene expression in microarray samples and (B) biological replicates of pericytes, endothelial cells and other mesenchymal cells (n=3) by qPCR. Expression was normalized to the housekeeping gene *B2M*. MP – muscle pericytes, LP – lung pericytes, PlaP – placenta pericytes, PancP – pancreas pericytes, BP – brain pericytes, HUAEC – human umbilical arterial endothelial cells, HUVEC – human umbilical venous endothelial cells, HSAVEC – human saphenous vein endothelial cells, HDBEC – human dermal blood endothelial cells, HBMEC – human brain microvascular endothelial cells, Adi – adipocytes, MSC – mesenchymal stem cells, Fib – fibroblasts, SMC – smooth muscle cells. Values are mean±SD, *p<0.05, **p<0.01, ***p<0.001, n= number of independent experiments.

To confirm the expression of *S1PR3* and *PTGER2* in mouse pericytes, a protocol for the isolation of a mural cell-enriched population via FACS was established (Figure 8). The lung was chosen as a model organ, since it is highly vascularized and will as such provide sufficient cells for gene expression analysis. Therefore, lungs from adult mice (8-12 weeks) were resected and digested for preparation of single cell suspensions. Collagenase IV turned out to be the most efficient digestion enzyme. For subsequent FACS, cells were gated according to SSC-A and FSC-A to exclude cell debris. Doublets were removed by FSC-H and FSC-A gating. Leukocytes (CD45 positive), erythrocytes (TER119 positive), lymphatic endothelial cells (LYVE1 positive), alveolar epithelial cells (Podoplanin, PDPN positive) and FxCycle positive cells (dead cells) were excluded. FxCycle$^-$ CD45$^-$TER119$^-$LYVE1$^-$PDPN$^-$CD31$^-$ and FxCycle$^-$CD45$^-$TER119$^-$LYVE1$^-$PDPN$^-$CD31$^+$ were sorted for subsequent gene expression analysis.

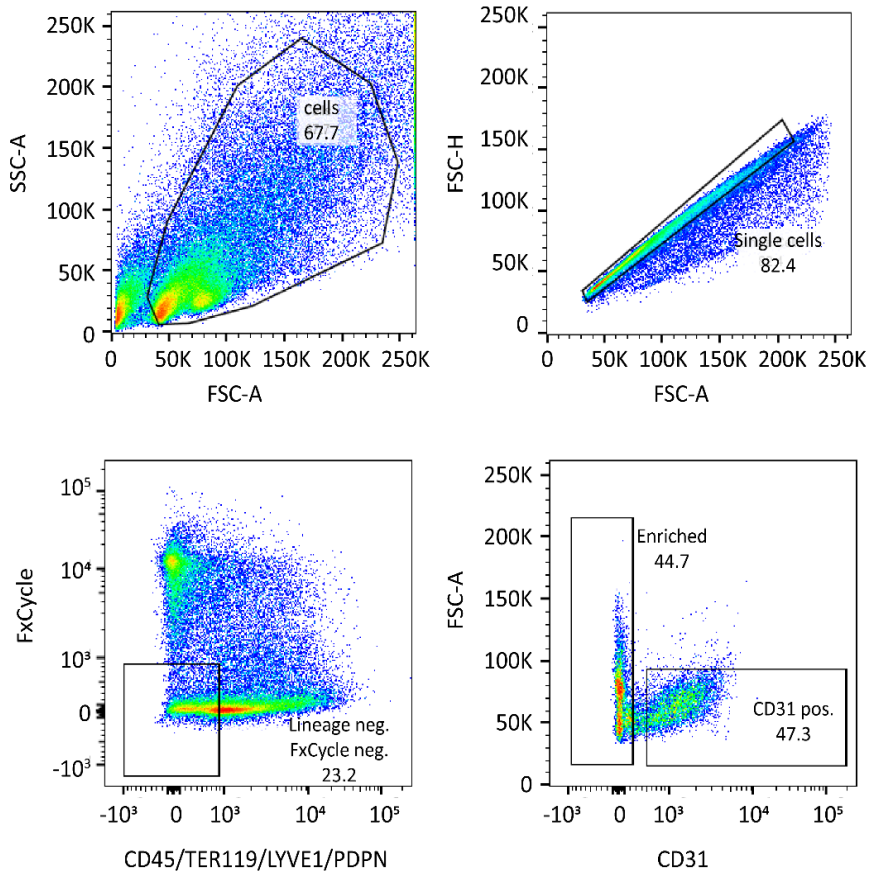

Figure 8: Isolation of a mural cell-enriched population from the murine lung
Representative FACS schemes for the isolation of a mural cell-enriched population. FxCycle$^-$ CD45$^-$TER119$^-$LYVE1$^-$PDPN$^-$CD31$^-$ and FxCycle$^-$CD45$^-$TER119$^-$LYVE1$^-$PDPN$^-$CD31$^+$ cells were sorted for gene expression analysis.

The purity of the sorted cells was confirmed by qPCR (Figure 9) detecting the expression of EC markers (*Cd31, Vegfr2, Cdh5*), pericyte markers (*Ng2, Desmin, Pdgfrb*), a fibroblast marker (*Pdgfrα*) and the novel pericyte markers (*S1pr3, Ptger2*). Pericyte markers, except for *Desmin*, and the fibroblast marker *Pdgfrα* were higher expressed in the mural cell enriched population (FxCycle$^-$CD45$^-$TER119$^-$LYVE1$^-$PDPN$^-$CD31$^-$) compared to the EC population (Figure 9C), whereas endothelial makers were primarily expressed in the EC compartment (FxCycle$^-$ CD45$^-$TER119$^-$LYVE1$^-$PDPN$^-$CD31$^+$) (Figure 9B). *S1pr3* and *Ptger2* were exclusively expressed in the mural cell enriched population (Figure 9A).
Together, these experiments validated *S1PR3* and *PTGER2* as pericyte-specific transcripts *in vitro* and *in vivo* both in human and mouse.

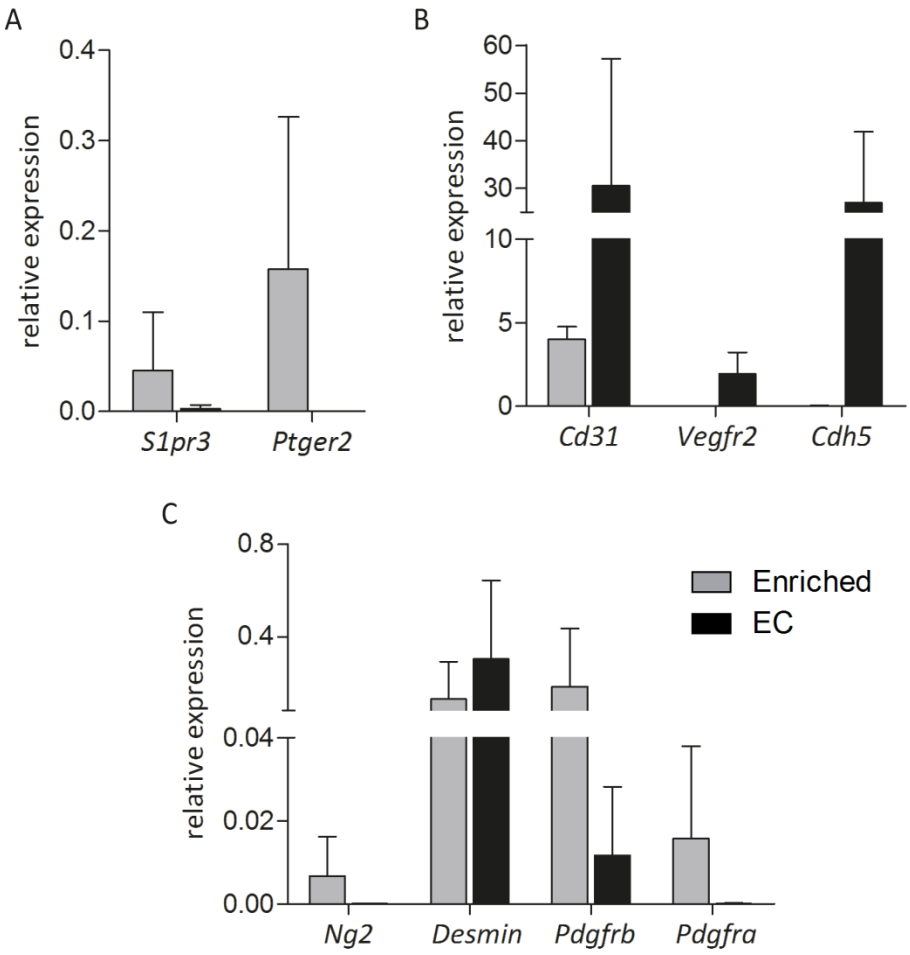

Figure 9: Mural cell enriched population express *S1pr3* and *Ptger2*
(A) Quantification of *S1pr3* and *Ptger2*, (B) EC- and (C) pericyte-/fibroblast-specific marker gene expression in the isolated mural cell enriched population (FxCycle$^-$CD45$^-$TER119$^-$LYVE1$^-$PDPN$^-$CD31$^-$) and isolated EC (FxCycle$^-$ CD45$^-$TER119$^-$LYVE1$^-$PDPN$^-$CD31$^+$) by qPCR (n=2). *Hprt* was used as housekeeping gene. n= number of independent experiments.

2.2 S1PR3 signals via $G\alpha_i$ and $G\alpha_q$

S1PR3 has been described to signal via the three Gα proteins: $G\alpha_i$, $G\alpha_{12/13}$ and $G\alpha_q$ (An et al., 1998; Ancellin and Hla, 1999). In order to investigate which S1PR3 pathways are active in pericytes, downstream signaling molecules were analysed upon S1P stimulation in *S1PR3* silenced *vs*. control-silenced pericytes. Extracellular signal-regulated kinase 1/2 (ERK 1/2) is known to be phosphorylated upon S1P activation of $G\alpha_i$ (Tao et al., 2009). S1P stimulation only of siControl transfected pericytes showed phosphorylation of ERK 1/2 in a time-dependent manner (Figure 10A) but no significant increase in phosphorylation of ERK 1/2 if S1PR3 was silenced with two different siRNAs (Figure 10A) or TY52156, a selective S1PR3 receptor antagonist (Figure 10B) (Murakami et al., 2010). *S1PR3* was down-regulated by approximately 90% after 48 h and 70-80% after 72 h using two different siRNAs (Figure 11). $G\alpha_i$ can be inhibited by the ADP-ribosylating activity of pertussis toxin (PTX) (Gunther et al., 2000). $G\alpha_i$ inhibition prevented the phosphorylation of ERK 1/2 after S1P stimulation in pericytes (Figure 10C). In summary, these data demonstrate that S1PR3 signals via $G\alpha_i$ in pericytes.

For analysis of the $G\alpha_{12/13}$ pathway, downstream signaling molecules of RhoA were investigated. RhoA is described to be an effector of the myosin light chain phosphatase (MLCP), which regulates myosin light chain (MLC) phosphorylation of myosin II (Amano et al., 2010). S1P stimulation of pericytes resulted in a time-dependent increase of MLC phosphorylation (Figure 12). Selective inhibition of S1PR3 by TY52156 prevented the phosphorylation of pMLC2 after S1P stimulation. In conclusion, these data indicate that S1PR3 regulates MLC phosphorylation potentially via $G\alpha_{12/13}$ signaling in pericytes.

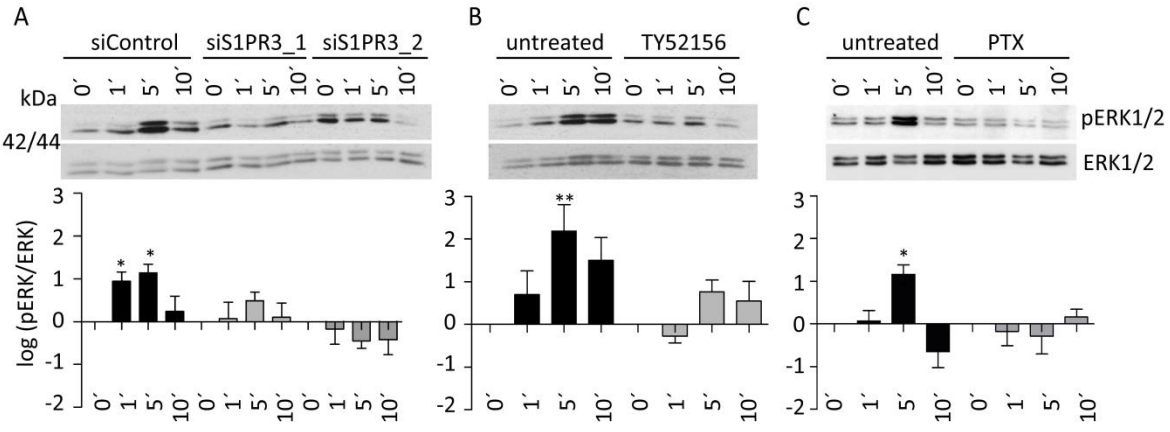

Figure 10: S1PR3 signals via $G\alpha_i$ in human pericytes

(A) Representative immunoblotting images and corresponding quantifications for pERK/ERK1/2 in 1 µM S1P treated (0, 1, 5, 10 min) BP upon silencing of *S1PR3* (n=5), (B) treatment with S1PR3 inhibitor TY52156 (1 µM, 4h, n=4) or with (C) the $G\alpha_i$ inhibitor pertussis toxin (PTX, 200 ng, 4h, n=3). *p<0.05, **p<0.01, ***p<0.001, n= number of independent experiments.

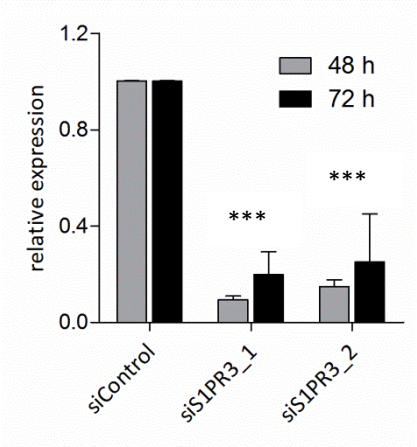

Figure 11: *S1PR3* knockdown upon siRNA transfection
Quantification of *S1PR3* gene expression in BP upon siRNA mediated silencing of S1PR3 after 48 h (n=3) and 72 h (n=3). *Hprt* was used as housekeeping gene. *p<0.05, **p<0.01, ***p<0.001, n= number of independent experiments.

S1PR3 signaling to $G\alpha_q$ was examined by calcium release assay as activation of $G\alpha_q$ is described to result in increased intracellular calcium levels (Hirota et al., 2007). Pericytes, silenced for *S1PR3* by siRNAS or S1PR3 inhibitor TY52156, were preincubated with the fluorescent dye Rhod4. The intensity of Rhod4 increases upon binding to Ca^{2+}. 10 sec upon stimulation with S1P, the rapid release of Ca^{2+} from the endoplasmatic reticulum into the cytosol was measured as increase of fluorescence intensity over time (Figure 13A). After 3 min, cytosolic Ca^{2+} levels were back to basal levels. siRNA- or TY52156-mediated silencing of S1PR3 in pericytes significantly reduced Ca^{2+} from the endoplasmatic reticulum. The area under the curve of the fluorescent signals was calculated for all conditions (Figure 13B). Thus, S1PR3 signals via $G\alpha_q$ in pericytes.

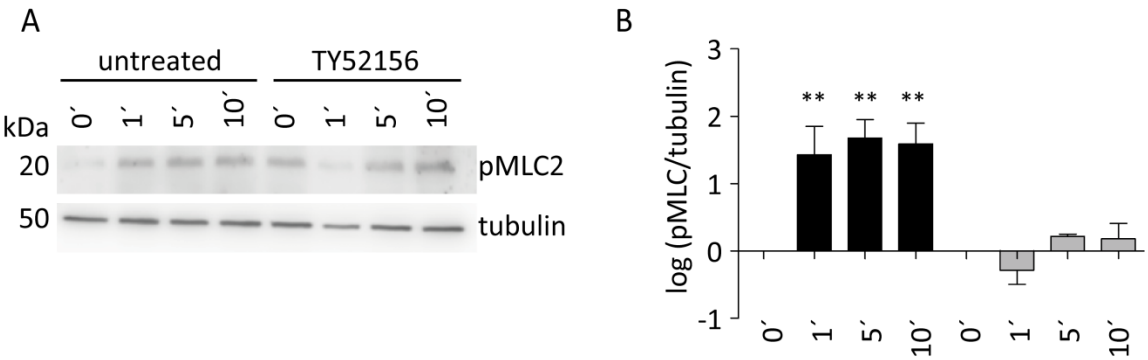

Figure 12: S1PR3 inhibition results in reduced MLC phosphorylation
(A) Representative immunoblotting images for pMLC2/tubulin in 1 µM S1P treated (0, 1, 5, 10 min) BP upon treatment with 1 µM S1PR3 inhibitor TY52156 for 4 h (n=3). (B) Corresponding quantifications for immunoblot experiments (in A) of pMLC/tubulin. *p<0.05, **p<0.01, ***p<0.001, n= number of independent experiments.

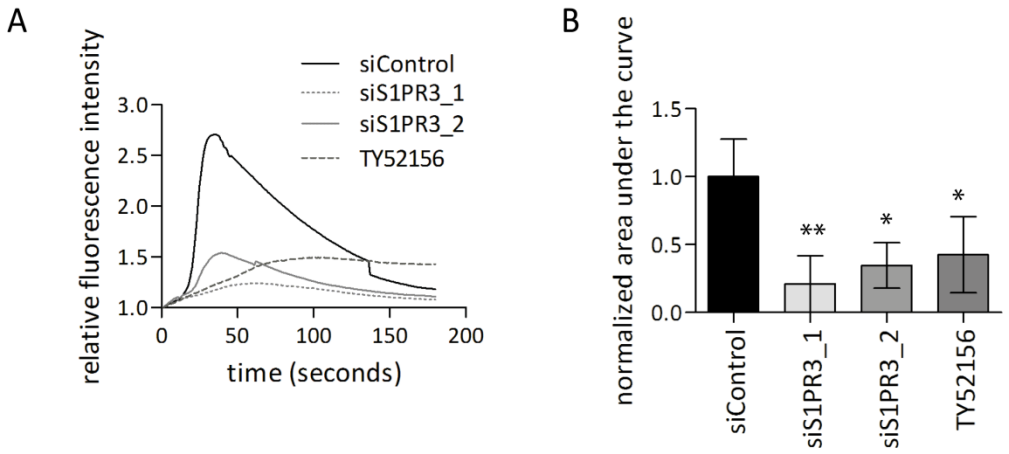

Figure 13: S1PR3 signals via $G\alpha_q$ in human pericytes
(A) Calcium release analysis of stimulated (S1P, 1 µM) BP after *S1PR3* silencing or treatment with the S1PR3 inhibitor Ty52156 (1 µM). (B) Quantification of the area under the curve of the relative fluorescent intensities shown in A (n=3). *p<0.05, **p<0.01, ***p<0.001, n= number of independent experiments.

To exclude that S1PR1 may be responsible for the remaining effects upon *S1PR3* silencing, S1PR1 mRNA and protein expression was investigated in pericytes. Comparing *S1PR1* and *S1PR3* expression in the microarray data (described above) of pericytes from different organs with different endothelial cells, showed an inverse expression of both receptors (Figure 14A). *S1PR3* was exclusively expressed in pericytes, whereas *S1PR1* was strongly expressed in EC, but absent in pericytes. This result was confirmed in biological replicates with BP and HUVEC. Again, *S1PR1* showed very low mRNA and protein expression in pericytes (Figure 14B, C), suggesting that S1PR1 does not play a role in pericytes.

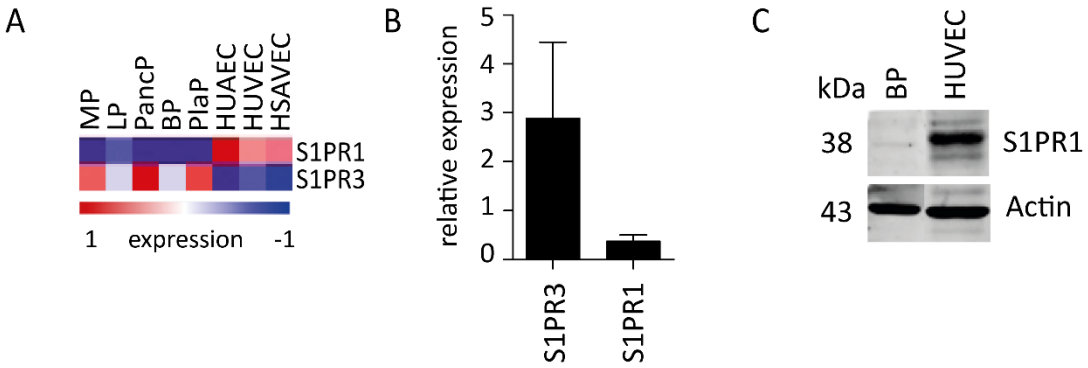

Figure 14: S1PR1 is not expressed by pericytes
(A) Heatmap of *S1PR1* and *S1PR3* in primary human pericytes, endothelial cells and different mesenchymal cells. (B) Quantification by qPCR of *S1PR1* and *S1PR3* in BP. *B2M* was used as housekeeping gene (n=2). (C) Immunoblotting of S1PR1 in BP and HUVEC. βActin was used as loading control (n=1). MP – muscle pericytes, LP – lung pericytes, PancP – pancreas pericytes, BP – brain pericytes, PlaP – placenta pericytes, HUAEC – human umbilical arterial endothelial cells, HUVEC – human umbilical venous endothelial cells, HSAVEC – human saphenous vein endothelial cells. n= number of independent experiments.

2.3 Establishment of a co-culture system of pericytes and EC

EC and pericytes are in close contact. Both interact closely via paracrine and juxtacrine signaling based on their anatomical relationship. In a biological setting, pericytes are always associated with EC, whereas EC exist without pericyte contacts (see chapter 1.2.4). To gain functional insights of S1PR3 and PTGER2 in pericytes and contacting EC, a co-culture system of *S1PR3* or *PTGER2* silenced pericytes and EC was established. Shortly, *S1PR3* or *PTGER2* were silenced in pericytes before culturing on a monolayer of EC (Figure 15A). After 24 hours of co-culturing, pericytes and EC were separated via FACS. For subsequent FACS, cells were gated according to SSC-A and FSC-A to exclude cell debris. Doublets were removed by SSC-H and SSC-A gating. $CD31^+$ endothelial cells and pericytes marked with an integrated membrane label were collected (Figure 15B). RNA of both populations was sent for gene expression profiling.

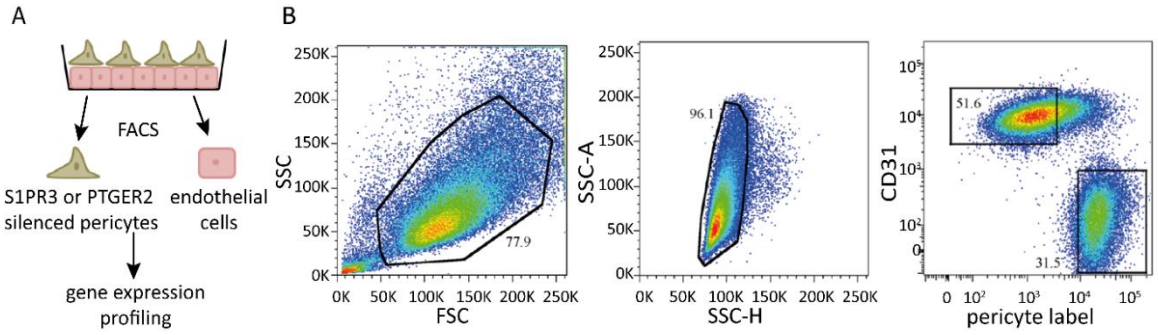

Figure 15: BP and EC gene expression profiling upon co-culture
(A) Scheme depicting the workflow for gene expression profiling of BP and EC upon co-culturing. *S1PR3* or *PTGER2* silenced BP and primary EC were co-cultured for 24 h and separated by FACS followed by gene expression profiling. (B) Representative FACS sorting schemes for the separation of BP and EC after co-culturing. $CD31^+$ cells and pericyte $label^+$ (PKH) cells were sorted for microarray analysis.

2.4 Functional analysis of S1PR3 and PTGER2

To verify the robustness of the generated expression profiles, the expression of cell-specific genes was examined. Pericytes showed a significant knockdown of *S1PR3* and *PTGER2* in the corresponding datasets (Figure 16A). EC had a low expression intensity of *S1PR3* and *PTGER2* and no expression change upon *S1PR3* or *PTGER2* knockdown in the respective co-cultured pericytes (Figure 16B). Both populations expressed cell-specific genes (Figure 16C). Pericytes were *NG2/CSPG4*- and *ACTA2* (αSMA)-positive, while EC were *CD31*-positive. The data confirms the purity of both populations after separation via FACS.

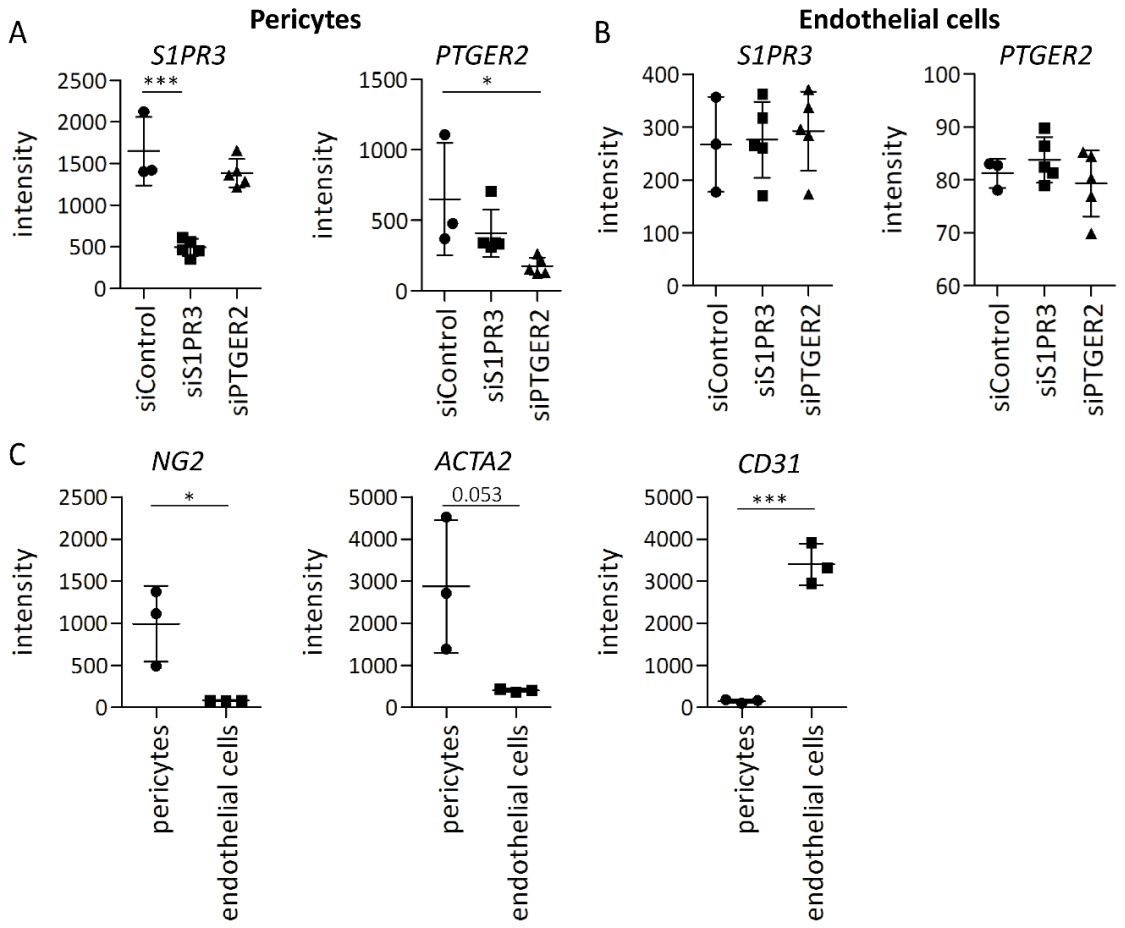

Figure 16: Pericytes and endothelial cells express cell-specific genes after co-culture
(A) Quantification of the *S1PR3* and *PTGER2* expression (mean intensity, microarray) in pericytes- and (B) endothelial cells (n=3-6). (C) Pericyte marker (*NG2*, *ACTA2*) and endothelial cell marker (*CD31*) expression in EC and BP. *p<0.05, **p<0.01, ***p<0.001, n= number of independent experiments.

The expression data of non-silenced vs. *S1PR3* or *PTGER2* silenced pericytes as well as the corresponding EC were evaluated by separate analysis (Figure 17). Both, *S1PR3* and *PTGER2* silenced pericytes, showed differentially expressed genes (log2FC threshold 0.4/-0.4, 143 [*S1PR3*]/ 262 [*PTGER2*] genes). However, gene expression changes in EC were not as pronounced as in the respective pericytes (log2FC threshold 0.2/-0.2, 13 [*S1PR3*]/ 10 [*PTGER2*] genes). This small number of differentially expressed genes in EC could not be validated by qPCR (data not shown). Therefore, the following chapters will be confined to the analysis of *S1PR3* and *PTGER2* in pericytes.

In pericytes, genes with a significant fold change of 30% in the silenced vs non silenced pericyte population were evaluated by Molecular Signature Database Analysis (MSigDB). MSigDB allows to generate an overlap of differentially expressed genes in pericytes with the existing collection of annotated gene sets (Subramanian et al., 2005). Hallmark gene sets, representing genes that are involved in biological processes, and Reactome gene sets, deriving from the Reactome pathway database, were used for analysis.

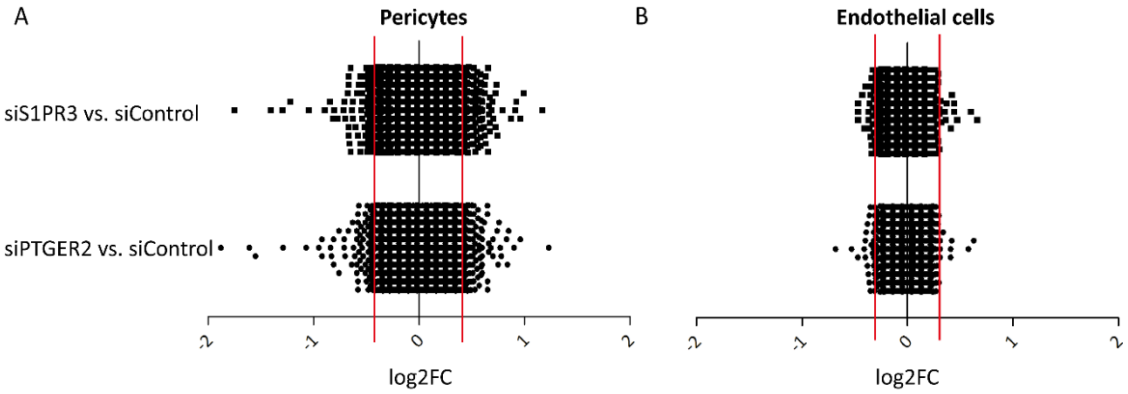

Figure 17: Separate gene expression analysis of pericytes and EC after co-culture
(A) Separate gene expression analysis of pericytes silenced for *S1PR3* or *PTGER2* and corresponding (B) EC after 24h of co-culture. Depicted is the differential expression profile according to the log2 Fold Change (FC). Red line indicates the log2FC threshold (pericytes: log2FC 0.4/-0.4; EC: log2FC 0.2/-0.2) used for analysis.

2.4.1 Microarray analysis prompts towards S1PR3 interference with the actin/myosin skeleton in pericytes

To gain insights into the functional role of S1PR3 in pericytes, gene expression data was analysed. Among the top genesets, overlapping with significantly regulated genes, MTORC1 signaling (FDR=1.88x10^{-03}) and cell junction organization, cell-ECM interaction and cell-cell communications (FDR=2.59/2.68x10^{-03}; Figure 18A, B, C) were identified . To complement these findings, co-culture experiments with *S1PR3* silenced pericytes were performed and gene expression of particular genes was validated by real time (RT) quantitative PCR (qPCR). Asparagine synthetase (ASNS), included in the MTORC1 signaling gene set, was upregulated upon S1PR3 knockdown (Figure 18D). ASNS is involved in amino acid metabolism and regulates mTORC1 activity (Krall et al., 2016). Differentially regulated genes (*MPRIP, MYH10, SDC1*) of the cell-cell and cell-ECM genesets were successfully validated (Figure 18E). Myosin phosphatase rho interacting protein (*MPRIP*) targets the myosin phosphatase and therefore regulates myosin light chain phosphorylation. MPRIP binds the myosin phosphatase but also directly RhoA resulting in myosin phosphatase regulation by RhoA (Surks et al., 2003). MPRIP is known to influence pericyte cytoskeletal remodeling (Durham et al., 2014). Myosin heavy chain 10 (MYH10) is a non-muscle myosin and described to be involved in cell polarity, adhesion and migration (Bresnick, 1999). Syndecan 1 (SDC1) is a transmembrane (type I) heparan sulfate proteoglycan and mediates cell binding, signaling and cytoskeletal organization (Beauvais et al., 2009). These results suggest a role of S1PR3 in cell morphology in respect of actin-myosin skeleton, migration and adhesion.

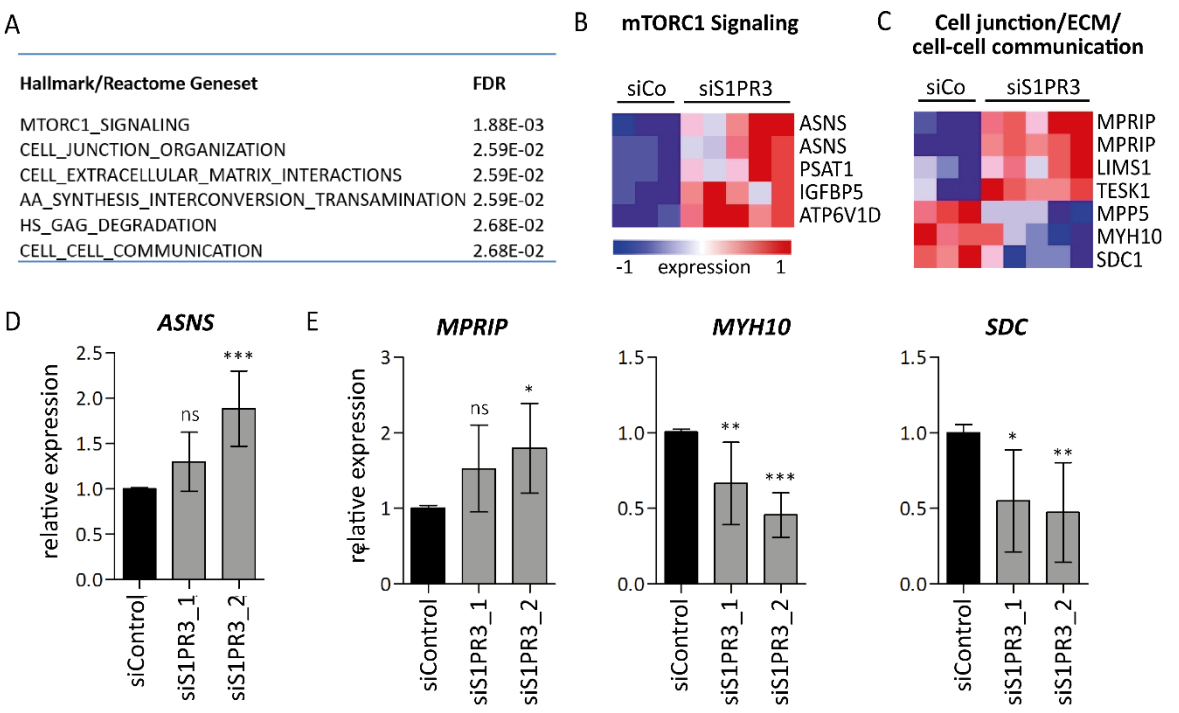

Figure 18: Molecular Signature Database analysis of BP silenced for *S1PR3* co-cultured with EC
(A) Molecular Signature database (Hallmark, Reactome) analysis of *S1PR3* silenced BP vs. control-silenced (siCo) BP after co-culture with EC. (B, C) Heatmap of differently regulated genes (Genesets ´mTORC1 Signaling´ and ´Cell junction organization/cell-ECM interactions/cell-cell communication´) in pericytes silenced for *S1PR3*. (D, E) Validation of corresponding genes of mTORC1 signaling (D) and cell junction/ECM/cell-cell communication (E) by qPCR in microarray samples and biological replicates (n=5). *p<0.05, **p<0.01, ***p<0.001, ns=non significant, n= number of independent experiments.

To verify the biological relevance, functional *in vitro* assays of *S1PR3* silenced pericytes were performed. Cell migration towards a gradient (FCS, conditioned media of HUVEC) of *S1PR3* silenced pericytes was significantly decreased, as seen by xCELLigence real time cell analysis (RTCA) or Boyden chamber assay (Figure 19A and B). The xCELLigence system is an electronical Boyden chamber assay that allows quantitative kinetic measurements in real-time without the use of labeling. These results go in line with the diminished phosphorylation of MLC2 upon *S1PR3* silencing (Figure 12A and B). Since *S1PR3* silenced pericytes are less migratory and expression of genes (*MYH10, SDC1*), responsible for cell adhesion and cell-ECM interaction were downregulated upon *S1PR3* knockdown, adhesion assays were performed. However, adhesion of *S1PR3* silenced pericytes on a monolayer of EC (Figure 19C) as well as mono-cultured pericytes using xCELLigence system (data not shown) was not changed.

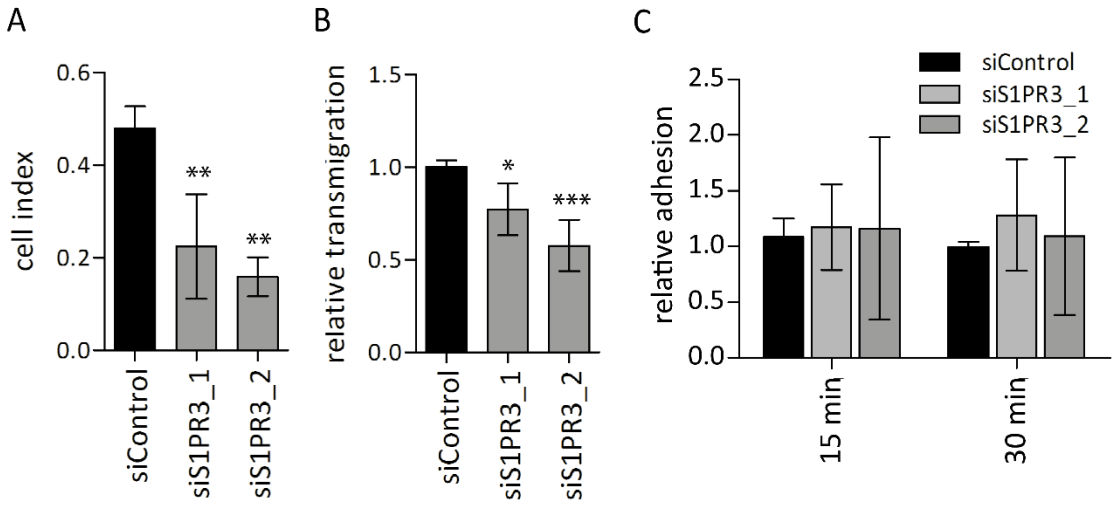

Figure 19: Reduced migration of *S1PR3* silenced pericytes
(A, B) Migration analysis of mono-cultured *S1PR3* silenced pericytes using (A) xCELLigence system (n=4) and (B) Boyden chamber assay (B, n=5). The migration was iniitated by using a FCS (xCELLigence) or conditioned HUVEC media (Boyden chamber assay) gradient. (C) Adhesion analysis of *S1PR3* silenced pericytes (n=3) on EC. *p<0.05, **p<0.01, ***p<0.001, ns=non significant, n= number of independent experiments.

Even though cell adhesion was not changed in *S1PR3* silenced pericytes, the morphology of the cells appeared different compared to control cells. Knockdown cells showed increased cell size, validated by image analysis of Phalloidin-positive area per cell (DAPI positive nucleus, Figure 20A and B). To gain further insight, live cell imaging was performed using Holomonitor microscope (Alm et al., 2013). The Holomonitor allows real-time imaging while the cells are cultured under standard conditions. Images of the cells are calculated based on the phase-shift of light through the cells compared to bypassed light. Thus, several cellular parameters can be measured at the same time. The analysis of *S1PR3* silenced pericytes confirmed the change of morphology concerning cell volume and cell thickness compared to the corresponding control (Figure 20C). In summary, *S1PR3* in pericytes interferes with the actin-myosin cytoskeleton of the cells resulting in increased migration and reduced cell size.

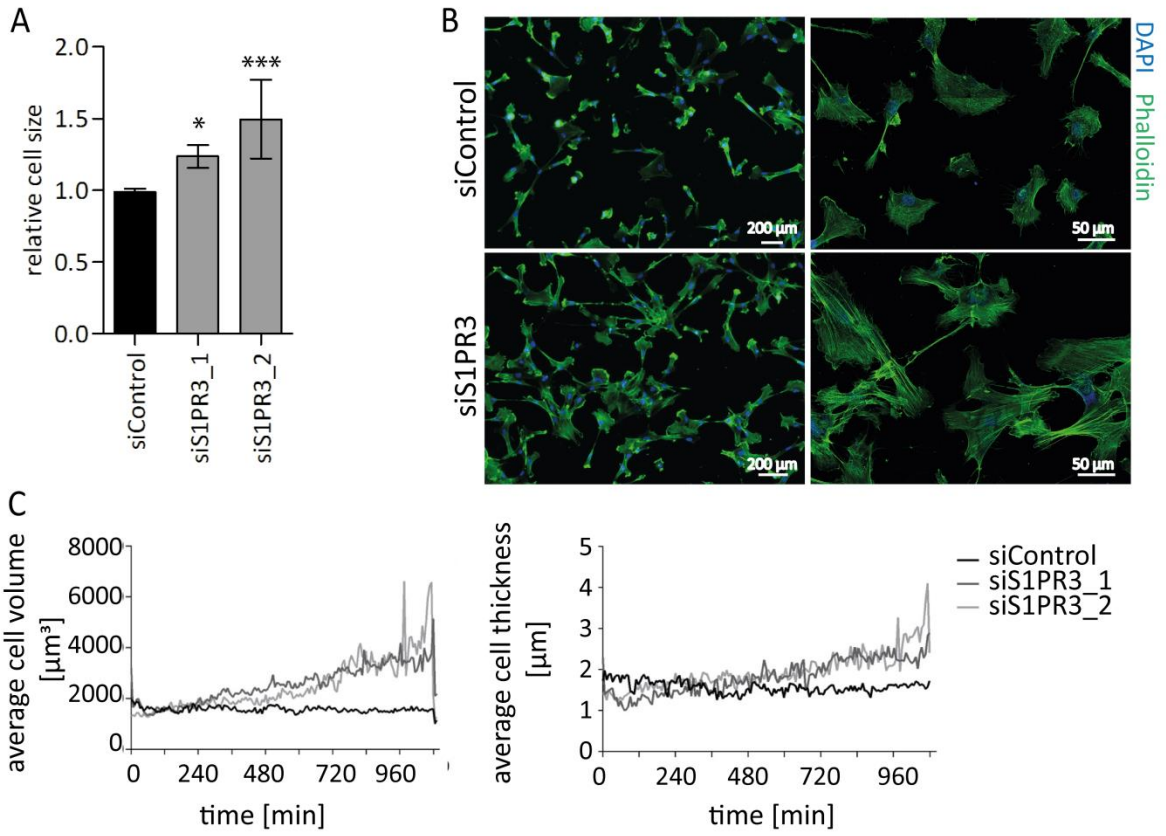

Figure 20: Increased cell size of *S1PR3* silenced pericytes
(A) Cell size analysis of *S1PR3* silenced BP upon stimulation with 1 µM S1P for 6 h (n=6). (B) Representative images of phalloidin staining (20x, left; 63x, right) of *S1PR3* silenced BP upon S1P (1 µM) stimulation for 6 h. (C) Representative analysis of average cell volume and cell thickness using Holomonitor software upon *S1PR3* knockdown (24 h pst siRNA) compared to control cells for 18 hours (n=2). *p<0.05, **p<0.01, ***p<0.001, n= number of independent experiments.

2.4.2 PTGER2 regulates pericyte proliferation

Gene expression profiling data of *PTGER2* silenced pericytes was analysed according to the *S1PR3* analysis (see chapter 2.4). MSigDB analysis revealed Il2-STAT5 signaling (FDR=5.82x10^{-05}), apoptosis (FDR=7.96x10^{-05}) and mitotic spindle (FDR=1.62x10^{-03}) of the Hallmark genesets having the most significant overlap with the differentially expressed genes upon *PTGER2* silencing (Figure 21A). Six proliferation regulating genes were identified in the mitotic spindle geneset (Figure 21B), most notably the significantly downregulated genes Kinesin-associated protein 3 (*KIFAP3*) and tuberous sclerosis protein 1 (*TSC1*), two negative regulators of cell division (Figure 21C). Conversely, the apoptosis geneset included pro- (*SMAD7*, *CASP3*, *GSN*) and anti-apoptotic (*BCL2L1*, *IGFR2*) genes (Figure 21D), mostly being downregulated (Figure 21E).

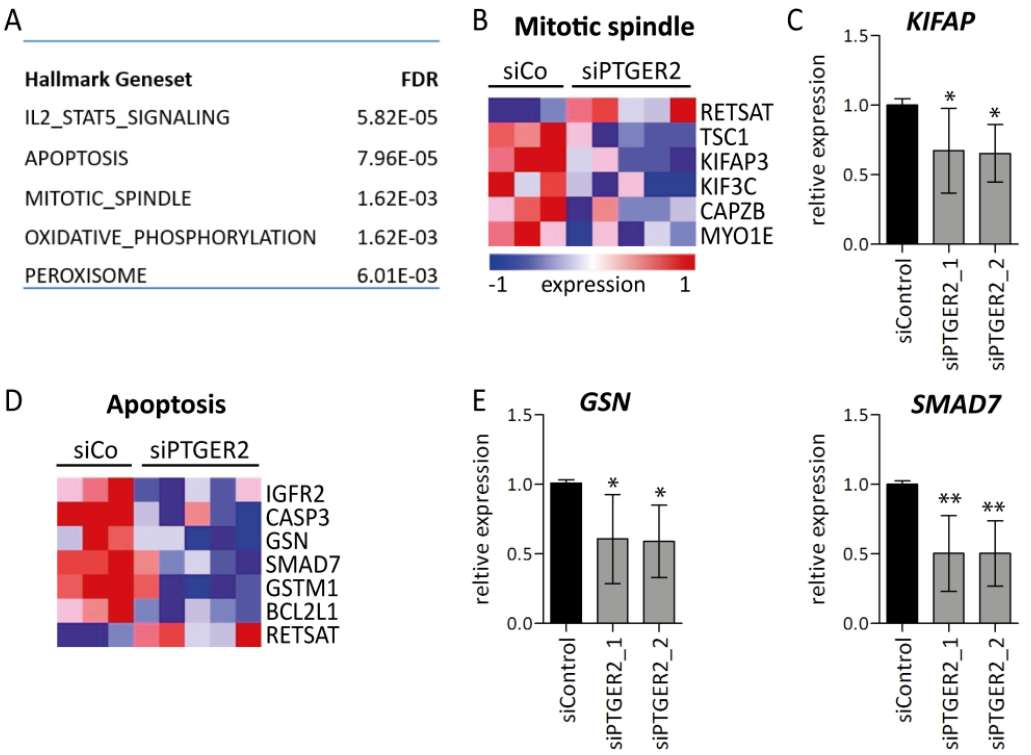

Figure 21: Molecular Signature Database analysis of BP silenced for *PTGER2* co-cultured with EC
(A) Molecular Signature database (Hallmark) analysis of *PTGER2* silenced BP after co-culture with EC. Gene sets with an FDR<10^{-3} are indicated. (B) Heatmap of differently regulated genes (Geneset ´mitotic spindle´) in pericytes silenced for *PTGER2* vs. control (siCo). (C) Quantification and validation of a corresponding gene (*KIFAP*) in biological replicates (n=3). (D) Heatmap of differently regulated genes (Geneset ´Apoptosis´) in pericytes silenced for *PTGER2* vs. control. (E) Quantification of corresponding genes (*GSN, SMAD7*) in biological replicates (n =3). *p<0.05, **p<0.01, ***p<0.001, n= number of independent experiments.

Corresponding to the downregulation of negative regulators of proliferation (Figure 21B and C), proliferation analysis of mono-cultured *PTGER2* silenced pericytes using the xCELLigence system revealed a significant increase of proliferation compared to control silenced cells (Figure 22A). However, silencing of *PTGER2* in pericytes did not change the level of apoptosis (Annexin V FACS) upon co-culture with EC (Figure 22B). Thus, PTGER2 signaling in pericytes influences the proliferation of pericytes *in vitro*.

In summay, successfully identified novel pericyte markers S1PR3 and PTGER2 have functional relevance in pericyte biology which was verified *in vitro*.

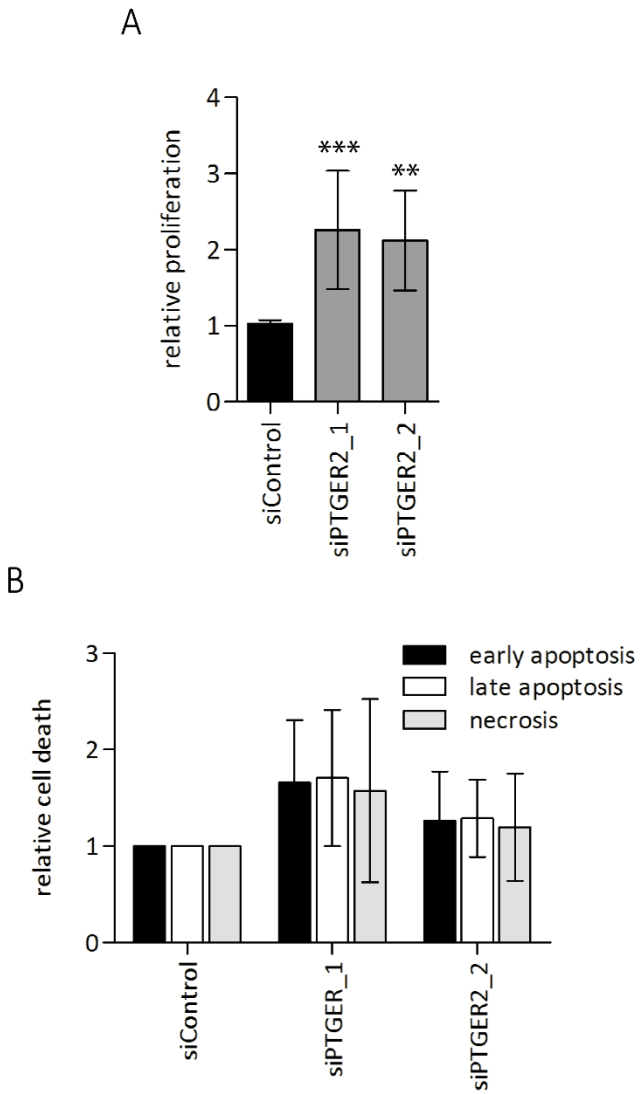

Figure 22: Increased proliferation in *PTGER2* silenced pericytes
(A) Proliferation analysis of mono-cultured *PTGER2* silenced pericytes using xCELLigence system (n=3). (B) Cell death (n=3) analysis of co-cultured *PTGER2* silenced pericytes with EC using Annexin V staining. *p<0.05, **p<0.01, ***p<0.001, n= number of independent experiments.

2.5 Generation of conditional *S1pr3* mice using CRISPR/Cas

To enable the analysis of S1pr3 and Ptger2 in pericytes *in vivo,* mouse models for the conditional deletion of these genes are required. The conditional knockout mouse for *Ptger2* was kindly provided by the lab of Prof. Katrin Andreasson. However, *S1pr3* conditional mice are not available. Therefore, CRISPR/Cas technology was used to generate a conditional mouse line. The strategy was to flank major parts of the coding sequence (exon 2) with LoxP sites (Figure 23). CRISPR/Cas is a new approach in the field of genome engineering for *in vivo* verification of target genes by using clustered regularly interspaced short palindromic repeats (CRISPRs) and CRISPR-associated protein-9 nuclease (Cas9) (Jinek et al., 2012; Mali et al., 2013). Originally, CRISPR systems are bacterial immune mechanisms that adapt and protect them from viral or plasmid nucleic acids (Barrangou et al., 2007; Fineran and Charpentier, 2012; Horvath and Barrangou, 2010; Wiedenheft et al., 2012). The CRISPR II system of *S. pyogenes* was adapted for targeted genome editing (Jinek et al., 2012). It is based on the initiation of a nuclease (Cas9) induced double strand break (DSB) at the gene locus of interest, which can then either be repaired by insertions and deletions (indels) via non-homologous end joining (NHEJ) or lead to specific nucleotide changes by homologous directed repair (HR). Here, the loxP sites should be introduced via HR. To induce site-specific DSBs, two major components have to be introduced into cells: a Cas9 nuclease and a guide RNA (gRNA) that directs the nuclease to the specific DNA sequence by RNA-DNA complementary base pairing. The specific DNA target site has to be directly 5´ next to a protospacer adjacent motif (PAM, 5´-NGG) that is absolutely necessary for target binding (Mali et al., 2013). CRISPR/Cas is described to be more simple and precise than other methods used for DNA editing so far (Cong et al., 2013).

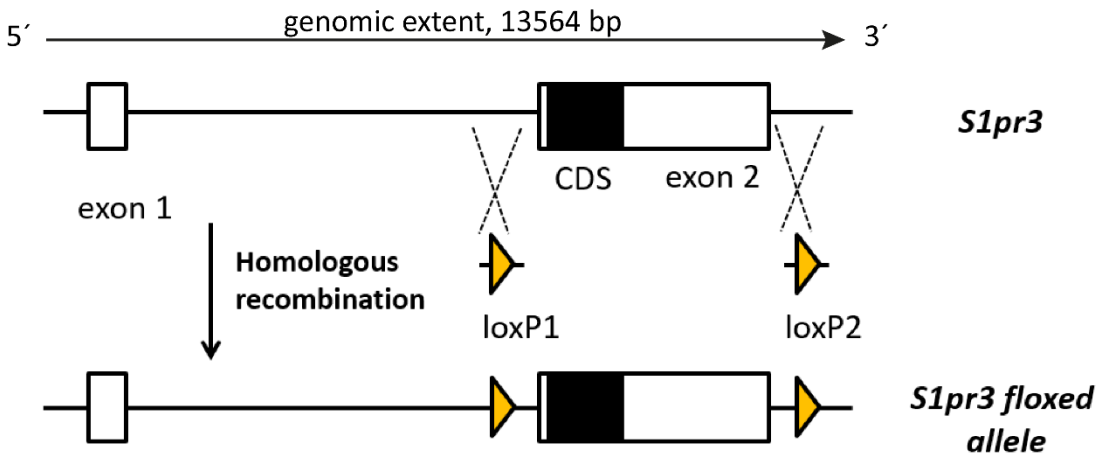

Figure 23: *S1pr3* gene locus with integrated loxP sites
Schematic of the *S1pr3* gene locus before and after loxP site integration. The loxP sites, flanking exon 2, are integrated via homologous recombination using CRISPR/Cas technology. CDS - coding sequence.

2.5.1 Double Nicking enables efficient genome editing *in vitro* and *in vivo*

RNA-guided nucleases are known to induce site specific DSB. However gRNAs can bind DNA loci that show few mismatches, leading to off-target cleavage events (Hsu et al., 2013). Therefore, the double nickase system, favored to reduce off-target effects due to its higher specificity, was used. The nickase (Cas9n) has an aspartate-to-alanine substitution (D10A) and lost the ability to induce DSBs, but instead cuts only one strand of DNA. The concept of the double nickase system is that two specific gRNAs induce two single strand breaks in close proximity resulting in a cleavage of the target site with efficiencies similar to Cas9 wildtype (WT) system (Figure 24A). Simultaneously, off-target effects are reduced (Cong et al., 2013).

To establish the CRISPR/Cas based integration of two LoxP sites *in vitro* and *in vivo,* the bicistronic vector px335 (nickase) and px330 (wildtype) expressing gRNA and Cas9 were amplified. An EGFP locus expressed under a CMV promotor was cloned into px330 and px335 to be able to proof transfection efficiency. To proof the target-specific cleavage and the homologous directed repair *in vitro*, a primary mouse embryonic fibroblast cell line (NIH3T3) was used. For the validation of the cleavage site, the following site-specific mutation was confirmed using the surveyor mutation assay (Figure 24B). First, NIH3T3 cells were transfected with the plasmids, expressing the eGFP reporter, the nuclease Cas9n and gRNAs, designed by the online tool of the Zhang laboratory. The efficiency of transfection was on average 50% (Figure 24C).

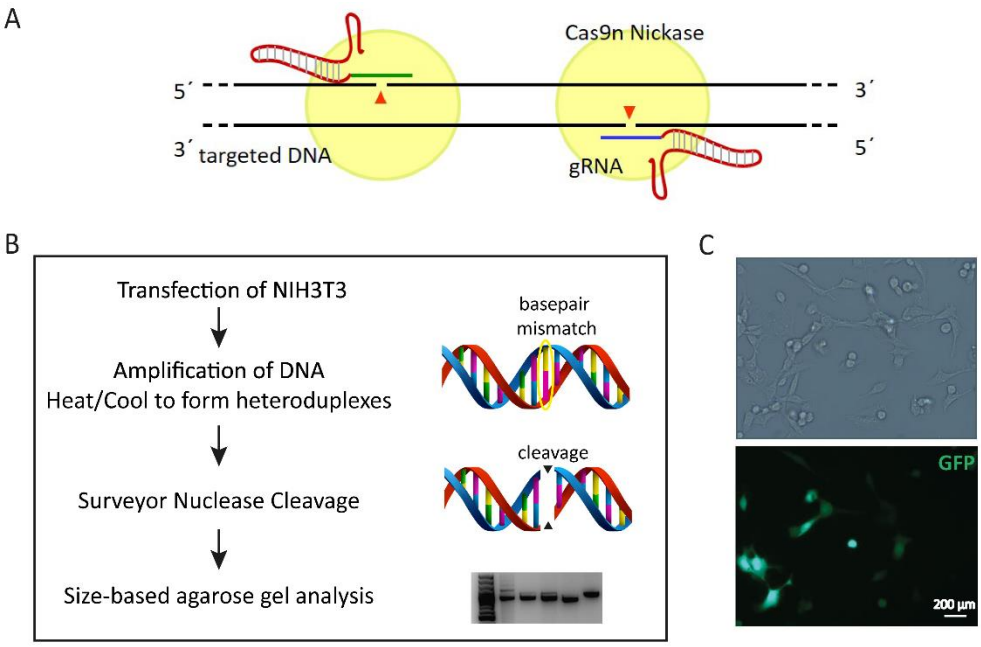

Figure 24: Principle of surveyor mutation assay
(A) Schematic of the CRISPR/Cas mechanism using Cas9n nickase that generates single-stranded cleavage. (B) Schematic protocol for the surveyor mutation assay. NIH3T3 cells were transfected with the CRISPR/Cas plasmid. PCR amplification of the DNA was performed following heating/cooling cycles to generate heteroduplexes (basepair mismatches). The Surveyor Nuclease cuts specifically at basepair mismatches. The fragments were analysed with size-based agarose gels. (C) Representative images of NIH3T3 cells (brightfield, 20x, top; GFP fluorescence, 20x, bottom) transfected with CRISPR/Cas plasmids.

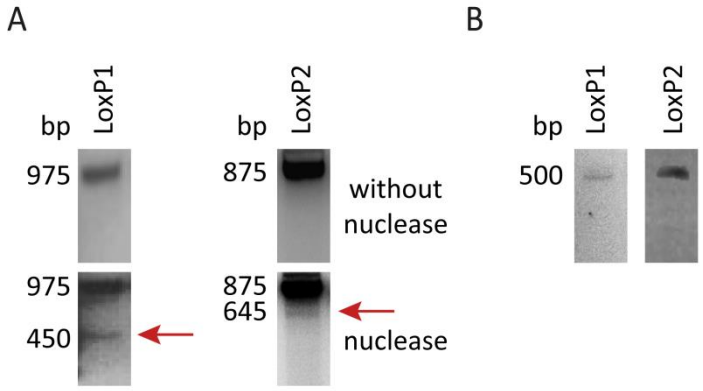

Figure 25: Site-specific cleavage and LoxP site integration *in vitro*
(A) Representative agarose gel images of PCR amplified DNA fragments from NIH3T3 cells treated with CRISPR/Cas plasmids specifically targeting LoxP integration site of LoxP 1 and LoxP 2. DNA products were treated with or without surveyor nuclease. Specific digestion fragments are indicated with a red arrow. (B) Representative agarose gel images of integrated LoxP sites 1 and 2 using a primer binding specifically to the LoxP sequence.

Upon DNA isolation, PCR amplification of the DNA locus of interest was performed following heating and cooling cycles to melt and reassemble the DNA strands. Since not all cells were transfected and the cleavage process did not occur in all transfected cells, hetero-duplexes were build. The specialized nuclease (surveyor nuclease) digests the DNA only on 3´-side of mismatches, revealing different sized DNA fragments, that can be analysed by agarose gel electrophoresis (Figure 22B). Transfection of NIH3T3 cells with the corresponding CRISPR/Cas plasmids for LoxP site 1 (LoxP1) or 2 (LoxP2) resulted in specific digestion fragments (450bp for LoxP1; 645bp for LoxP2) after treatment with surveyor nuclease (Figure 25A, bottom). Agarose gel analysis of untreated DNA showed only one specific PCR amplicon in both cases (Figure 25A, top). This suggests that the chosen gRNAs directed the nuclease to the target sequence.
Homologous recombination of DNA templates (containing the 34 bp LoxP sequence) was validated by transfection of NIH3T3 cells with the CRISPR/Cas plasmids including the corresponding pairs of gRNA and the single stranded DNA template. After DNA isolation of the cells, PCR amplification of the DNA loci LoxP 1 and LoxP 2 were performed using a primer specifically binding to the LoxP sequence. In case of LoxP integration, a PCR amplicon will be detectable. Here, homologous recombination was confirmed with both LoxP sites in NIH3T3 cells (Figure 25B).
After verifying efficient LoxP integration *in vitro*, the efficiency of the double nickase system to target the *S1pr3* locus was analysed *in vivo*. To assess toxicity of the constructs and the efficiency of integration *in vivo* a pilot test was performed (Figure 26A). Accordingly, the DNA template as well as the mRNA of Cas9n and the corresponding gRNAs were injected into the cytosol of zygotes. Within three days, the targeted zygotes developed to morulae under cell culture conditions and PCR analysis of single morula was performed. 75% of zygotes survived the injection and 66% of these zygotes developed to morulae (Figure 26B). In total, one morula was positive for both LoxP sites. Moreover, LoxP 2 integration showed significantly higher efficiency (68%) compared to LoxP 1 integration (4%). This result confirms that double nicking using the designed gRNAs and DNA fragments allows specific genome editing of the S1pr3 locus *in vivo*. To improve the recombination efficiency of LoxP 1, a higher concentration of the LoxP 1 constructs was injected in the new experiment (Figure 26C). Following injection, zygotes were developed to

two cell stage embryos under culture conditions before surgical transfer into pseudo-pregnant recipient mice. The higher concentration (total 350 ng/µl) did not increase the toxicity as seen in the percentage of transferred embryos. Twenty-one F0 pups were born (Figure 26C). As seen before, differences in the efficiencies of LoxP 1 (9.5%) and LoxP 2 (81%) integration were observed. Two pups carried both LoxP sites. However, the F1 generation (F0 crossed with WT mice) were either positive for one or the other LoxP site indicating that the LoxP sites were integrated on different alleles in both mice. Furthermore, sequencing of the *S1pr3* locus often revealed indels and deletions instead of homologous directed integration (data not shown).

A

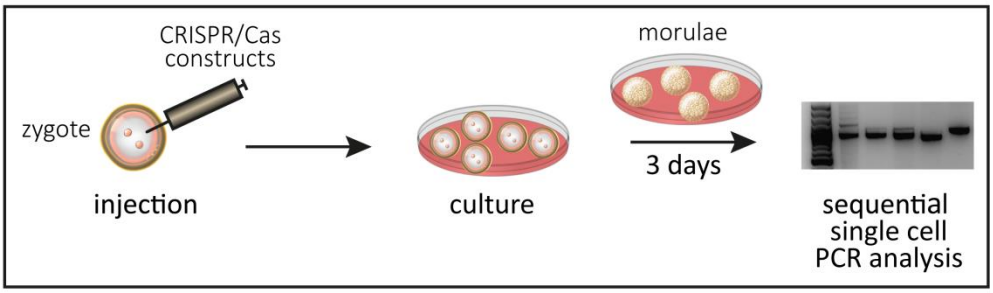

B Pilot Test ´Cas9n´

	No. of injected zygotes	No. of zygotes surviving injection	No. of zygotes developing to morulae	No. of embryos with LoxP site 1 or 2	No. of embryos with both LoxP sites
S1pr3	50 (25/25)	38 (75%)	25 (66%)	LoxP 1 (4%) LoxP 2 (68%)	1 (4% of morulae)

C Experiment ´Cas9n´

	No. of injected zygotes	No. of zygotes survived injection	No. of embryos transferred (% of injected zygotes)	No. of F0 pups born	No. of F0 pups with one flox site	No. of F0 pups with both flox sites	No. of F0 pups with both flox sites on one allele
S1pr3	376	279	269 (72%)	21 (7.8%)	2 (9.5%)/ 17 (81%)	2	0

Figure 26: Determination of the success rate using Cas9n nickase to target the *S1pr3* locus *in vivo*
(A) Schematic protocol for a pilot test of the Cas9n efficiency targeting the *S1pr3* locus *in vivo*. CRISPR/Cas constructs were injected in the cytosol of zygotes. Upon 3 days of culturing morulae developed which were genotyped using sequential single cell PCR analysis. (B) Results of the pilot test using Cas9n to target the *S1pr3* locus. (C) Results of the Cas9n constructs in zygotes that were implanted into foster mothers.

2.5.2 SCR7 reduces efficiency in combination with double nickase

To reduce the probability of indels and promote HR, a new strategy using SCR7 was pursued. DSBs induce DNA repair through NHEJ or HR (Figure 27A). In a normal setting, NHEJ induced indels occur more frequently than HR mediated genome editing, since NHEJ takes place throughout the whole cell cycle, whereas HR is restricted to S- and G2-phase (Deriano and Roth, 2013). SCR7, a DNA ligase IV, was first described as an anti-cancer drug (Ma et al., 2016). Yet, by inhibiting NHEJ SCR7 is described to shift the balance and increase the efficiency of HR (Lin et al., 2016; Ma et al., 2016). Therefore, zygotes were treated with SCR7 after injection of double nickase constructs. Additionally, the concentrations of the constructs were more shifted towards the LoxP 1 site and reduced for the LoxP 2 site. After transfer into mice, eight-teen pups were born (Figure 27B). The discrepancy between LoxP 1 and LoxP 2 efficiency was reduced. Nevertheless, the integration of both LoxP sites in one mouse or on one allele was not successful using the combination of the double nickase and SCR7. Besides, indels were even more detectable compared to the approach using double nickase alone (data not shown).

A

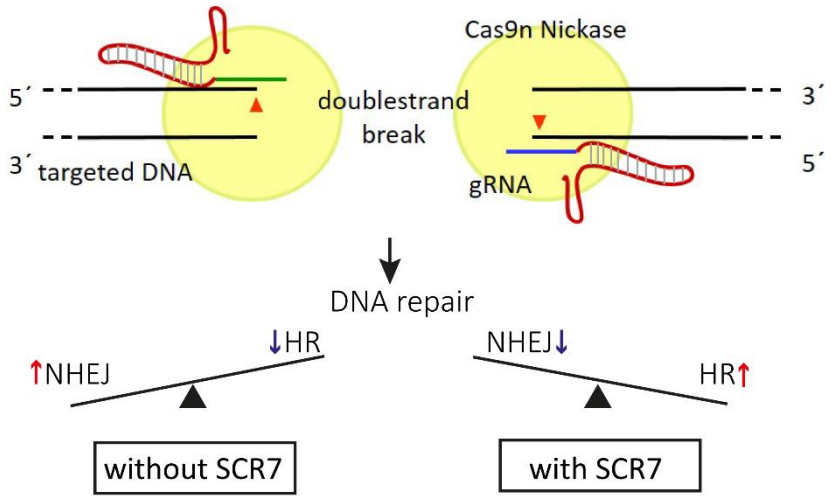

B Experiment ´SCR7´

	No. of injected zygotes	No. of zygotes survived injection	No. of embryos transferred (% of injected zygotes)	No. of F0 pups born	No. of F0 pups with one flox site	No. of F0 pups with both flox sites	No. of F0 pups with both flox sites on one allele
S1pr3	390	N.A.	319 (82%)	18 (6%)	1 (6%)/ 2 (12%)	0	0

Figure 27: Determination of the success rate using Cas9n nickase in combination with SCR7 to target the *S1pr3* locus *in vivo*

(A) Schematic for the principle of SCR7 (Ligase IV inhibitor) on DNA repair. Upon double strand breaks two different DNA repair mechanism (Non-homologous end-joining, NHEJ; Homologous recombination, HR) can occur. In normal conditions (without SCR7) NHEJ prevails, however with the use of SCR7 the balance shifts to homologous recombination due to the blockage of Ligase IV. (B) Results of the Cas9n constructs with SCR7 in zygotes that were implanted into foster mothers.

2.5.3 Wildtype nuclease mediates genome editing with increased efficiency

To increase the efficiency of homologous recombination, the wildtype Cas9 nuclease was used for further *in vivo* studies. The Cas9 nuclease induces a DSB with the help of one single specific gRNA (Figure 26A). Initially, the target-specific cleavage and homologous directed repair of the new constructs (Cas9 and gRNA) were proven *in vitro* (data not shown). *In vivo*, the survival (97%) and the integration efficiency (LoxP 1 and LoxP 2: 26%) were increased compared to the double nickase (Figure 28B). Additionally, the integration of both LoxP sites was similarly effective. In total, 3 morulae showed positive recombination of LoxP 1 and LoxP 2.

To further increase the probability of integrating both LoxP sites on one allele, the integration was performed sequentially (Figure 29A). Briefly, zygotes were injected with Cas9 WT constructs for LoxP 1 insertion. Afterwards male mice, homozygous or heterozygous for LoxP 1, were bred with C57BL/6N female mice to generate zygotes. Subsequently, these LoxP 1 positive zygotes were injected with LoxP 2 constructs. In total, 34% of the born pups were positive for LoxP 1 (Figure 29B), of which four homozygous and two heterozgyous male mice were used for the generation of LoxP 1 positive zygotes (data not shown). The integration efficiency of LoxP 2 was less compared to the pilot test (Figure 29B). Albeit, seven mice were identified with both LoxP sites.

A

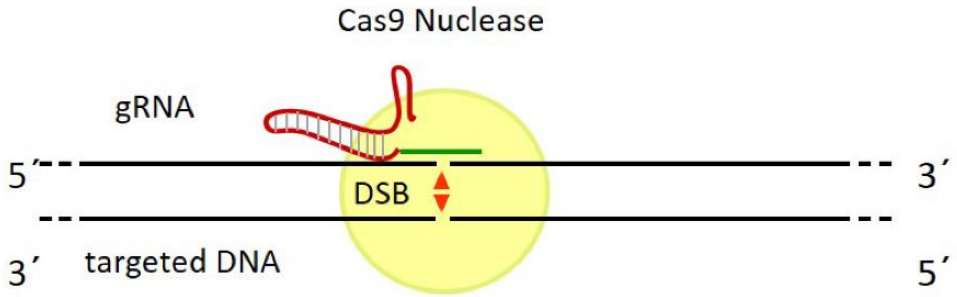

B Pilot Test ´Cas9 WT´

	No. of injected zygotes	No. of zygotes surviving injection	No. of zygotes developing to morulae	No. of embryos with LoxP site 1 or 2	No. of embryos with both LoxP sites
S1pr3	38	37 (97%)	35 (95%)	LoxP 1 (9, 26%) LoxP 2 (9, 26%)	3 (8% of morulae)

Figure 28: Determination of the success rate using Cas9 WT to target the *S1pr3* locus *in vivo*
(A) Schematic of the CRISPR/Cas mechanism using Cas9 WT. The Cas9 WT enzyme generates double strand breaks upon specific binding of one gRNA to the DNA region of interest. (B) Results of the pilot test using Cas9 WT to target the *S1pr3* locus.

A

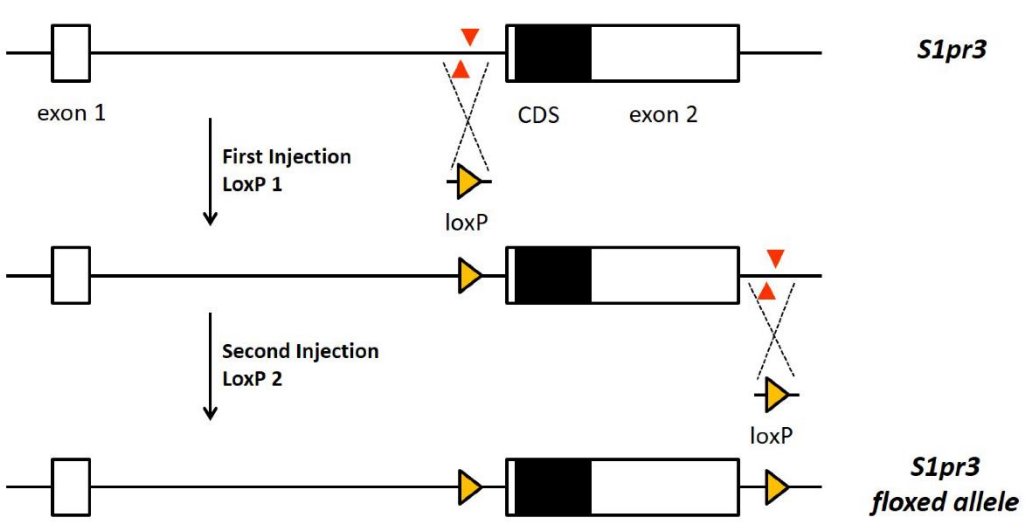

B Experiment ´Cas9 WT sequential´

	No. of injected zygotes	No. of zygotes survived injection	No. of embryos transferred (% of injected zygotes)	No. of F0 pups born	No. of F0 pups with one flox site	No. of F0 pups with both flox sites	No. of F0 pups with both flox sites on one allele
LoxP 1	327	N.A.	283 (87%)	61 (21%)	21 (34%)	--	--
LoxP 2	413	N.A.	339 (82%)	83 (24%)	9 (11%)	7 (78%)	2 (29%)

Figure 29: Sequential integration workflow of LoxP sites into the *S1pr3* gene locus
(A) Schematic protocol of sequential integration of the 2 LoxP sites in the *S1pr3* gene locus. LoxP 1 was solely integrated with the first CRISPR/Cas construct injection. LoxP 1 positive male F0 mice were used to breed LoxP 1 positive zygotes. These zygotes were injected with CRISPR/Cas constructs for LoxP 2. (B) Results of the sequential injection of LoxP 1 and 2 using Cas9 WT enzyme targeting the S*1pr3* locus.

To confirm the presence of both LoxP sites on the same allele and the germline transmission of the floxed allele, breedings with the corresponding floxed mice and WT mice was initiated. Genotyping of the F1 generation (LoxP 1: 185 bp [wt]/219 bp [floxed], LoxP 2: 186 bp [wt]/ 220 bp [floxed]) revealed litters of two floxed mice carrying the floxed allele (Figure 27B and 28B). Sanger sequencing of the floxed allele verified the integration of intact LoxP sites (Figure 30A). In summary, conditional mice for *S1pr3* were successfully generated by applying the CRISPR/Cas technology.

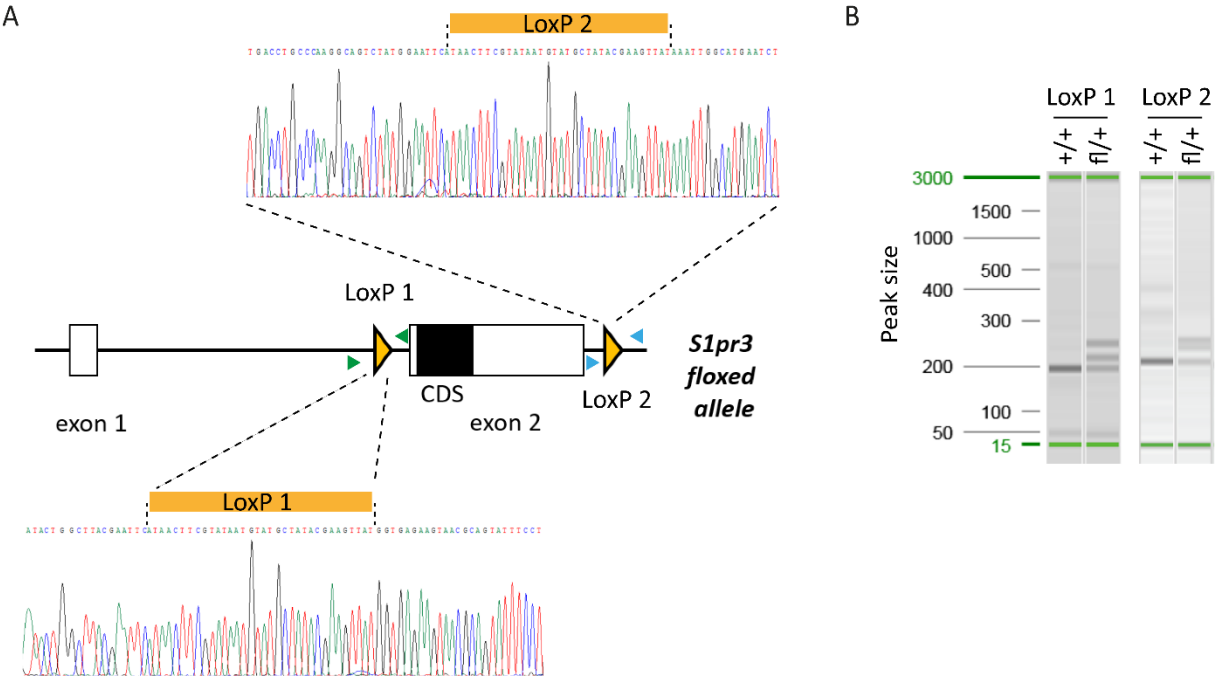

Figure 30: Germline transmission of the *S1pr3* conditional allele
(A) Schematic of the *S1pr3* gene locus with two integrated LoxP sites. Relative positions of the genotyping primers for LoxP 1 (green triangles) and LoxP 2 (blue triangles) are indicated. Representative DNA sequences of the 2 PCR amplicons spanning the targeted locus confirmed the presence of two intact LoxP sites. (B) PCR products amplified from the two genotyping primer sets for LoxP 1 and LoxP 2. The smallest band represents the wildtype allele (+/+) and the middle band represents the floxed allele (fl/+). The third band is unspecific. CDS, coding sequence.

3 Discussion

Many different markers have been described to identify and characterize pericytes. However, none of these markers is exclusively pericyte-specific (Armulik et al., 2011). Based on the results of a systematic expression profiling screen of cultured pericytes isolated from different organs and other mesenchymal cells (Figure 6), the present study was aimed at identifying pericyte-specific transcripts in the mesenchymal lineage and their contribution to vascular function in general and in pericytes specifically. Employing a combination of cellular and biochemical experiments, the study demonstrates that i) *S1PR3* and *PTGER2* are pericyte-specific transcripts in the mesenchymal lineage in mouse and human in the vascular niche; ii) S1PR3 signals via divers signaling pathways ($G\alpha_i$, $G\alpha_q$ and presumably $G\alpha_{12/13}$) in pericytes; iii) pericyte-specific deletion of *S1PR3* in pericytes co-cultured with EC results in transcriptional regulation of cell junction and cell-ECM interaction genes; iv) pericyte migration and cell size as well as signaling pathways of the actin-myosin skeleton are regulated by S1PR3 signaling in pericytes (Figure 31); v) pericyte-specific deletion of *PTGER2 in vitro* increases proliferation by transcriptional down-regulation of proliferation inhibitors; vi) CRISPR/Cas technology can be applied to generate *S1pr3* conditional knockout mice by using Cas9 WT in a sequential approach.

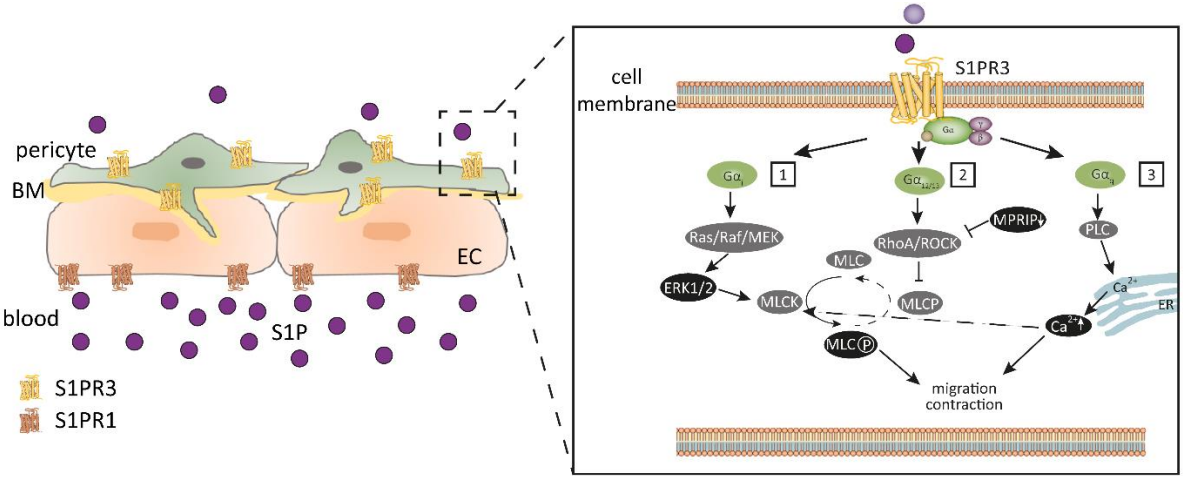

Figure 31: S1PR3 signaling in pericytes
Schematic illustration of the proposed S1P/S1PR3 signaling in pericytes. EC predominantly express S1PR1, whereas pericytes express S1PR3. Under physiological conditions the maintenance of a S1P gradient from blood to tissue is important for vascular function (blood>tissue). S1PR1 signaling in EC sustains vessel integrity. In contrast, S1PR3 signaling is low under physiological conditions due to low S1P concentration in the tissue. However, if S1P is binding to S1PR3 it can signal via different pathways: 1) S1PR3 can signal via $G\alpha_i$ leading to phosphorylation of ERK1/2 via Ras/Raf/MEK pathway. ERK1/2 is known to positively regulate myosin light chain kinase (MLCK) resulting in phosphorylation of myosin light chain (MLC). 2) S1PR3 signals via $G\alpha_{12/13}$ through RhoA and ROCK resulting in the inhibiton of myosin light chain phosphatase (MLCP). Furthermore, upon expression of S1PR3, myosin phosphatase Rho-interacting protein (MPRIP) is downregulated. This results in more RhoA activity, less MLCP activity and increased MLC phosphorylation. 3) S1PR3 signals via $G\alpha_q$ by the induction of calcium release from the endoplasmatic reticulum (ER). All three pathways result in migration/contraction of pericytes. Genes marked in grey indicate literature evidence, whereas genes marked in black were investigated in this study. Basement membrane, BM.

3.1 Challenges of the identification of pericytes

Pericytes have gained increasing attention as functionally significant contributors in physiological and pathological angiogenesis (Bergers and Song, 2005). Although the current definition of a mature pericyte as an embedded cell in the BM is accepted, the identification of pericytes and the phenotypic discrimination from other mural and/or mesenchymal cells are still challenging (Armulik et al., 2011; Bergers and Song, 2005). Mural cells are described to be a continuum of phenotypes reaching from SMC on large caliber vessels to pericytes ensheathing capillaries (Armulik et al., 2011). The term continuum stresses the complexity in discriminating ontogenetic related SMC and pericytes, but also the difficulties in distinguishing pericytes with a great mesenchymal potential from other cells of mesenchymal origin (Bergers and Song, 2005; Crisan et al., 2008a). This is highly dependent on the unavailability of an uniquely expressed marker for pericytes (Armulik et al., 2011). This study identified pericyte-specific transcripts in mesenchymal lineages. Human primary pericytes from different organs were used for a microarray expression analysis. The different pericytes were purchased from companies (BP and PlaP) or obtained from the laboratory of Dr. Bruno Peault (MP, PancP, LP). Even though the isolation protocols of the pericytes vary, the purity of cells was checked by pericyte marker expression (Crisan et al., 2008b, 2008c). Additionally, pericytes show typical morphological features (elongated cell shape and long cell processes) of mesenchymal cells. However, each cell type used for the microarray differed in morphology. Interestingly, pericytes possess tissue-specific cell morphology (Figure 4). This might reflect the organ-/tissue-dependent diversity in pericyte functions (Bergers and Song, 2005). Indeed, clustering of the microarray data revealed organ-specific expression profiles in pericytes, except for PancP (Figure 5). The expression of established pericyte markers is strongly dependent on several criteria including species, vessel type, organ, pathological or activation state of the vessel (Armulik et al., 2011; Bergers and Song, 2005). This is in line with the observed divers pericyte marker expressions in the microarray analysis. Whereas LP, PancP and BP predominantly expressed NG2 (*CSPG4*), MP and PlaP primarily expressed Endosialin (Figure 5).

Even though, pericytes and EC may originate of a common progenitor cell (Yamashita et al., 2000), EC do not express typical pericyte markers (Figure 5). Given the fact that established pericyte markers are known to be expressed in other cells of mesenchymal origin, it was not suprising that also fibroblasts, adipocytes and MSC expressed these markers (Figure 5). In fact, pericytes act as perivascular stem cell niche and can transdifferentiate into osteocytes, chondrocytes and adipocytes (Crisan et al., 2008a; da Silva Meirelles et al., 2008). Close ontogenic relationship is also given between pericytes and SMC/fibroblast, since their progenitor cells (mesothelial cells) undergo EndMT and can transdifferentiate into these three cell entities (Hall, 2006). Although the fibroblasts of two different companies express some pericyte markers (*PDGFRβ, ACTA2, CD248*), they are also positive for the fibroblast-specific transcript S100A4 in contrast to pericytes (Figure 4). As the microarray-based expression analysis was performed with strict parameters to identify only transcripts expressed by pericytes, established pericyte markers (Table 1) did not appear in the pericyte-specific transcript list (Figure 6).

As SMC have not been included in the expression analysis, expression levels of *S1PR3* and *PTGER2* were validated in biological replicates of SMC (Figure 7B). *PTGER2* expression was not detectable in SMC. However, SMC expressed *S1PR3* at comparable expression levels as pericytes, which was consistent with published studies describing S1PR3 in SMC (Mousseau et al., 2012a, 2012b; Ryu et al., 2002; Wamhoff et al., 2008). The classical concept of mural cells differentiates SMC and pericytes. Instead, emerging evidence indicates a range of intermediate mural cell phenotypes between the prototypical SMC and pericytes (Armulik et al., 2011; Díaz-Flores et al., 2009). Based on their close relationship, the proper phenotype of the cells used for the microarray can not be stated. Marker expression (S1PR3 and PTGER2) along the vascular bed needs to be analysed *in vivo*. However, this is limited by the unavailability of S1PR3- and PTGER2-specific antibodies.

In vivo, the expression of *S1pr3* and *Ptger2* was high in an isolated mural cell enriched population compared to the endothelial compartment (Figure 9). The mural cell-enriched population was isolated by a negative selection approach due to the unavailability of working FACS antibodies against established pericyte markers (NG2, PDGFRβ). Leukocytes, erythrocytes, lymphatic endothelial cells alveolar epithelial cells and FxCycle positive cells (dead cells) were excluded from the mouse lung cell suspension. The remaining cell population was sorted according to CD31 expression in CD31 positive (EC) and CD31 negative cells (mural cell enriched) (Figure 8). Pericyte- and EC-specific gene expression analysis confirmed adequate purity of the populations. *Pdgfrα*, known as pan-fibroblast marker (Driskell et al., 2013), was higher expressed in the mural cell enriched population, indicating the presence of fibroblasts in this population. However, *Pdgfrα* is known to be expressed in a subpopulation of pericytes in the lung (Hung et al., 2013). Furthermore, this study demonstrated that fibroblasts do not express *S1PR3* and *PTGER2* (Figure 6 and 7). Nevertheless, expression analysis in this population for pericyte markers showed strong enrichment compared to the EC compartment (Figure 9).

Hence, this study identified *S1PR3* as mural cell-specific and *PTGER2* as pericyte-specific transcript in human and mouse within the mesenchymal lineage.

3.2 Human and mouse pericytes express functional S1PR3

In this study, the significantly higher expression of *S1PR3* in human pericytes of different tissues in comparison to other mesenchymal cells was discovered by microarray-based gene expression profiling and was confirmed on RNA level. This is in line with recently published publications, showing that S1PR3 is enriched in Pdgfrβ-/Ng2-positive brain pericytes (He et al., 2016) and that hepatic stellate cells, the pericytes of the liver, express *S1PR3* (Liu et al., 2011). However, S1PR3 expression was also detectable in SMC (Figure 7B). In accordance with that, few publications described the expression of a functional S1PR3 in SMC (Mousseau et al., 2012a, 2012b; Ryu et al., 2002; Wamhoff et al., 2008). These data reflect the heterogeneity of mural cells and the difficulties to distinguish pericytes from SMC depending on the markers used in each study (as discussed above). Some studies suggest S1PR3 expression in endothelial cells (van Hooren et al., 2014; Nussbaum et al., 2015; Waeber et al., 2004). In this and another recent study by He *et al.* (He et al., 2016), *S1PR3* expression in EC was barely detectable compared to pericytes and the

expression seemed to be dependent on culture conditions (HUVEC, see Figure 7A and B). Furthermore, *S1PR3* expression is known to be upregulated under pro-inflammatory conditions (Fischer et al., 2011a), which could explain the *S1PR3* expression in endothelial cells *in vivo* in inflammation models (Nussbaum et al., 2015). The availability of exclusively global *S1PR3* knockout mice stresses the difficulty to state which *S1PR3* expressing cells are causing angiogenic phenotypes (Kono et al., 2004). Our understanding of S1PR3 protein expression levels, though, is challenged by the fact that S1PR3 and S1PR1 are highly homolog and there is no commercially available antibody detecting specifically S1PR3. Therefore, investigators have to rely heavily on mRNA expression profiles, even though expression studies were done on protein levels showing S1PR3 expression on benign and malignant human tissues (Wang et al., 2014).

The results of the present study show for the first time that indeed S1PR3 signals via $G\alpha_i$ and $G\alpha_q$ (Figure 10 and 13) in pericytes (An et al., 1998, 1999; Ancellin and Hla, 1999). Analysis of downstream signaling of RhoA ($G\alpha_{12/13}$) revealed reduced phosphorylation of MLC2 upon S1PR3 inhibition (Figure 12). However, MLC phosphorylation is not only described to be regulated by RhoA, but also by ERK and calcium (Amano et al., 2010; CHENG et al., 2015; Hong and Grabel, 2006; Turner et al., 1999), illustrating the complexity of MLC phosphorylation regulation (Figure 31). Accordingly, further investigations of the regulation of MLC phosphorylation and the involvement of RhoA ($G\alpha_{12/13}$) are required by using MEK, ROCK and/or PLC inhibitors. Nevertheless, literature suggests that there is a complex and dynamic interplay of signaling pathways in the regulation of myosin phosphorylation (Cheng et al., 2015; Kaneko-Kawano et al., 2012). In summary, S1PR3 interferes with the signaling that regulates the actin-myosin skeleton.

In accordance with this, S1PR3 has a functional role in pericytes. Pericytes, silenced for *S1PR3*, show less migratory capacity and increased cell size (Figure 19 and 20). These results are in line with the pro-migratory effect seen in S1PR3 expressing hepatic stellate cells (Liu et al., 2011) and SMC (Mousseau et al., 2012a, 2012b; Ryu et al., 2002; Shimizu et al., 2012) via ERK1/2 and MAPK activation upon S1P stimulation. Furthermore, PDGFB/PDGFRβ and S1P/S1PR3 signaling act synergistically on SMC migration (Mousseau et al., 2012b). Apart from that, microarray-based gene expression profiling of *S1PR3* silenced pericytes, co-cultured with EC, revealed differentially regulated genes overlapping with gene sets involved in cell junction organization, cell-ECM interaction, cell-cell communications and mTORC1 signaling. Similarly, S1P induced migration involves mTOR and ERK signaling in SMC (Tanski et al., 2005). Additionally, S1PR3 dependent regulation of MPRIP and subsequent dephosporylation of MLC (Durham et al., 2014) identified in pericytes (Figure 12, 18 and 31) point to the molecular mechanism by which S1PR3 regulates migration. SDC1 is a heparin sulfate proteoglycan and is part of the glycocalyx. It binds various components of the ECM and is an important regulator of cell-cell and cell-ECM interactions (Zeng, 2017). A relation between EC-expressed S1PR1 and syndecan 1 on protecting the glycocalyx was described (Zeng, 2017; Zeng et al., 2014). However, the relationship between pericyte-expressed SDC1 and S1PR signaling is not explored. Still, the downregulation of SDC1 upon *S1PR3* silencing in pericytes suggests an impairment of growth factor binding or ECM binding that is necessary for pericyte migration.

S1PR1 is the major S1P receptor in EC and signals upon S1P binding that is delivered by the blood in micromolar concentrations (Gaengel et al., 2012). The activation of S1PR1 leads to the inhibition of angiogenic sprouting and stabilization of endothelial VE-cadherin at the endothelial junctions. In short, S1PR1 signaling on EC maintains blood vessel integrity by protecting blood vessels against abnormal angiogenic signals (Gaengel et al., 2012; Xiong and Hla, 2014). EC serve as the gatekeeper between the circulation and the tissue by maintaining the S1P gradient. Through synthesis and export of S1P into the blood, EC control high S1P concentrations in circulating fluids. Whereas by controlling the intracellular crossing of S1P, EC sustain the low concentration on the abluminal side (Olivera et al., 2013). In a physiological scenario, pericytes that are located on the abluminal side, are exposed to a low S1P concentration suggesting minor S1PR3 signaling in pericytes. This is in line with the less migratory phenotype in pericytes upon *S1PR3* silencing described in this study (Figure 19). Concurrently, S1PR1 signaling on EC maintains vessel integrity (Gaengel et al., 2012). Under certain pathophysiological conditions (inflammation and cancer), an increase of the S1P concentration in the tissue may occur (Olivera et al., 2013). In context of cancer and allergic inflammation, mast cells are considered to be stimulated and alter S1P homeostasis (Olivera, 2008; Olivera and Rivera, 2011). Furthermore, cancer and stromal cells can turn on S1P production while diminishing the degradation of S1P (Bandhuvula and Saba, 2007; Colié et al., 2009; Takabe et al., 2010). This alteration in the S1P concentration in the tissue may activate S1PR3 signaling on pericytes and lead to a pro-migratory phenotype and partial disruption of vessel integrity. However, this hypothesis needs to be proven *in vivo* experiments in *S1PR3* conditional knockout mice using inflammatory or cancer models.

In summary, this study identifies S1PR3 as novel mural cell marker and shows for the first time the functional role of S1PR3 in pericytes influencing the actin-myosin skeleton. Yet, the interplay of S1P signaling in EC and pericytes needs further investigation by the use of pericyte-specific deletion of *S1pr3* in mice.

3.3 Pericyte-specific expression of PTGER2

Specific *PTGER2* expression in human pericytes from different organs was for the first time discovered in this study (Figure 6). The expression of *PTGER2* was exclusively observed in pericytes and almost absent in other mesenchymal cells in the vascular niche, analysed by a microarray based transcriptomic profiling and validated on RNA level (Figure 7). Only few publications indicate the expression of PTGER2 in mesangial cells, the specialized pericytes in the kidneys (Jaffer et al., 1995; Kennedy-Lydon et al., 2013). Jaffer *et al.* suggest an effect of PGE2 on mesangial migration, most probably via EP2 (*PTGER2*) (Jaffer et al., 1995). In contrast, *PTGER2* silenced BP did not show any difference in migration in this study (data not shown). This suggests an organ-specific influence of PGE2/EP2 signaling on the migration of pericytes. Interestingly, *PTGER2* was not expressed in SMC (Figure 7). Yet, Yau *et al.* describe EP2 (*PTGER2*) expression (protein) and functional contribution in SMC (Yau and Zahradka, 2003). In contrast, EP2 is absent on SMC of the small intestine (Dey et al., 2006). Even though EP2 protein expression has been published (Aoki et al., 2011; Yau and Zahradka, 2003), not a single commercially available

antibody has been validated to specifically bind EP2. The functional role of EP2 on SMC proliferation is in line with the proliferation phenotype seen in pericytes (Figure 22) (Yau and Zahradka, 2003). However, the effects in SMC seem to be dependent on the status (quiescent or proliferative) of the cells (Yau and Zahradka, 2003).

PGE2 is a factor with a short half-time and therefore typically functions in an autocrine way or on cells in close proximity (paracrine) (Funk, 2001). Few publications indicate that pericyte express PGE2 suggesting an autocrine signaling of PGE2 and EP2 on pericytes (Giurdanella et al., 2015; Jaffer et al., 1995). In addition, EC express PGE2 (Hsu et al., 1993; Milne et al., 2001). Their close anatomical relationship may suggest that EC are a source of PGE2 that can act in a paracrine manner on pericytes via the EP2 receptor.

The PGE2/EP2 axis regulates angiogenesis. However, which mechanism or cells are the major contributor is still not fully explored. Some studies claim that EP2 expression on EC effects EC motility and survival (Kamiyama et al., 2006; Sakurai et al., 2011). This is contrast to this study, showing exclusive expression of *PTGER2* in pericytes, whereas EC are devoid of *PTGER2* (Figure 7). The majority of publications discussing EP2 and angiogenesis are in the context of tumor angiogenesis. It is known that the tumor microenvironment including tumor endothelial cells show morphological, epigenetic and gene expression changes compared to their healthy counterparts (Dudley, 2012). However, this study exclusively investigated the role of EP2 in the physiological setting. Global deletion of EP2 decreases the number of intestinal polyps in $Apc^{\Delta 716}$ mice with reduced tumor vascular density (Seno et al., 2002; Sonoshita et al., 2001). Mostly, PGE2/EP2 is said to act on tumor cells resulting in release of VEGF and induction of angiogenesis (Eibl et al., 2003; Jain et al., 2008; Seno et al., 2002; Wang and Klein, 2007; Xiong et al., 2005). Albeit, these studies are all performed in global EP2 knockout mice or by using EP2 inhibitors. To investigate the role of different EP2 expressing cells on (tumor) angiogenesis, cell-specific EP2 deletion needs to be performed *in vivo*.

PGE2 is a main mediator in inflammation and regulates cytokine expression of immune cells via EP2 (Jing et al., 2003; Johansson et al., 2013; Ricciotti and FitzGerald, 2011). Pericytes are described to contribute to the immunological defense of the vaculature by secreting chemokines, expressing adhesion molecules and attracting immune cells (Navarro et al., 2016; Pieper et al., 2013; Stark et al., 2013). Whether PGE2/EP2 signaling in pericyte plays a role in inflammatory processes needs to be further elucidated.

Overall, this study identifies *PTGER2* as a specifically expressed transcript of pericytes in the mesenchymal niche with a contribution to pericyte function. However, further investigations concerning potential influence of pericyte-expressed *PTGER2* on angiogenesis and inflammation needs to be performed *in vivo*.

3.4 Challenges of CRISPR/Cas technology

In this study, the generation of *S1pr3* floxed mice was performed using the newly emerging technique CRISPR/Cas. Different approaches were used to establish an efficient system to specifically introduce two LoxP sites into the DNA. Genome engineering refers to techniques that introduce targeted and permanent modifications into the genome. Until recently, gene targeting in mouse embryonic stem (ES) cells by plasmid-based homologous recombination was the gold standard for investigating gene functions and was 2007 awarded by the Nobel Prize in Physiology and Medicine (Capecchi, 1989). This method was a breakthrough since former techniques created transgenic mice based on the random incorporation of DNA via DNA injection into fertilized eggs. However, targeted gene editing by ES cells is impeded by several factors including low efficacy targeting rate, effortful screening and culturing of ES cells, chimeric mouse production and subsequent breeding to acquire germline transmission of the genetic modification (Capecchi, 2001, 2005; Sato et al., 2016).

In the past decade, genome editing using programmable sequence-specific DNA binding nucleases emerged. The nucleases induce DSBs and stimulate DNA repair mechanism (NHEJ and HR) by which the gene is disrupted or gene modifications can be introduced. These site-specific nucleases comprising of zink-finger nucleases (ZFNs), transcriptions activator-like effector nucleases (TALENs) and Clustered Regularly Interspaced Short Palindromic Repeats/CRISPR-associated protein-9 nuclease (CRISPR/Cas), are powerful tools to induce site-specific modifications (Gaj et al., 2013). CRISPR/Cas is the most recently established technique and was used in this study, since it demonstrates advantages in comparison to ZFNs and TALENs (Falahi et al., 2015; Jinek et al., 2012). ZFNs exert more off-target effects (non-specific DNA modifications) and TALENs are highly sensitive to methylation of the targeted DNA and their design is complex and time consuming (Falahi et al., 2015; Valton et al., 2012). Based on publications, describing off-target effects by the Cas9 nuclease, the first approach was performed with the Cas9n nickase (Figure 24 and 26). The specificity of CRISPR/Cas is determined by the sequence of the gRNA (guide RNA). However, mismatches (up to 5) in the gRNA can retain the cleavage activity dependent on the mismatch positions in the gRNA, and result in off-target effects in the genome (Cho et al., 2014; Cong et al., 2013; Fu et al., 2013; Hsu et al., 2013). Intriguingly, the usage of Cas9n and corresponding gRNAs avoids off-target mutations through the higher specificity (Cho et al., 2014; Shen et al., 2014) and sustains efficiency (Cho et al., 2014; Shen et al., 2014). This study shows that Cas9n was able to introduce two LoxP sites flanking exon 2 of *S1pr3*. However, the recombination efficacy strongly depends on the gene locus (Figure 26B and C), as published before (Miyaoka et al., 2016). An increase of the concentration (25 to 50 ng/µl) of the LoxP 1 constructs did not substantially improve the recombination efficiency of the LoxP 1 site. The low recombination efficiency of the LoxP 1 may explain that only few mice with both LoxP sites, but not located on the same allele, were generated. However, changes in the concentrations of injected CRISPR/Cas constructs (see Table 44) balanced the recombination efficiency of LoxP 1 and LoxP 2. In publications, the concentrations of injected CRISPR/Cas constructs vary from 50 ng/µl to 250 ng/µl in total (Lee and Lloyd, 2014; Wang et al., 2013). However, in general even the highest concentrations are

suggested to be low toxic when injected into the cytoplasm of the zygote (Wang et al., 2013). In this study, the maximal total injected concentration of 350 ng/µl into the cytoplasm of the zygote did not show higher toxicity but did also not result in increased efficacy (Figure 26C).

Recombination efficiency can be improved up to 19-fold by the Ligase IV inhibitor SCR7 via blockage of the NHEJ pathway (Figure 27A) (Lin et al., 2016). In this study, SCR7 treatment did not increase recombination efficiency (Figure 27B). In the majority of publications, SCR7 was co-injected with the CRISPR/Cas constructs into the zygotes. In this study, zygotes were incubated with SCR7, before and after injection. This procedure was described in the context of NHEJ inhibitor treatment of cells (Maruyama et al., 2015) and was well established in the transgenic service (DKFZ) for genome editing experiments with the Cas9 WT. Moreover, publications stating the increase of genome editing upon SCR7 treatment, are all performed with Cas9 WT (Chu et al., 2015; Maruyama et al., 2015; Singh et al., 2015). This suggests that the combination of SCR7 and Cas9n are not as efficient as with Cas9 WT.

Insertion of two LoxP sites flanking *S1pr3* using Cas9 WT (Figure 26A) with published concentrations (Wang et al., 2013) revealed a high survival rate of the injected zygotes and high and equal efficiencies of both LoxP sites (Figure 26B). This implies that the region of the LoxP 1 was not as accessible as the LoxP 2, since in case of Cas9n transfection the recombination of LoxP 1 was less efficient. Here, two nucleases have to bind in close proximity and in a narrow time frame to induce the DSB. As discussed above, the Cas9 WT harbors the risk of off-target effects. To minimize this risk, designed gRNAs with the highest quality scores were chosen. The quality score considers target specificity and possible off-target matches, meaning the higher the quality score, the fewer off-target matches in the genome. Additionally, intergenic off-targets may be considered as acceptable, since off-targets on different chromosomes will not necessarily be co-segregated with the floxed allele, when transgenic mice are back-crossed. However, whole genome sequencing will be necessary to fully exclude unspecific alterations in the genome.

In both Cas9n approaches (Figure 26 and 27) the insertion of both LoxP sites on the same allele was not successful due to low efficiency of one LoxP site. In addition to the usage of Cas9 WT, a sequential approach (Figure 29A) was established to increase the probability of the insertion of both LoxP sites on one allele. This approach also prevented the origin of deletions arising from the simultaneous cleavage up- and downstream of exon 2. Whereas LoxP 1 was integrated with a similar efficiency (Figure 29B) as in the pilot experiment (Figure 28B), recombination of LoxP 2 was less efficient (Figure 29B). Subsequent analysis of the genome of the born mice revealed integration of both LoxP sites on one allele and germline transmission was confirmed in the F1 generation (Figure 30).

CRISPR/Cas is currently described to be the simplest, most precise and versatile method of genome editing. However, the homologous recombination of LoxP sites is highly gene locus and nuclease (Cas9 or Cas9n) dependent and can therefore lead to a time-consuming establishment of the best and efficient conditions. Yet, the sequential LoxP integration strategy turned out to be a suitable approach for the generation of a conditional *S1pr3* knockout mouse. The availability of

this new mouse line will help to answer pivotal questions about the role of S1PR3 in pericyte biology. For instance, crossing to Ng2-Cre reporter mouse line will enable the cell-specific manipulation of *S1pr3 in vivo*.

4 Materials and Methods

4.1 Materials

4.1.1 Chemicals

Chemicals were purchased from the following companies:

Table 2 Chemicals

Company
AppliChem (www.applichem.com)
Carl Roth (www.carl-roth.de)
Gerbu (www.gerbu.de)
Merck (www.merk.de)
Roche (www.roche-applied-science.com)
Sigma-Aldrich (www.sigmaaldrich.com)

4.1.2 Vectors

The vectors px330 and px335 were purchased from Addgene (Figure 31). The EGFP vector CVU55762 that was used for cloning of px335+EGFP (Figure 32) was kindly provided by Dr. Soniya Savant.

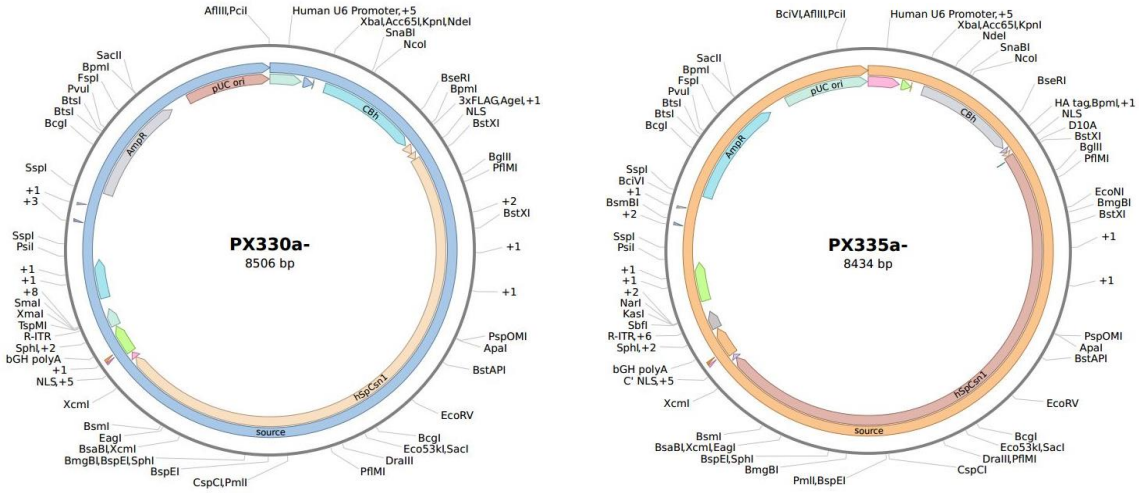

Figure 32: Vectormaps of the gRNA and Cas9 WT (px330) or Cas9n (px335) expressing plasmids
Vector maps were generated with the software Benchling (www.benchling.com).

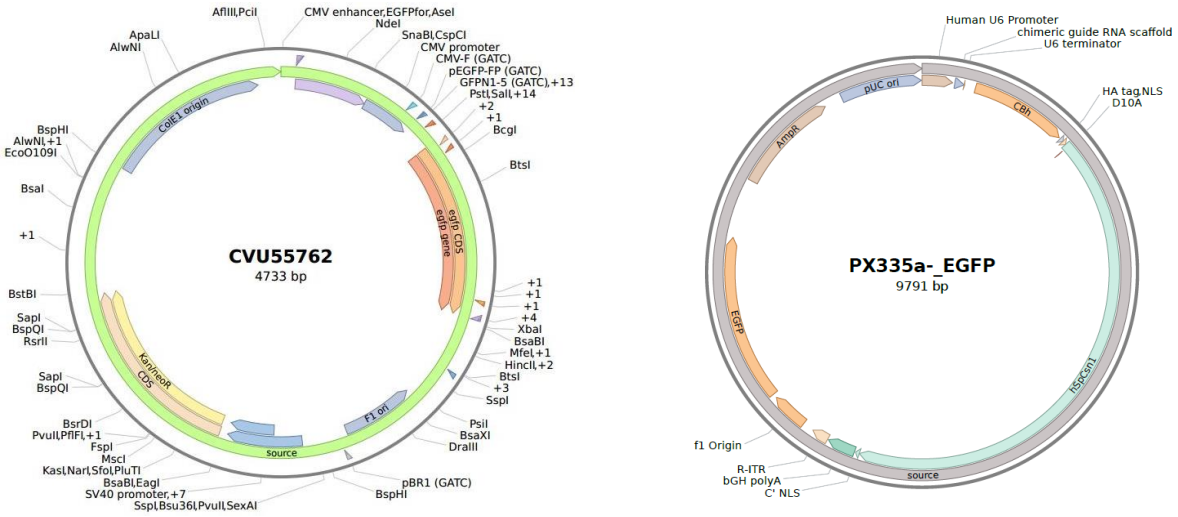

Figure 33: Vector maps of the EGFP vextor CVU55762 and px335+EGFP
Vector maps were generated with the software Benchling (www.benchling.com).

4.1.3 Primers and Oligonucleotides

All primers were purchased from MWG Biotech and Sigma Aldrich.

Table 3 Cloning Primers

Target	Primer name	Sequence (5'-3')
CVU55762	Px335_EGFP_for	GGGCTATTCTTTTGATTTAATGGAGTTCCGCGTTACATAA
CVU55762	Px335_EGFP_rev	ATCGGCAAAATCCCTTAGTCGCGGCCGCTTTACTT

Table 4 Surveyor mutation assay Primers

Target	Primer name	Sequence (5'-3')
S1pr3 Intron 1	S1pr3_I1_Sur_for	GCCACACTCAAAGTTCACGT
S1pr3 Intron 1	S1pr3_I1_Sur_rev	TCCCGGAGAGTGTCATTTCC
S1pr3 Intron 2	S1pr3_I2_Sur_for	TCATTTGCCAGTGTCTGCAG
S1pr3 Intron 2	S1pr3_I2_Sur_rev	CCCTCTGCCCTCTGACTTAG
LoxP	LoxP_for	CTTCGTATAATGTATGCTATACGAAG

Table 5 Oligonucleotides used in combination with the Cas9 Nickase

Description	Oligo name	Sequence (5'-3')
gRNA 1 Intron 1	S1PR3_Intron1_Nicko_Seq1	AAACGCTCCCACGTGGTGGGTGAGC
gRNA 2 Intron 1	S1PR3_Intron1_Nicku_Seq1	AAACGGCACCAGGAAATACTGCGTC
gRNA 1 Intron 2	S1PR3_Intron2_Nicko_Seq4	AAACTCTATCACCTCTGACCTGCC
gRNA 2 Intron 2	S1PR3_Intron2_Nicku_Seq4	AAACATTTTGCGATCTGGAGCATAC
DNA template Intron 1	S_I1_Nickou_Seq1_HDR_for	TACAGCTGGGAATACTGGCTTATCAGCTCCCAC GTGGTGGGTGAGAAGTAACGCAGTATATAACTT CGTATAATGTATGCTATACGAAGTTATTGCCTGG AGATTTCCAAGTGGAAGCTTGCTCGTTTCTGCTG CAGTTACAGGATTCACAGA
DNA template Intron 2	S_I2_Nickou_Seq4_HDR_for	CCACCCCCAGTTCCACCTTCCCGCCGTCTATCACC TCTGACCTGCCCAAGGCAGTCTATGATAACTTCG TATAATGTATGCTATACGAAGTTATAAATTGGCA TGAATCTTTTCAAGTGTTTCTGACAAGTTATCCCT TTTCCCACCCCTGAGG

Table 6 Oligoucleotides used in combination with the Cas9 WT

Description	Oligo name	Sequence (5'-3')
gRNA Intron 1	S1PR3_Intron1_Nicko_Seq1	AAACGCTCCCACGTGGTGGGTGAGC
gRNA Intron 2	S1PR3_Intron2_Nicku_Seq4	AAACATTTTGCGATCTGGAGCATAC
DNA template Intron 1	S_I1_Nickou_Seq3_HDR_for	CCCTCACTTTTCCTCATCCTGAGAAAAATCTGATT CCCTCTACAGCTGGGAATACTGGCTTACATAACT TCGTATAATGTATGCTATACGAAGTTATGGTGA GAAGTAACGCAGTATTTCCTGGTGCCTGGAGAT TTCCAAGTGGAAGCTTGCTCGTTTC
DNA template Intron 2	S_I2_Nickou_Seq4_HDR_for	CCACCCCCAGTTCCACCTTCCCGCCGTCTATCACC TCTGACCTGCCCAAGGCAGTCTATGATAACTTCG TATAATGTATGCTATACGAAGTTATAAATTGGCA TGAATCTTTTCAAGTGTTTCTGACAAGTTATCCCT TTTCCCACCCCTGAGG

Table 7 In vitro transcription Primers

Target	Primer name	Sequence (5'-3')
gRNA 1 Intron 1 (Nickase)	S1_T7_gRNA_for	TTAATACGACTCACTATAGGCTCACCCACCACGTGGGA
gRNA 2 Intron 1 (Nickase)	S2_T7_gRNA_for	TTAATACGACTCACTATAGGACGCAGTATTTCCTGGTGCC
gRNA 1 Intron 2 (Nickase)	S11_T7_gRNA_for	TTAATACGACTCACTATAGGCAGGTCAGAGGTGATAGA
gRNA 2 Intron 2 (Nickase)	S12_T7_gRNA_for	TTAATACGACTCACTATAGGTATGCTCCAGATCG CAAAATC
gRNA Intron 1 (Cas9 WT)	S1_T7_gRNA_for	TTAATACGACTCACTATAGGCTCACCCACCACGTGGGA
gRNA Intron 2 (Cas9 WT)	S12_T7_gRNA_for	TTAATACGACTCACTATAGGTATGCTCCAGATCG CAAAATC
each gRNA	uni_T7_gRNA_rev	AAAAGCACCGACTCGGTGCC
Cas9 WT/ Cas9n	Cas9_T7_for	TAATACGACTCACTATAGGGAGAATGTACCCATACGATG TTCCAGATTAC
Cas9 WT/ Cas9n	Cas9_rev	TCAGCGAGCTCTAGGAATTCTTAGCT

Table 8 Genotyping Primers

Genotype	Primer name	Sequence (5'-3')
S1pr3$^{fl/fl}$	*S1pr3*$^{fl/fl}$ Intron 1 for	TCCCTCACTTTTCCTCATCCTG
	S1pr3$^{fl/fl}$ Intron 2 for	CGACAGATGTTATAACTTGTAGTG
	S1pr3$^{fl/fl}$ Intron 1 rev	GAAACCTCAGAGTGCGAATCTG
	S1pr3$^{fl/fl}$ Intron 2 rev	TCTTCTGTTTTTCCCTCAGGGG

Table 9 Sequencing Primers

Target	Primer name	Sequence (5'-3')
LoxP 1	*S1pr3*$^{fl/fl}$ Intron 1 for	TCCCTCACTTTTCCTCATCCTG
LoxP 2	*S1pr3*$^{fl/fl}$ Intron 2 for	CGACAGATGTTATAACTTGTAGTG
px335_1	SeqPx335_rev	CGCTAAAAACGGACTAGCCTT
px335_2	SeqPx335U6prom_for	GGACTATCATATGCTTACCGTAAC

4.1.4 TaqMan assays

All TaqMan assays were purchased from Applied Biosystems.

Table 10 TaqMan assays

Mouse probes	Ordering number	Human probes	Ordering number
Mm *Cd31*	Mm01242584_m1	Hs *ASNS*	Hs04186194_m1
Mm *Cdh5*	Mm03053719_s1	Hs *B2M*	Hs00984230_m1
Mm *Desmin*	Mm00802455_m1	Hs *GSN*	Hs00609272_m1
Mm *Hprt*	Mm00446968_m1	Hs *HPRT*	Hs02800695_m1
Mm *Ng2*	Mm00507257_m1	Hs *KIFAP3*	Hs00183973_m1
Mm *Pdgfra*	Mm00440701_m1	Hs *MPRIP*	Hs00819388_m1
Mm *Pdgfrb*	Mm00435546_m1	Hs *MYH10*	Hs00992055_m1
Mm *Ptger2*	Mm00436051_m1	Hs *PTGER2*	Hs04183523_m1
Mm *S1pr3*	Mm02620181_s1	Hs S1PR1	Hs01922614_s1
Mm *Vegfr2*	Mm01222421_m1	Hs *S1PR3*	Hs00245464_s1
		Hs *SDC1*	Hs00896423_m1
		Hs *SMAD7*	Hs00998193_m1

4.1.5 Restriction enzymes

All FastDigest Restriction Enzymes were purchased from Thermo Fisher Scientific.

Table 11 Restriction enzymes

Enzyme	Ordering number
AgeI (BshTI)	FD1464
BbsI (BpiI)	FD1014
NcoI	FD0573
PsiI (AanI)	FD2064

4.1.6 siRNA

All Silencer® Select siRNAs were purchased from Life technologies.

Table 12 siRNA

siRNA	ID
si*Control*	4390847
si*S1pr3_1*	s4454
si*S1pr3_2*	s4455
si*Ptger2_1*	s11448
si*Ptger2_2*	s11450

4.1.7 CRISPR/Cas and PCR/RT-qPCR reagents, nucleotides and buffers

Table 13 CRISPR/Cas, PCR and RT-qPCR reagents, nucleotides and buffers

Reagent	Company
10 x Coral Load PCR buffer	Qiagen
Ampicillin	Sigma-Aldrich
Cas9 mRNA	Tebu-bio
Cas9 Nickase mRNA	Tebu-bio
Direct PCR Lysis Reagent	PeqLab
DNase/RNase free H_2O	Gibco
dNTP mix (10mM each)	Fermentas
Ethidium bromide	Roth
O'Generuler 100bp Plus DNA ladder	Thermo Scientific
RedTaq® ReadyMix PCR Reaction Mix	Sigmal-Aldrich
TaqMan® Fast Advanced PCR Master Mix	Applied Biosystems
TOP10F competent cells	Invitrogen

4.1.8 Cells

Table 14 Human cells

Cells	Description	Company	Medium	Company
Adi	Adipocytes	PromoCell	Adipocyte medium	PromoCell
BP	Brain vascular pericytes	ScienceCell	Pericyte medium+suppl	Sciencell
Fib 1	Fibroblasts	Provitro	DMEM/10%FCS P/S	Gibco
Fib 2	Fibroblasts	PromoCell	DMEM/10%FCS P/S	Gibco
HaoSMC	Human aortic smooth muscle cells	PromoCell	DMEM/5%FCS P/S	Gibco
HBMEC	Human brain microvascular endothelial cells	Neuromics	ECGM MV2/ +suppl	PromoCell
HDBEC	Human dermal blood endothelial cells	PromoCell	ECGM MV/ +suppl	PromoCell
HSAVEC	Human saphenous vein endothelial cells	Promocell	ECGM MV/ 10%FCS+suppl	PromoCell
HUAEC	Human umbilical aortic endothelial cells	PromoCell	ECGM MV/ 10%FCS+suppl	PromoCell

Table 14 Human cells – continued

Cells	Description	Company	Medium	Company
HUVEC	Mixed primary isolated EC of several isolations from the human umbilical chord	PromoCell	Endopan	PAN-Biotech
LP	Lung pericytes	Kindly provided by Bruno Peault	Pericyte medium+suppl	ScienCell
MP	Muscle pericytes	Kindly provided by Bruno Peault	Pericyte medium+suppl	ScienCell
MSC 1	Mesenchymal stem cells (with collagen cell carrier)	Bioengineering	McCoys 5A Medium+suppl	Gibco
MSC 2	Mesenchymal stem cells (without collagen cell carrier)	Bioengineering	McCoys 5A Medium+suppl	Gibco
PancP	Pancreas pericytes	Kindly provided by Bruno Peault	Pericyte medium+suppl	ScienCell
PlaP	Placenta pericytes	PromoCell	Pericyte medium+suppl	ScienCell

Table 15: Mouse cells

Cells	Description	Company	Medium	Company
NIH3T3	Mouse embryo fibroblast cell line	Kindly provided by Dr. Courtney König	DMEM+Glutamax 10%FCS P/S	Gibco

4.1.9 Growth factors, proteins and enzymes

Table 16 Growth factors, proteins and enzymes

Growth factor	Company
Collagenase IV	Sigma Aldrich
DNase I	Roche
FastAP Thermosensitive Alkaline Phosphatase	Thermo Fisher Scientific
Proteinase K	Gerbu
Q5® High-Fidelity DNA Polymerase	New England Biolabs
RNase free DNAse	Qiagen
S1P	Sigma-Aldrich
S1PR3 Inhibitor TY52156	Tocris
SCR7	Xcessbio Biosciences Inc
T4 Ligase	New England Biolabs

4.1.10 Cell culture reagents

Table 17 Cell culture reagents

Reagent	Company
Accutase	PAA
Collagen I	Isolated from rat tails
Dimethylsulfoxide (DMSO)	AppliChem
Dulbecco´s modified eagle medium (DMEM)	Gibco
Dulbecco´s phosphate buffered saline (PBS)	PAA
Endopan 3 + FCS + supplements	PAN-Biotech
Fatty acid free BSA	Sigma-Aldrich
Fetal Calf Serum (FCS, heat inactivated)	PAA
Gelatine	Sigma-Aldrich
Isopropanol	Sigma-Aldrich
Lipofectamine 2000	Thermo Fisher Scientific
Lipofectamine 3000	Thermo Fisher Scientific
Oligofectamine Reagent	Life Technologies
Opti-MEM I (1x) + GlutaMAX-I	Gibco
Penicillin/Strepomycin (100x 10^4U/10mg/ml)	PAA
Pertussis toxin	List Biological Laboratories
PKH 26 Red Fluorescent Linker Kit	Sigma-Aldrich
Trypan blue	Gibo
Trypsin-EDTA solution (10x)	PAA

4.1.11 Western blot reagents

Table 18 Western Blot reagents

Reagent	Company
Bovine Serum Albumine (BSA)	PAA laboratories
Nitrocellulose membrane	GE Healthcare
Orthovanadate	Sigma-Aldrich
PageRuler™ Prestained Protein Ladder	Thermo Scientific
Pierce ECL Western blotting substrate	Thermo Scientific
Immobilon-P PVDF membrane	Millipore
ReBlot Plus Strong Solution	Merck
Rotiphorese Gel 30	Carl-Roth
Super RX X-ray films	Fuji
SuperSignal™ West Dura Extended Duration Substrate	Thermo Fisher Scientific

4.1.12 Antibodies

Table 19 Primary antibodies

Antigen	Reactivity	Species	Dilution	Conjugate	Company	Ordering number
Actin	human	rabbit	1:5000	-	Santa Cruz	Sc-1616_r
CD31	human	mouse	1:200	Apc-Cy7	BD Bioscience	563653
CD31	mouse	rat	1:200	Pe-Cy7	BD Pharmingen	561410
CD45	mouse	rat	1:400	FITC	BD Pharmingen	553080
ERK1/2	human	rabbit	1:1000	-	Santa Cruz	Sc-94
LYVE1	mouse	rat	1:250	FITC	eBioscience	53-0443
PDPN	mouse	hamster	1:100	AF488	eBioscience	53-5381
pERK1/2	human	mouse	1:1000	-	Cell Signaling	9106 S
S1PR1	human	rabbit	1:1000	-	Santa Cruz	Sc-25489
TER119	mouse	rat	1:200	FITC	BD Pharmingen	561032
tubulin	human	mouse	1:1000	-	Sigma-Aldrich	T8203

Table 20 Secondary antibodies

Reactivity	Species	Dilution	Conjugate	Company	Ordering number
mouse IgG	rabbit	1:10000	HRP	DAKO	P0260
rabbit IgG	goat	1:5000	HRP	DAKO	P0448

4.1.13 Kits

Table 21 Kits

Agilent RNA 6000 Nano Kit	Agilent technologies
Arcturus PicoPure RNA Isolation Kit	Life Technologies
DNeasy Blood & Tissue Kit	Qiagen
GenElute Mammalian Total RNA Purification Kit	Sigma-Aldrich
Gibson® Assembly Cloning Kit	New England Biolabs
MEGAclear Kit	Life Technologies
MEGAshortscript T7 Kit	Life Technologies
mMESSAGE mMACHINE T7 ULTRA Kit	Life Technologies
NucleoBond-Xtra Maxi Kit	Macherey-Nagel
PCR qiaquick purification kit	Qiagen
Pierce Bicinchoninic acid (BCA) Protein Assay Kit	Thermo Scientific
PureLink™ Quick Plasmid Miniprep Kit	Invitrogen
Qiaquick gel extraction kit	Qiagen
Quantitect Reverse Transcription Kit for cDNA Synthesis	Qiagen
QuantiTect Whole Transcriptome Kit	Qiagen
Reagent	Company
Surveyor mutation assay	Transgenomic

4.1.14 Staining reagents

Table 22 Staining reagents

Reagent	Company
Annexin V	eBioscience
Annexin V Binding buffer	eBioscience
Fluorescent mounting medium	DAKO
FxCycle	Invitrogen
Hanks buffer 20mM Hepes	Biomol
Hoechst Dye 33258, 1mg/ml	Sigma-Aldrich
Phalloidin AF488	Invitrogen
Pluronic® F-127	Biomol
Rhod4	Biomol
Roti-Histofix 4% (pH 7)	Carl Roth

4.1.15 Consumables

Table 23 Consumables

Consumable	Company
384 well plates	Roche
Boyden chambers 8.0 µm	Corning
Cannula (18G, 19G, 27G)	BD
Cell culture dishes (6cm,10cm)	TPP
Cell scraper	Corning
Cell strainer	BD Falcon
Cover slips 12mm	VWR
Cryotubes	Carl-Roth
FACS tubes	BD Falcon
Filter containing pipette tips	Biozym
Ibidi µ-slide	Ibidi
Microscope cover glasses	VWR international
Microscope glass slides	Menzel-Gläser
E-Plate 16 (Proliferation xCELLigence)	Omni Life Science
Cim Plate (Migration xCELLigence)	Omni Life Science
Mini PP tubes	Greiner
Pipette tips	Nerbe
Reaction tubes (0.5ml, 1.5ml, 2ml)	Eppendorf
Reaction tubes (15ml, 50 ml)	Greiner
Sealing foil	Applied Biosystems
Sterile pipette	Corning
Syringes	Dispomed
Tissue culture 6 well/24 well plates	Greiner

4.1.16 Equipment

Table 24 Equipment

Equipment	Company
Agarose gel documentation system	Peqlab
Agilent 2001 Bioanalyzer	Agilent technologies
Amersham Imager 600	GE Healthcare
Aria FACS Sorter	BD
Bacterial incubator	Heraeus
Bacterial incubator/shaker	Edmund Bühler GmbH
BioRad gel casting system	BioRad
BioRad gel running system	BioRad
BioRad Western Blotting equipment	BioRad
Canto II	BD
Cell culture hood	Thermo Fisher Scientific
Cell culture incubator	Thermo Fisher Scientific
Cell Observer	Zeiss
Cell^R microscope	Olympus
Centrifuge	Beckman Coulter
Classic E.O.S film developer	Agfa
Countess automated cell counter	Invitrogen
Developing cassette Western Blot	Amersham Bioscience
Freezing box	Thermo Fisher Scientific
Heating block	Eppendorf
Holomonitor microscope	Phiab
iMark™ Microplate Reader	BioRad
Light cycler 480	Roche
Multistep pipette	Eppendorf
Nanophotometer® N60	INTAS
Pipettes	ErgoOne
Power supply	BioRad
QIAxcel Advanced System	Qiagen
StepOnePlus Real-Time PCR System	Thermo Fisher Scientific
Table centrifuge (5417R)	Eppendorf
Thermocycler	Applied Biosystems
Tubes and adapters for flow incubation	Carl Roth
UV transluminator	Intas
Vortex	Neolab
Water bath	Julabo
xCELLigence	ACEA Biosciences

4.1.17 Softwares

Table 25 Softwares

Software	Company
Chromas Lite	http://chromas-lite.software.informer.com/2.1/
CRISPRdesign	http://crispr.mit.edu/
FACSDiva™	BD
Fiji	ImageJ
FlowJo	Miltenyi Biotec
Genepattern	http://software.broadinstitute.org/cancer/software/genepattern/
Graph Pad Prism	Graph Pad
Holostudio Software	Phiab
ImageQuant TL	GE Healthcare
Light Cycler 480 software	Roche
Molecular Signature Database	http://software.broadinstitute.org/gsea/index.jsp

4.1.18 Solutions and buffers

Solutions and buffers were prepared as follows:

Table 26 Solutions and buffers

Buffer	Composition	
5x Protein sample buffer	250 mM	Tris-HCl (pH 6.8)
	10%	SDS
	0.5%	Bromophenol blue solution
	50%	Glycerol
		add 10% β-mercaptoethanol prior to use
Blotting buffer (1x)	192mM	Glycine
	25mM	Trizma Base
LB Agar	12.0 g	Tryptone
	5.0 g	Yeast extract
	5.0 g	NaCl
	1.0 g	Glucose
		Add 1l H_2O
LB medium	12.0 g	Tryptone
	5.0 g	Yeast extract
	5.0 g	NaCl
	1.0 g	Glucose
	12 g/l	Agar
		Add 1l H_2O

Table 26 Solutions and buffers – continued

Buffer	Composition	
Morulae lysis buffer	18.75 µl	125µg/ml Proteinase K
	333 µl	100mM Tris-HCL (ph8.3)
	300 µl	100mM KCl
	300 µl	0.02% gelatin
	13.5 µl	0.45% Tween 20
	18 µl	60µg/ml yeast tRNA
	2017 µl	H_2O
Phosphate buffered saline (PBS)	1.34M	NaCl
	27mM	KCl
	200mM	Na_2HPO_4
	4.7mM	KH_2HPO_4
		adjust pH 7.4
RIPA lysis buffer	50mM	Tris-HCl pH 7.5
	150mM	NaCl
	1mM	EDTA
	1%	NP-40
	0.25%	Na-deoxycholate
	2mM	Na-orthovanadate
	1x	Protease inhibitor Mix G
Running buffer (1x)	192mM	Glycine
	25mM	Trizma Base
	0.1%	SDS
Separating gel (15%) (1Gel)	2.3ml	H_2O
	2.5ml	1.5M Tris-HCl pH 8.8
	100µl	10% SDS
	5ml	30% Acrylamide
	100µl	APS
Stacking gel (5%)	2.7ml	H_2O
	0.5ml	1M Tris-HCl pH 6.8
	40µl	10%SDS
	0.67ml	30% Acrylamide
	40µl	APS
Tris-Borate-EDTA buffer (TBE)	89 mM	Tris-HCL pH 7.5
	89mM	NaCl
	1mM	Tween-20
Tris-Buffered Saline Tween-20 (TBST)	10mM	Tris/HCl, pH 7.5
	100mM	NaCl
	0.1%	Tween-20

4.2 Methods

4.2.1 Cell culture methods

4.2.1.1 Cell maintenance

All cell types used in the present study were maintained at 37°C under sterile conditions, high humidity and 5 % CO_2 and were cultured in media as indicated (Table 14 and 15). Cells were checked for mycoplasma contamination on a regular basis. All primary cells were used between passage one and six and discarded afterwards. When cells reached 80-90% confluency, they were passaged and diluted 1:3 (HUVEC, HUAEC, HSAVEC, HBMEC, HDBEC, SMC, Adi), 1:5 (BP, MP, LP, PancP, PlaP, Fib, MSC) or 1:10 (NIH3T3). The medium was discarded and cells were washed with PBS. All cells were detached by accutase incubation at 37°C for 2 min, diluted in culture medium and centrifuged for 5 min at 200 g. The supernatant was discarded, the pellet was resuspended in culture medium and the desired cell dilutions were prepared. For HUVEC, cell plates were pre-incubated on 0.2 % gelatine at 37 °C for 30 min.

4.2.1.2 Cryopreservation and thawing of cells

Cryocultures were prepared for long-term storage of cells. For this purpose, cells were resuspended in cell-type specific media with 10 % DMSO and additional 10% of FCS than normal culture media. The cell suspension (1 ml) was transferred to a cryotube and the tubes were slowly frozen to -80 °C in an isopropanol containing freezing box overnight and were then transferred into liquid nitrogen for long-term storage. For thawing of cells, the cryotube was warmed at 37 °C for 2 min and the cells were resuspended in 10 ml pre-warmed culture medium and centrifuged for 3 min at 200 g. The supernatant was discarded and the pellet was resuspended in 10 ml culture medium and seeded into a 10cm cell culture dish.

4.2.1.3 Seeding of cells

For seeding specific number of cells for experiments, cells were detached as described in 4.2.1.1. Cells were counted by mixing 10 µl of cell suspension with 10 µl of trypan blue in an automated cell counting mashine according to manufacturer´s manual. Cell solutions with corresponding cell numbers were prepared and seeded accordingly in cell culture dishes or multiwall plates.

4.2.1.4 Transfection of pericytes with siRNA

Depending on the experiment, specific numbers of pericytes were seeded in different cell culture plates. Table 27 shows an overview of cell numbers and corresponding volumes of reagents needed for transfection. Briefly, cells were transfected 24 h after seeding with two independent silencer select *S1PR3/PTGER2* siRNAs or control siRNA using oligofectamine transfection reagent. siRNA (20 µM) and Opti-MEM(1x)+GlutaMAX-I (solution A) were mixed with equal amounts of oligofectamine and 100 µl Opti-MEM(1×)+GlutaMAX-I (solution B). Solution A and B were

incubated separately for 10 min at RT and then combined and incubated for another 30 min at RT. Pericytes were twice washed with Opti-MEM(1x)+GlutaMAX-I. The transfection mix was carefully dropped on the cells, covered with defined volume of media (see Table 27). After 4 hours of incubation, the medium was exchanged to pericyte medium (PM) with 2% FCS/ growth factors and penicillin/streptomycin. All assays were performed 48-72 hours post-transfection.

Table 27 Cell densities and siRNA transfection volumes

Cell densities and siRNA transfection volumes					
Plate	Cell number	siRNA	Oligofectamine	Opti-MEM	Plate
µ-slide	10 000	1 µl	0.5 µl	10 µl	80 µl
24-well	18 000	2 µl	1 µl	20 µl	160 µl
6-well	80 000	10 µl	5 µl	100 µl	800 µl
6 cm	250 000	25 µl	12.5 µl	250 µl	2 ml
10 cm	500 000	50 µl	25 µl	500 µl	4 ml

4.2.1.5 PKH labelling of pericytes and co-culture of HUVEC and BP

48 hours before co-culturing, pericytes were transfected with siRNA as described in 4.2.1.4. HUVEC were seeded one day before co-culturing to form a monolayer ($1.1x10^6$ HUVEC in 10 cm dish; 180 000 HUVEC in 6 well). Transfected pericytes (48 post transfection) were detached as described in 4.2.1.1. The cell pellet was resuspended in Diluent C and centrifuged at 300 g for 5 min at room temperature. Cells were stained in PKH red/Diluent C solution (1:250) in the dark at room temperature for 10 min. The staining was stopped by adding 1 ml of FCS. 5 ml of Endopan containing 3% FCS and supplements was added and centrifuged at 200 g for 5 min. The cell pellet was resuspended in 1 ml of Endopan medium and cells were counted as described in 4.2.1.3. Stained pericytes were seeded in a 1:2 ratio on the HUVEC monolayer in Endopan full medium.

4.2.1.6 Phalloidin staining of pericytes

Coverslips were coated with 0.2 % gelatine for 30 min at 37 °C. Pericytes were seeded at a density of 18 000 cells per 24 well and were transfected with siRNA (4.2.1.4). 48 hours after transfection, cells were washed once with PBS and fixed in 4 % PFA/H2O for 10 min at RT. After three washing steps (3x5 min) with TBST for permeabilization, cells were incubated with directly labelled phalloidin (Phalloidin-FITC) and Hoechst for 1 h at RT. The antibody solution was aspirated and cells were washed three times with TBST. Lastly, coverslips were mounted with Fluoromount G. Images were acquired using Zeiss Cell Observer. Analysis was performed using Fiji/ImageJ software. Phalloidin-positive area was normalized to the amount of Hoechst stained nuclei.

4.2.2 Cellular assays

4.2.2.1 PTX, TY52156 treatment of BP

For treating BP with pertussis toxin (PTX) or S1PR3 inhibitor TY52156, pericytes were seeded in 6 wells (100 000 pericytes) or 6 cm dishes (400 000 cells). Pericytes were treated with 1 µM inhibitor (dissolved in 100 % ethanol) or 200 ng of PTX (dissolved in PBS) with corresponding controls (100 % ethanol or PBS) for 4 hours in PM containing 0.5 % FCS without growth factors. Subsequently, cells were stimulated with S1P and harvested for further analysis.

4.2.2.2 S1P stimulation of BP

BP were transfected with siRNA (4.2.1.4) or treated with PTX or TY52156 (4.2.2.1) as described above. 48 hours after transfection or 4 hours after treatment, cells were starved in 0.5 % FCS in PM without growth factors for 2 hours. S1P powder was reconstituted in methanol (0.5 mg/ml) and aliquoted in 20 µl. The methanol was evaporated with nitrogen gas and the resulting S1P films were frozen at -20 °C. To prepare a working solution (200 µM) S1P films were dissolved in 130 µl of 0.4 % BSA (fatty acid free) in PBS and incubated at 37 °C for 15 min. For stimulation, the S1P stock was diluted in 0.1 % BSA (fatty acid free) in PM without FCS and supplements to a final concentration of 1 µM. Starvation medium was discarded and the S1P containing medium was added for 1, 5 or 10 min before cells were harvested with a cell scraper in 1 ml PBS on ice. For the 0 min stimulation control cells were directly scraped.

4.2.2.3 Transmigration assay

BP were transfected with siRNA targeting *S1PR3* and non-targeting siRNA as control (as described in 4.2.1.4).

Transmigration assay with xCELLigence system: 40 000 pericytes in PM containing 0.5 % FCS and no growth factors were seeded into the upper inserts containing electrodes in migration plates. PM containing 2 % FCS and growth factors was added in the lower chamber to create a gradient for the cells to migrate (72 hours). Cell migration was monitored with the xCELLigence system detecting changes in impedance every 30 min. Each condition (2 different targeting siRNAs, 1x siControl) was performed in triplicates.

Transmigration assay with Boyden chambers: 60 000 HUVEC were seeded in the 24 wells in Endopan containing 0.5 % FCS and no growth factors and were cultured overnight. On the next day, 70 000 pericytes in Endopan containing 0.5 % FCS and no growth factors were seeded onto the upper well of the 8.0 µm pore transwells and let adhere for 2 hours. Boyden chambers with seeded pericytes were positioned on top of the HUVEC monolayer with the conditioned media to create a gradient for the pericytes to migrate. After 6 hours, transmigration was stopped by fixation of the cells with histofix (4 % PFA). Transwells were washed three times with PBS and incubated with DAPI (in PBS, 1:2 000 for 30 min RT) to stain the cell nuclei. Transwells were washed three times with PBS and cells on the upper side of the filters were removed with a cotton

swab. Images were taken on the fluorescent microscope Olympus IX 71 and transmigrated cells (DAPI positive) were counted using Fiji/ImageJ software.

4.2.2.4 Calcium release assay

BP were seeded in 24 wells (18 000) and were transfected with siRNA or siControl as described above. For S1PR3 blockage with the inhibitor TY52156, equal numbers of cells (as transfected cells) were seeded in triplicates, but were left untreated during transfection procedure. Cells were treated as described in 4.2.2.1. All conditions were washed twice with Hanks buffer before adding 500 µl staining solution (0.02 % pluronic acid and 0.05% Rhod4 in Hanks buffer). The Inhibitor TY52156 and the corresponding control (100 % ethanol) were added in corresponding wells. Cells were incubated for 30 min at 37 °C and 5 % CO_2, following 30 min at room temperature in the dark. The calcium release was measured for 180 seconds by live-cell imaging using Olympus Cell^R microscope (20x). Pictures were taken every second. Cells were stimulated after 10 sec with 1 µM S1P. The increase in fluorescent intensities upon calcium release was quantified using Fiji/ImageJ software.

4.2.2.5 Holomonitor live cell imaging

The Holomonitor M4 is a microscope that allows non-invasive and label-free real-time imaging to monitor cell parameters such as cell area, volume, migration and cell count. Holographic images, resulting of phase-shift measurements, are taken in the incubator while imaging the cells (Alm et al., 2013).

Ibidi 8-well µ-slides were used for imaging. siRNA transfected pericytes (10 000, see Table 27) were seeded in 0.2% gelatine coated wells. 24 hours after transfection, live-cell imaging was started for 60 hours. Pictures were taken every 5 min. Analysis was performed using HoloStudio software.

4.2.2.6 Co-culture FACS

Transfected BP and HUVEC were co-cultured in 10 cm dishes as described in 4.2.1.5. After 24 hours of co-culture, cells were detached and incubated with an antibody against CD31 (APC-Cy7 labeled) for 30 min on ice. Cells were gated and sorted for two single positive populations: CD31-positive (EC) or PKH-positive (pericytes) cells. Double positive cells were excluded. Directly after the sort, cells were pelleted and lysed in RNA extraction buffer and frozen at -80°C.

4.2.2.7 Cell proliferation assay

Real-time and dynamic monitoring of cell proliferation was performed using xCELLigence system. 4000 pericytes in pericyte medium containing 2 % FCS and no growth factors were seeded into the inserts containing electrodes in proliferation plates. Cell proliferation was monitored with the xCELLigence system detecting changes in impedance every 30 min. Each condition (2 different targeting siRNAs, 1x siControl) was performed in triplicates.

4.2.2.8 Annexin V apoptosis assay

Annexin V apoptosis assay was performed to investigate the effect of *S1PR3* knockdown in pericytes cultured with HUVEC. Annexin V binds to phosphatidylserine, which is flipped to the cell surface upon cell apoptosis. *S1PR3* silenced pericytes were co-cultured with HUVEC in 6 wells as described above (4.2.1.5). After 24 hours of co-culturing, cell culture supernatant and PBS wash were collected to also include dead cells. Cells were detached and washed once in binding buffer. Subsequently, cells were stained with Annexin V-FITC (1:20 in binding buffer) for 15 min at room temperature. Additionally, cells were stained with FxCycle violet (1:1 000) for 30 min on ice to allow the discrimination of early, late apoptotic or necrotic cells. To distinguish endothelial cells from PKH-positive pericytes, cells were stained with CD31-APC-Cy7 (1:200). Single stained controls and an unstained control were used for compensation. Cells were gated in PKH-positive (pericytes) or APC-Cy7-positive (EC) populations. Each population was gated for Annexin V-positive, FxCycle-positive and Annexin-V/FxCycle-double-positive cells. Quantification of the analysis was performed using FlowJo software.

4.2.2.9 Adhesion assay

BP were transfected with siRNA targeting *S1PR3* and siControl in 6 wells as described in 4.2.1.4. One day after transfection, HUVEC (36 000) were seeded in 0.2 % gelatine coated 24 wells and were cultured overnight. The next day, transfected pericytes were detached and stained with PKH (see 4.2.1.5). BP (18 000) were seeded on top of the monolayer in Endopan containing 3 % FCS and supplements and allowed to adhere for 15 or 30 min. Non-adherent cells were carefully removed by washing. Attached cells were fixed with Histofix (4 % PFA) and imaged using the fluorescent microscope Olympus IX 71. Attached cells (PKH-positive) were counted using Fiji/ImageJ software. Each condition was performed in triplicates.

4.2.3 Biochemical methods

4.2.3.1 Protein isolation and concentration determination for immunoblotting

For protein extraction from stimulated pericytes, cells were washed once with ice-cold PBS and scraped in 1 ml PBS. After centrifugation, the pellet was dissolved in RIPA lysis buffer (6 well: 100 µl, 10cm dish: 300 µl). Whole cell lysates were centrifuged for 10 min at full speed at 4°C and supernatants were separated from the cell debris. Protein concentration was measured using Pierce BCA Assay according to manufacturer´s instructions. Defined protein concentrations of the samples were generated by diluting them in RIPA buffer. Samples were boiled in 5x protein sample buffer at 95 °C for 5 min and used directly for immunoblotting or were stored at -20 °C.

4.2.3.2 SDS-Polyacrylamide gel electrophoresis (PAGE) and Western blot

Proteins were separated according to their molecular weight by 10% (ERK1/2) or 12% (MLC, RhoA) SDS-PAGE with the BioRad gel casting and running system in 1x running buffer. Gel electrophoresis was started at 80 V to allow the proteins to enter the gel. After 30 min the voltage

was increased to 120 V for 1 h. 7 µl of PageRuler™ Prestained Protein ladder was used to determine the size of the proteins. After electrophoresis, proteins were blotted on a nitrocellulose membrane (ERK1/2) or on a PVDF-membrane (MLC) at 0.4 A for 70 min in 1x blotting buffer. The PVDF membrane was equilibrated for 20 sec in 100 % methanol and afterwards in 1x blotting buffer.

Unspecific binding of antibodies to the membrane was prevented by subsequent blocking with 3 % BSA/TBST for 1h at RT. For immunodetection of the desired proteins, primary antibodies (see Table 19) were diluted in 3 % BSA/TBST and incubated overnight at 4 °C. Three times washing with TBST removed unbound and unspecific bound antibody. Afterwards, the membrane was incubated with the corresponding horse-radish-peroxidase (HRP)-coupled secondary antibodies diluted in TBST (see Table 20) for 1h at RT. After three washing steps with TBST membranes were developed using Pierce ECL Western Blotting Substrate or SuperSignal™ West Dura Extended Duration Substrate according to manufacturer´s instructions. The membranes were exposed to Super RX X-ray films (2 sec to 30 min) and developed in the Classic E.O.S. film developer or using Amersham Imager 600. Signal intensities were either set in relation to a housekeeping gene (α-tubulin) or corresponding non-phosphorylated proteins served as control for their phosphor-protein signal.

4.2.4 Molecular biological methods

4.2.4.1 RNA isolation

RNA of FACS-sorted mouse pericytes was isolated with the Arcturus PicoPure RNA Isolation Kit. Cells were centrifuged at 500 g and 4°C for 5 min and the pellet was resuspended in 50 µl Arcturus PicoPure extraction buffer. RNA was isolated according to manufacturer´s instructions. RNA was eluted in 11 µl RNase free H_2O and RNA concentrations were measured using NanoPhotometer® N60. RNA of cell culture cells was isolated using GenElute Mammalian Total RNA Purification Kit according to the manufacturer´s instructions. Cells were lysed with 100-300 µl lysis buffer and RNA was eluted in 30 µl RNase free H_2O and stored at -80°C.

4.2.4.2 Reverse transcription of RNA

Reverse transcription was performed using the QuantiTect Reverse Transcription Kit according to the manufacturer's instructions. Briefly, 1 µg RNA was combined with 2 µl 7xDNA Wipeout buffer and the total volume was adjusted to 14 µl with RNase-free H_2O. Genomic DNA digestion was performed for 2 min at 42°C. Afterwards, 1 µl reverse transcriptase, 4 µl 5xRT-buffer and 1 µl RT-Primer mix were added. Reverse transcription was accomplished at 42°C for 30 min and then stopped by 3 min incubation at 95°C. The cDNA was diluted 1:20 in H_2O for qPCR. cDNA was stored at -20°C.

RNA of FACS-sorted mouse cells was transcribed with QuantiTect Whole Transcriptome Kit according to manufacturer´s instructions.cDNA was diluted 1:100 and stored at -20°C.

4.2.4.3 Real time (RT) - qPCR

Relative gene expression was determined by RT-qPCR of synthesized cDNA. TaqMan-based RT-qPCR was used to detect differences of mRNA transcription levels. The Taqman mono-color hydrolysis probe method is based on using fluorescently labeled oligonucleotide probes that bind the gene of interest flanked by the forward and reverse primer. Taqman probes are labeled with a fluorophore (FAM) at the 5' end and a quencher at the 3' end that blocks fluorescence emission. The exonuclease activity of the Taq-polymerase allows the cleavage of the Taqman probe during amplification. Thereby, FAM fluorescence is detectable that is proportional to the amount of the amplified product. Reactions were performed in 96 or 384 well plates. One reaction contained the following components:

Table 28 TaqMan RT-qPCR reaction mix

TaqMan RT-qPCR reaction mix	
	1x
cDNA	3 µL
Taqman Fast Advanced Master Mix	5 µl
TaqMan gene expression assay	0.5 µl
ddH_2O	1.5 µL

Each reaction was performed in triplicates. Lightcycler®480 System (348 well plate) or StepOnePus Real-Time PCR System (96 well plate) was used for RT-qPCR with the following protocol:

Table 29 TaqMan RT-qPCR program

TaqMan RT-qPCR program			
Step	Temperature [°C]	Time [sec]	
Pre-denaturation	95	30	
Denaturation	95	2	45x
Amplification	60	20	

RT-qPCR data analysis was performed according to the ΔΔCT method (Livak and Schmittgen, 2001). Briefly, CT values of the genes of interest were normalized to the respective CT values of the indicated housekeeping genes for each sample (ΔCT). Afterwards, normalized CT values of the samples of interest were compared to normalized CT values of control samples (ΔΔCT). Respective fold changes (FC) were calculated from the ΔΔCT values.

$$\Delta CT = CT_{\text{gene of interest}} - CT_{\text{housekeeping gene}}$$

$$\Delta\Delta CT = \Delta CT_{\text{sample of interest}} - \Delta CT_{\text{control sample}}$$

$$\text{fold change} = 2^{-\Delta\Delta CT}$$

In case of data sets without internal control, relative expression was calculated by $2^{-\Delta CT}$.

4.2.4.4 Microarray

For gene expression analysis, microarrays were performed by the DKFZ Genomics and Proteomics core facility (Heidelberg). Briefly, RNA was isolated with the GenElute Mammalian Total RNA Purification Kit and RNA quantity and quality were checked using the Agilent RNA 6000 Pico Kit on an Agilent 2001 Bioanalyzer. Only RNA samples with a RIN value of > 6.0 were eligible for microarray analysis. RNA was reverse transcribed into cDNA. cDNA was hybridized on a HumanHT-12 Expression BeadChip Array (Ilumina) according to manufacturer´s protocol.

Cell and RNA preparation of the expression analysis of different primary human pericytes compared to other mesenchymal cells was performed by Dr. Zulfiyya Hasanov. For this microarray analysis, only significantly differentially expressed ($p \leq 0.05$) with mean intensities >400 in pericytes and <400 in the other mesenchymal cells were considered.

For the microarray analysis of co-cultured pericytes, expression levels measured in the *S1PR3/ PTGER2* silenced cells were normalized to the non-silencing controls. Only genes with a significantly differential expression ($p \leq 0.05$) and a log2FC of 0.4/-0.4 compared to control were considered for Molecular Signature Database analysis (Hallmark and Reactome gene sets).

4.2.5 Mouse lung pericyte isolation by FACS

For isolation of lung mouse pericytes, the tissue was digested by collagenase IV and pericytes were purified by FACS. Mice (8-12 weeks) were sacrificed and lungs of adult mice were surgically removed and cut into small pieces. Subsequently, lungs were digested with DMEM containing 1 mM $CaCl_2$, 80 U/ml collagenase IV and 0.2 % DNaseI at 37 °C for 30 min and additionally 15 min. Digested organs were passed through 18G and 19G cannula syringes to achieve single-cell suspensions. Afterwards, digestion was stopped with FCS and the single-cell suspension was passed through a 100 µm cell strainer. To identify lymphatic, blood and alveolar epithelial cells, cells were stained for PDPN, LYVE1, CD45 and TER119 (antibodies listed in Table 19) and CD31 (Table 19) for 30 min at 4 °C in PBS /5 % FCS. Dead cells were excluded by FxCycle staining

(1:1000) that was added shortly before FACS. Unstained and single stained control cells were used for compensation. Mural cell enriched cells ($FxCycle^-CD45^-TER119^-LYVE1^-PDPN^-CD31^-$ cells) and EC ($FxCycle^-CD45^-TER119^-LYVE1^-PDPN^-CD31^+$ cells) were sorted with a BD Biosciences FACS Aria Cell Sorter. Cells were centrifuged (300 g, 5 min), 50 µl RNA lysis buffer (of the picopure RNA isolation kit) was added and cells were immediately frozen at -80°C. In total, 5 mouse lungs were pooled for one FACS sample.

4.2.6 CRISPR/Cas establishment

4.2.6.1 gRNA and template design

gRNAs for the double Nickase and the WT Cas9 approach were designed by using the online tool CRISPRdesign (http://crispr.mit.edu/). Pairs of gRNAs (Table 5, 6) were chosen with the highest quality score. The quality score considers target specificity and possible off-target matches. The gRNAs were designed with overhang sequences 5´- CTTC- 3´ (sense) and 3´- CAAA- 5´ (antisense oligo) which are complementary to overhangs generated by BbsI digestion. The oligos were ordered as high purity salt-free purified single-stranded oligos from eurofins.

For the DNA template design (Table 5, 6), the 34 bp LoxP sequence (ATAACTTCGTATAATGTATGC-TATACGAAGTTAT) was flanked by 50-80 bp long homology arms of the gene region of interest. To avoid degradation of the template by Cas9, intact PAM sequences (5´ -NGG- 3´) within the DNA template were converted by inserting silent mutations. The DNA template was ordered as high-performance liquid chromatography (HPLC) purified single-stranded DNA (ssDNA) from Sigma-Aldrich.

4.2.6.2 Cloning of CRISPR/Cas plasmids

Amplification and purification of plasmids

For recovering the bicistronic expression vector px335 (double nickase and gRNA), bacteria of the glycerol stock were streaked on agar plates containing the appropriate antibiotic (ampicillin) and were incubated at 37°C for 12-16 hours. For the amplification of single clones, 5 ml of LB medium (Mini) containing ampicillin were inoculated with single colonies and incubated at 37°C on a shaker (300 rpm) for 12-16 hours. Plasmid DNA purification was performed using PureLinkTM Quick Plasmid Miniprep Kit according to manufacturer´s instructions. To confirm the validity of the plasmid, an enzymatic digestion with NcoI was performed, containing the following components:

Table 30 NcoI digestion mix

NcoI digestion mix	
	1x
DNA (400 ng)	X µL
NcoI FastDigest	1 µL
10 x FastDigest Buffer	1 µL
ddH_2O	X µL
total	20 µL

DNA fragment sizes were checked using agarose gel electrophoresis. After confirming the correctness of single clones, 1 ml of the Mini-prep was transferred into a bigger volume of 300 ml of LB medium and was incubated at 37°C and 300 rpm for 12-16 h. The bacterial cells were harvested by centrifugation at 4500-6000 g for 30 min at 4°C. Plasmid purification was performed using NucleoBond-Xtra Maxi kit according to manufacturer´s guidelines. DNA was eluted in 400 µl water and measured using NanoPhotometer® N60. Glycerol stock of the vectors was prepared by suspending bacterial cells of 1 ml of the Mini in 1 ml of 20% glycerol. Gylcerol stock was stored at -80 °C.

Cloning of EGFP in px330 and px335

From the plasmid CVU55762, the EGFP coding sequence and the corresponding CMV promotor were amplified using flanking primers with an overhang complementary to the insertion region of the px335 plasmid (Table 3). For the amplification, a high fidelity proofreading polymerase (Q5® High-Fidelity DNA Polymerase) was used with following reaction mix and PCR protocol:

Table 31 EGFP amplification PCR mix

EGFP amplification PCR mix	
	1x
px335_EGFP_for (Primer for)	1.25 µL
px335_EGFP_rev (Primer rev)	1.25 µl
dNTPs (10mM)	0.5 µl
5 x Reaction Buffer	5 µL
5x Q5 High GC Enhancer	5 µl
Q5 Polymerase	0.25 µl
DNA (100 ng)	X µl
ddH_2O	X µl
total	25 µl

Table 32 EGFP PCR program

EGFP PCR program			
Step	Temperature [°C]	Time	
1	98	30 sec	
2	98	10 sec	25 x
3	61	30 sec	
4	72	2 min	
5	72	10 min	
6	4	forever	

PCR product was purified by using the PCR Qiaquick purification kit according to manufacturer´s instructions. The PCR product was eluted in 30 µl H_2O. The plasmid px335 was digested with the restriction enzyme PsiI (Table 33). The reaction was stopped at 65°C for 15 min. The digested DNA was loaded on an agarose gel and bands were excised and purified using the Qiaquick gel extraction kit according to manufacturer´s instructions.

Table 33 PsiI digestion mix

PsiI digestion mix	
	1x
DNA (4000 ng)	X µL
PsiI FastDigest	4 µL
10 x FastDigest Buffer	4 µL
ddH_2O	X µL
total	20 µL

The Gibson Assembly® Cloning Kit from New England BioLabs was used to assemble the EGFP fragment and the plasmid px335. The Gibson Assembly is based on the efficient joining of overlapping DNA fragments. The Assembly was performed with a molar vector : insert ratio of 1:3 for 30 min. The assembly and the subsequent transformation of Top10F competent cells were performed according to manufacturer´s guidelines. The next day, single colonies were amplified (Mini) and a NcoI digestion was performed (see Table 30). Sequencing (see primers Table 9) confirmed the integration and correct orientation of EGFP.

gRNA annealing and cloning in px335 vector

The vector px335+EGFP was digested and dephosphorylated with BbsI and alkaline phosphatase for 30 min at 37°C (see Table 34) before ligating the respective gRNA into the vector. The digested vector was purified by gel electrophoresis using Qiaquick gel extraction kit according to manufacturer´s instructions. Before ligation, single-stranded gRNAs were phosphorylated and

annealed (see Table 35, 36). Ligation of the annealed gRNAs and the digested px335+EGFP was performed with a molar vector to insert ratio of 1:3 for 2 h at RT (see Table 37). Transformation of Top10F competent cells was performed according to manufacturer´s instructions.

Table 34 BbsI digestion mix

BbsI digestion mix	
	1x
DNA (1000 ng)	X µL
BbsI FastDigest	1 µL
10 x FastDigest Buffer	2 µL
Fast Alkaline Phosphatase	1 µl
ddH_2O	X µL
total	20 µL

Table 35 Annealing program

Annealing program		
Step	Temperature [°C]	Time
1	37	30 min
2	95 to 25	5 min and then ramp down 5°C/min

Table 36 Annealing of gRNAs

Annealing of gRNAs	
	1x
gRNA for (100 µM)	1 µL
gRNA rev (100 µM)	4 µL
10 x T4 Ligation Buffer	1 µL
ddH_2O	6.5 µl
T4 PNK	0.5 µl
total	10 µL

Table 37 Ligation reaction mix

Ligation reaction mix	
	1x
Digested px335+EGFP (50 ng)	X µL
Phosphorylated and annealed oligo	X µL
10 x T4 Ligation Buffer	2 µL
T4 Ligase	1 µl
ddH_2O	X µL
total	20 µL

The integration was confirmed by BbsI/AgeI digestion. In case of correct ligation of the gRNA into px335+EGFP, the BbsI enzyme is not able to bind and cut, whereas AgeI can digest the plasmid (plasmid fragment sizes: 5646 bp and 4145 bp). In case of incorrect integration of the gRNA, BbsI and AgeI are able to digest the plasmid (plasmid fragment sizes: 5646, 3151 and 972 bp). Plasmid fragment sizes were analysed by agarose gel electrophoresis. Additionally, plasmids were sequenced to validate gRNA integration (see primers Table 9). Confirmed plasmids were amplified (see 4.2.6.2).

4.2.6.3 *In vitro* verification of CRISPR/Cas-dependent genome modifications

Transfection of NIH3T3

Transfection of NIH3T3 cells with px335+EGFP containing the respective gRNA was performed using Lipofectamine 2000 reagent according to manufacturer´s guidelines. Briefly, 100.000 NIH3T3 cells were seeded in 24 wells. The day after, cells were transfected with 500 ng DNA (250 ng per gRNA) with the lowest concentration of Lipofectamine (2 µl) indicated in the manual. After 48 hours, genomic DNA was isolated using the DNeasy Blood & Tissue Kit according to manufacturer´s guidelines.

For transfection of NIH3T3 cells with the gRNA and the nuclease-containing plasmids and the DNA template, the reagent Lipofectamine 3 000 was used according to manufacturer´s instructions. Cells were seeded in 12 well plates and were transfected with 1 000 ng of DNA (330 ng per gRNA and 330 ng template) and 1.5 µl Lipofectamine 3 000. After 48 hours, genomic DNA was isolated using the DNeasy Blood & Tissue Kit according to manufacturer´s guidelines.

Surveyor mutation assay

The analysis of Cas9-induced repaired DSB and subsequent mismatches in the DNA was analysed using the Surveyor Mutation Detection Kit from Transgenic. This kit is based on the ability of an endonuclease only cleaving DNA at sites of mismatches resulting in distinct restriction fragments, which can be detected by agarose gel electrophoresis.

The DNA region of the expected mismatches was amplified by primers resulting in a PCR product of about 1000 bp with the high fidelity proofreading polymerase Q5® to prevent DNA synthesis errors (see Table 38, 39). The PCR product was purified using PCR Qiaquick purification kit according to manufacturer´s instructions. The digestion of the PCR products with the surveyor nuclease and the analysis with agarose gel electrophoresis was performed according to the manufacturer´s guidelines.

Table 38 Surveyor PCR program

Surveyor PCR program		
Step	Temperature [°C]	Time
1	98	30 sec
2	98	10 sec
3	58	30 sec
4	72	1 min
5	72	2 min
6	4	forever

Table 39 Surveyor PCR mix

Surveyor PCR mix	
	1x
Primer for 10 µM (see Table 4)	2.5 µL
Primer rev 10 µM (see Table 4)	2.5 µl
dNTPs (10mM)	1 µl
5 x Reaction Buffer	10 µL
5x Q5 High GC Enhancer	10 µl
Q5 Polymerase	0.5 µl
DNA (100 ng)	X µl
ddH_2O	X µl
total	50 µl

PCR analysis for LoxP integration

LoxP integration into the genome of transfected NIH3T3 cells with CRISPR/Cas plasmids and DNA template was confirmed by PCR analysis (see Table 40, 41). A primer binding directly to the LoxP site was used. In case of LoxP integration, a PCR product (PCR product size: LoxP 1 and 2 500 bp) could be detected with agarose gel electrophoresis.

Table 40 LoxP PCR mix

LoxP PCR mix	
	1x
LoxP_for 10 µM	1 µL
Primer rev 10 µM (see Table 7)	1 µl
dNTPs (10 mM)	0.5 µl
5 x Reaction Buffer	5 µL
5x Q5 High GC Enhancer	5 µl
Q5 Polymerase	0.25 µl
DNA (100 ng)	X µl
ddH_2O	X µl
total	25 µl

Table 41 LoxP PCR program

LoxP PCR program		
Step	Temperature [°C]	Time
1	98	30 sec
2	98	10 sec
3	58	30 sec
4	72	1 min
5	72	2 min
6	4	forever

4.2.6.4 *In vitro* transcription and quality control for *in vivo* application of CRISPR/Cas

In vitro transcription

For transcription of Cas9n mRNA and gRNA from the plasmids, the T7 promoter was added to Cas9n coding region by PCR amplification (see Table 42, 43). T7-Cas9n product was gel purified using Qiaquick gel extraction kit and served as template for *in vitro* transcription (IVT) using mMESSAGE mMACHINE T7 ULTRA Kit (Life Technologies) according to manufacturer´s instructions. T7 promoter was added to gRNA by PCR amplifications using primer listed in Table 7. The T7-gRNA PCR product was gel purified by Qiaquick gel extraction kit. 350 ng of the PCR product were used as template for *in vitro* transcription (IVT) using MEGAshortscript T7 kit (Life Technologies) according to manufacturer´s instructions. Both, Cas9n mRNA and gRNA were purified by MEGAclear kit (Life Technologies) and eluted in RNase-free water according to manufacturer´s guidelines.

For the double nickase/SCR7 experiment as well as for the following Cas9 WT experiments, commercially available Cas9n and Cas9 WT mRNA were used for the injection.

Table 42 IVT PCR Mix

IVT PCR mix	
	1x
Primer for 10µM (see Table 7)	2 µL
Primer rev 10 µM (see Table 7)	2 µl
dNTPs (10 mM)	2 µl
5 x Reaction Buffer	20 µL
5x Q5 High GC Enhancer	20 µl
Q5 Polymerase	1 µl
DNA (2 ng)	X µl
ddH_2O	X µl
Total	100 µl

Table 43 IVT PCR program

IVT PCR program		
Step	Temperature [°C]	Time
1	98	30 sec
2	98	10 sec
3	58	1 min
4	72	1 min
5	72	2 min
6	4	forever

Bioanalyzer

For the analysis of quality and quantity of gRNA and Cas9n mRNA, the Agilent RNA 6000 Nano Kit was used on an Agilent 2001 Bioanalyzer according to manufacturer´s guidelines. Samples were immediately frozen at -80°C. In case of the necessity to thaw already used transcribed mRNA samples, Bioanalyzer analysis was repeated before injecting *in vivo*.

4.2.6.5 One-cell embryo injection

All *in vivo* experiments in the context of the CRISPR/Cas establishment were performed by Frank van der Hoeven and Ullrich Kloz (Transgenic Service, DKFZ). All animal experiments were approved by the local regulatory committee (Bezirksregierung Karlsruhe, Germany; permit: G-154-14).
Briefly, C57BL/6N female mice (5-8 weeks old) were super ovulated and mated overnight with C57BL/6N male mice (older than 7 weeks). On the next day, zygotes were harvested from the ampullae of super ovulated females. The gRNAs, Cas9n or Cas9 mRNA and the DNA templates were injected into the cytoplasm of zygotes.
For the pilot experiment, injected zygotes were incubated in 5.5 % CO2 at 37 °C for 2-3 days until they developed to morulae. For experiments, in which the 2-cell stage embryos should be transferred into the uterus of pseudo-pregnant mice, injected zygotes were cultured for 24 hours before oviduct transfer in mouse embryo culture medium KSOM. In the case of SCR7 treatment, zygotes were incubated for 1 h with 50 µM SCR7 before injection. Injected zygotes were incubated further 24 hours with 50 µM SCR7 previous to embryo transfer.
Used concentrations of Cas9n/Cas9 WT, each gRNA and each DNA template is listed as follows:

Table 44 Nucleotide concentrations for zygote injections

Concentrations for zygote injections			
experiment	Cas9n/Cas9 WT (ng/µl)	gRNA (ng/µl)	DNA template (ng/µl)
Pilot test ´Cas9n´	100	25	50
Experiment ´Cas9n´	100	50	75
Experiment ´SCR7´	80	LoxP 1: 80 LoxP 2: 15	LoxP 1: 90 LoxP 2: 80
Pilot test ´Cas9 WT´	100	75	75
Experiment ´Cas9 WT sequential´	100	75	75

4.2.6.6 Genotyping/ Sequencing PCR

Genotyping of morulae was performed by PCR of genomic DNA. Morulea were lysed in 10 µl morulea lysis buffer for 10 min at 56°C and afterwards 10 min at 95°C. 2 µl of supernatant were directly used for the genotyping PCR (see Table 8). 2 µl of this PCR product were used for subsequent PCR2. Morula lysate was stored at -20°C for later re-genotyping.
Genotyping of mice was performed by PCR of genomic DNA extracted from mouse tails. Tails were lysed in 100 µl DirectPCR Lysis Reagent with 10 µg proteinase K at 55 °C and 300 rpm overnight. The next day, proteinase K activity was stopped by incubating the tail lysate for 15 min at 95°C. The lysate was centrifuged at full speed for 5 min and 2 µl supernatant was directly used for the genotyping PCR. Lysates were stored at -20°C for later re-genotyping.
The genotyping/sequencing PCRs for the different alleles were performed using RedTaqMix and primers as depicted in Table 8 and 45. *S1pr3*$^{fl/fl}$ genotyping generates a wild-type and a mutant

band of 185 bp/219 bp (LoxP 1) and 186bp/220 (LoxP 2), respectively. The PCR was performed with an Applied Biosystems thermocycler according to the PCR programs shown in Table 46. The PCR reactions were analysed by 2% agarose gel electrophoresis or with QIAxcel Advanced system according to manufacturer´s instructions.

Table 45 S1pr3$^{fl/fl}$ genotyping PCR mix

***S1pr3*$^{fl/fl}$ genotyping PCR mix**	
	1x
dd H_2O	9.5 µL
RedTaq Mix	12.5 µL
Primer S1pr3$^{fl/fl}$ for (10µM)	1 µL
Primer S1pr3$^{fl/fl}$ rev (10µM)	1 µL
DNA	2 µL

Table 46 S1pr3fl/fl genotyping PCR program

S1pr3$^{fl/fl}$ genotyping PCR program			
Step	Temperature [°C]	Time	
1	94	3 min	
2	94	1 min	35x
3	62	2 min	
4	72	1 min	
5	72	10 min	
6	4	forever	

4.2.6.7 Agarose gel electrophoresis

Agarose gel electrophoresis was used to separate DNA fragments obtained in the genotyping PCR reaction. Agarose was dissolved in 1x TBE buffer to generate 2% [w/v] agarose gels. 5 µl ethidium bromide was added to 100 ml gel. The entire PCR mix of the genotyping reaction and 7 µl of the O'Generuler 100 bp Plus DNA ladder were loaded onto the gel. Electrophoresis was performed at 140 V for 45 min. Bands were detected with a UV transluminator and band size was determined relative to the DNA ladder.

4.2.6.8 DNA extraction from agarose gels

For sequencing PCR amplicons, DNA bands of desired size were cut out of the agarose gel. DNA extraction was performed with the QIAquick Gel Extracton Kit according to the manufacturer´s guidelines.

4.2.6.9 Sequencing

The sequencing of plasmids or genomic DNA was performed by GATC Biotech. Purified genomic or plasmid DNA was diluted to an end concentration of 10-20 ng/µl. Primers (see Table 9) were used at a concentration of 10 pmol/µl.

4.2.7 Statistical analysis

Statistical analysis was performed using GraphPad Prism Software. Unless otherwise stated, data are expressed as mean±s.d. Statistical significance was determined by ANOVA followed by Dunnett´s Multiple Comparison Test. A p-value of less than 0.05 was considered statistically significant and marked by asterisks (*P<0.05, **P<0.01, ***P<0.001). n represents the number of independent mice or *in vitro* treated cell culture samples analysed per group.

Abbreviations

A	Ampere
Abcc9	ATP-binding cassette, subfamily C (CFTR/MRP)
Acta2	Smooth muscle actin gene
ACTA2	Alpha actin 2
Adi	Adipocytes
AF	Alexa Fluor
Angpt1	Angiopoietin 1
Anpep	Amino peptidase N
APS	Ammonium persulfate
ASNS	Asparagine synthetase
B2M	B2- Microglobulin
BBB	Blood brain barrier
BCA	Bicinchoninic acid
BCL2L1	B-cell lymphoma 2 like protein 1
bFGF	basic FGF
BM	Basement membrane
bp	Base pair
BP	Brain pericytes
BSA	Bovine serum albumin
c	Concentration; Centi
Ca^{2+}	Calcium
Cas	CRISPR-associated
Cas9n	Nickase
CASP3	Caspase 3
CCDC34	Coiled-coil domain containing 34
CD	Cluster of differentiation
CDH5	Cadherin 5
cDNA	Complementary DNA
Cer	Ceramide
CNS	Central nervous system
CO_2	Carbon dioxide
Col7A1	Collagen type 7 alpha 1 chain
COX	cyclooxygenase
CRISPR	Clustered Regularly Interspaced Short Palindromic Repeats
CT	Threshold cycle
Cu	Copper
DAPI	4´, 6-diamidino-2-phenylindole
DLK1	delta-like 1 homolog
DMEM	Dulbecco’s modified Eagle's medium
DMSO	Dimethyl sulfoxide
DNA	Deoxyribonucleic acid
DNase	Deoxyribonuclease
dNTP	Deoxynucleoside triphosphate
DP	Prostaglandin D2 receptor
DPH3	Diphthamide biosynthesis 3
ds	Double stranded
DSB	Double-strand break
EC	Endothelial cells
ECL	enhanced chemiluminescence

ECM	Extracellular matrix
EDG	Endothelial differentiation gene
EDTA	Ethylenediaminetetraacetic acid
eGFP	Enhanced green fluorescent protein
ELOF1	Elongation factor 1 homolog
EndMT	Endothelial mesenchymal transition
EP2	Prostaglandin E2 receptor
ER	Endoplasmatic reticulum
ERK	Extracellular signal-regulated kinase
ETOH	ethanol
FACS	Fluorescence activated cell sorting
FAK	Focal adhesion kinase
FC	Fold change
FCS	Fetal calf serum
FDR	False discovery rate
Fib	Fibroblasts
FITC	Fluorescein isothiocyanate
For	Forward
FP	Prostaglandin F receptor
FSC	Forward scatter
GSL	Glycosphingolipid
GSN	Gelsolin
GTP	Guanosine-triphosphate
h	hours
H_2O	Water
HBMEC	Human brain microvascular endothelial cells
HCl	Hydrochloric acid
HDBEC	Human dermal blood endothelial cells
HPRT	Hypoxanthin-guanin-phosphoribosyltransferase
HR	Homologous recombination
HRP	Horseradish peroxidase
Hs	Human
HSAVEC	Human saphenous vein endothelial cells
HSC	Hepatic stellate cells
HSPG	Heparan sulfate proteoglycans
HUAEC	Human umbilical artery endothelial cells
HUVEC	Human umbilical vein endothelial cells
Ifitm1	Interferon induced transmembrane protein 1
IGFR2	Insulin-like growth factor receptor 2
Indels	Insertions and deletions
IP	Prostacyclin receptor
Kcnj8	potassium inwardly rectifying channel, subfamily J
kD	Kilo Dalton
KDR	Kinase insert domain receptor
LoxP	Locus of crossover in P1
LP	Lung pericytes
LYVE1	lymphatic vessel endothelial hyaluronan receptor 1
MAPK	Mitogen-activated protein kinase
Min	Minutes
MMP	Metalloproteases
MP	Muscle pericytes
MPRIP	Myosin phosphatase Rho interacting protein

mRNA	Messenger ribonucleic acid
MRPL55	Mitochondrial ribosomal protein L5
Ms	Mouse
MSC	Mesenchymal stem cells
MSigDB	Moleculare Signature Database
MTORC1	Mammalian target of rapamycin complex 1
MYH10	Myosin heavy chain 10
NG2	Neural/glial antigen
NHEJ	Non-homologous end joining
NRP	Neuropilin
NSAID	Nonsteroidal anti-inflammatory drug
O_2	oxygen
Opti-MEM	Optimized Minimal Essential Medium
p	pico
PAM	Protospacer adjacent motif
PancP	Pancreas pericytes
PBS	Phosphate buffered saline
PCR	Polymerase chain reaction
Pdgfb	Platelet-derived growth factor beta
PDGFRα	Platelet derived growth factor receptor α
PDGFRβ	Platelet-derived growth factor receptor β
PDPN	Podoplanin
PECAM1	Platelet endothelial cell adhesion molecule 1
PFA	Paraformaldehyde
PGD_2	Prostaglandin D2
PGDS	Prostaglandin D synthase
PGE2	Prostaglandin E2
PGES	Prostaglandin E synthase
PGF2α	Prostaglandin F2α
PGFS	Prostaglandin F synthase
PGG_2	Prostaglandin G2
PGH_2	Prostaglandin H2
PGI_2	Prostaglandin I2/Prostacyclin
PGIS	Prostaglandin I synthase
PGT	Prostaglandin transporter
pH	power of hydrogen
PI3K	Phosphoinositide-3-kinase
PlGF	Placental growth factor
PLA2	Phospholipase A2
PlaP	Placenta pericytes
PLCy	Phospholipase C
PPAR	Peroxisome proliferator-activated receptor
PTGER1-4	Prostaglandin E Receptor 1-4
PTX	Pertussis toxin
Rev	Reverse
RGS5	Regulator of G-protein signaling 5
RNA	Ribonucleic acid
RNase	Ribonuclease
RT	Room temperature
RTCA	Real time cell analyzer
RT-qPCR	Real time-quantitative polymerase chain reaction
S100A4	S100 calcium-binding protein A4

S1P	Sphingosine-1-phosphate
S1PR1-5	Sphingosine-1-phosphate receptor 1-5
SDC1	Syndecan 1
SDS	Sodium dodecyl sulfate
SDS-PAGE	Sodium dodecyl sulfate polyacrylamide gel electrophoresis
Sec	Seconds
SGPP	Sphingosine-1-phosphate phosphatases
siRNA	Small interfering RNA
SM	Sphingomyelin
SMA	Smooth muscle actin
SMAD7	Mothers Against Decapentaplegic Homolog 7
SMC	Smooth muscle cells
SPHK	Sphingosine kinase
SPNS	Sphingosine-1-phosphate transporter
SSC	Side scatter
Taq	Thermus aquaticus
Tek	TEK tyrosine kinase, endothelial
TGFβ	Transforming growth factor β
Tie	Tyrosine kinase with immunoglobulin-like and EGF-like domains
Tm	Melting temperature
TP	Thromboxane receptor
TSC1	Tuberous sclerosis protein 1
TXA_2	Thromboxane A2
TxAS	Thromboxane synthase
U	Unit
UV	Ultra violet
V	Volt
v/v	Volume/volume (volume concentration)
VEGF	Vascular endothelial growth factor
VEGFR	Vascular endothelial growth factor receptor
Vtn	Vitronectin
WB	Western Blot
Zic1	Zink finger protein 201

Publications

Hasanov, Z.*, Ruckdeschel, T.*, König, C., Mogler, C., Kapel, S.S., Korn, C., Spegg, C., Eichwald, V., Wieland, M., Appak, S., Augustin, H.G. (2017). Endosialin promotes atherosclerosis through phenotypic remodeling of vascular smooth muscle cells. Arterioscler Thromb Vasc Biol. *37*, 495-505. * equal contribution

Roth, L., Prahst, C., Ruckdeschel, T., Savant, S., Weström, S., Fantin, A., Riedel, M., Héroult, M., Ruhrberg, C., Augustin, H.G. (2016). Neuropilin-1 mediates vascular permeability independently of vascular endothelial growth factor receptor-2 activation. Sci. Signal. *9*, ra42.

Teichert, M.*, Milde, L.*, Holm, A., Staniczek, L., Gengenbacher, N., Savant, S., Ruckdeschel, T., Hasanov, Z., Srivastava, K., Hu, J., Hertel, S., Bartol, A., Schlereth, K.*, Augustin, H.G* (2017). Pericyte-expressed Tie2 controls angiogenesis and vessel maturation. Nat.Commun. in press * equal contribution

References

Abramovitz, M., Adam, M., Boie, Y., Carrière, M., Denis, D., Godbout, C., Lamontagne, S., Rochette, C., Sawyer, N., Tremblay, N.M., et al. (2000). The utilization of recombinant prostanoid receptors to determine the affinities and selectivities of prostaglandins and related analogs. Biochim. Biophys. Acta *1483*, 285–293.

Abramsson, A., Berlin, Ö., Papayan, H., Paulin, D., Shani, M., and Betsholtz, C. (2002). Analysis of Mural Cell Recruitment to Tumor Vessels. Circulation *105*, 112–117.

Adams, R.H., and Alitalo, K. (2007). Molecular regulation of angiogenesis and lymphangiogenesis. Nat. Rev. Mol. Cell Biol. *8*, 464–478.

Alison, M.R., Nicholson, L.J., and Lin, W.-R. (2011). Chronic inflammation and hepatocellular carcinoma. Recent Results Cancer Res. Fortschritte Krebsforsch. Progres Dans Rech. Sur Cancer *185*, 135–148.

Alitalo, K. (2011). The lymphatic vasculature in disease. Nat. Med. *17*, 1371–1380.

Allende, M.L., Yamashita, T., and Proia, R.L. (2003). G-protein-coupled receptor S1P1 acts within endothelial cells to regulate vascular maturation. Blood *102*, 3665–3667.

Alm, K., El-Schich, Z., Miniotis, M.F., GjörloffWingren, A., Janicke, B., and Oredsson, S. (2013). Cells and holograms – holograms and digital holographic microscopy as a tool to study the morphology of living cells.

Amano, H., Ito, Y., Suzuki, T., Kato, S., Matsui, Y., Ogawa, F., Murata, T., Sugimoto, Y., Senior, R., Kitasato, H., et al. (2009). Roles of a prostaglandin E-type receptor, EP3, in upregulation of matrix metalloproteinase-9 and vascular endothelial growth factor during enhancement of tumor metastasis. Cancer Sci. *100*, 2318–2324.

Amano, M., Nakayama, M., and Kaibuchi, K. (2010). Rho-Kinase/ROCK: A key regulator of the cytoskeleton and cell polarity. Cytoskelet. Hoboken Nj *67*, 545–554.

An, S., Goetzl, E.J., and Lee, H. (1998). Signaling mechanisms and molecular characteristics of G protein-coupled receptors for lysophosphatidic acid and sphingosine 1-phosphate. J. Cell. Biochem. Suppl. *30–31*, 147–157.

An, S., Bleu, T., and Zheng, Y. (1999). Transduction of intracellular calcium signals through G protein-mediated activation of phospholipase C by recombinant sphingosine 1-phosphate receptors. Mol. Pharmacol. *55*, 787–794.

An, S., Zheng, Y., and Bleu, T. (2000). Sphingosine 1-phosphate-induced cell proliferation, survival, and related signaling events mediated by G protein-coupled receptors Edg3 and Edg5. J. Biol. Chem. *275*, 288–296.

Ancellin, N., and Hla, T. (1999). Differential pharmacological properties and signal transduction of the sphingosine 1-phosphate receptors EDG-1, EDG-3, and EDG-5. J. Biol. Chem. *274*, 18997–19002.

Aoki, T., Nishimura, M., Matsuoka, T., Yamamoto, K., Furuyashiki, T., Kataoka, H., Kitaoka, S., Ishibashi, R., Ishibazawa, A., Miyamoto, S., et al. (2011). PGE2-EP2 signalling in endothelium is activated by haemodynamic stress and induces cerebral aneurysm through an amplifying loop via NF-κB. Br. J. Pharmacol. *163*, 1237–1249.

Armulik, A., Abramsson, A., and Betsholtz, C. (2005). Endothelial/pericyte interactions. Circ. Res. *97*, 512–523.

Armulik, A., Genové, G., Mäe, M., Nisancioglu, M.H., Wallgard, E., Niaudet, C., He, L., Norlin, J., Lindblom, P., Strittmatter, K., et al. (2010). Pericytes regulate the blood-brain barrier. Nature *468*, 557–561.

Armulik, A., Genové, G., and Betsholtz, C. (2011). Pericytes: developmental, physiological, and pathological perspectives, problems, and promises. Dev. Cell *21*, 193–215.

Asahina, K., Zhou, B., Pu, W.T., and Tsukamoto, H. (2011). Septum transversum-derived mesothelium gives rise to hepatic stellate cells and perivascular mesenchymal cells in developing mouse liver. Hepatol. Baltim. Md *53*, 983–995.

Augustin, H.G., Koh, G.Y., Thurston, G., and Alitalo, K. (2009). Control of vascular morphogenesis and homeostasis through the angiopoietin-Tie system. Nat. Rev. Mol. Cell Biol. *10*, 165–177.

Baffert, F., Le, T., Sennino, B., Thurston, G., Kuo, C.J., Hu-Lowe, D., and McDonald, D.M. (2006). Cellular changes in normal blood capillaries undergoing regression after inhibition of VEGF signaling. Am. J. Physiol. - Heart Circ. Physiol. *290*, H547–H559.

Balabanov, R., Washington, R., Wagnerova, J., and Dore-Duffy, P. (1996). CNS microvascular pericytes express macrophage-like function, cell surface integrin alpha M, and macrophage marker ED-2. Microvasc. Res. *52*, 127–142.

Balsinde, J., Winstead, M.V., and Dennis, E.A. (2002). Phospholipase A2 regulation of arachidonic acid mobilization. FEBS Lett. *531*, 2–6.

Bandhuvula, P., and Saba, J.D. (2007). Sphingosine-1-phosphate lyase in immunity and cancer: silencing the siren. Trends Mol. Med. *13*, 210–217.

Barón, M., and Gallego, A. (1972). The relation of the microglia with the pericytes in the cat cerebral cortex. Z. Für Zellforsch. Mikrosk. Anat. *128*, 42–57.

Barrangou, R., Fremaux, C., Deveau, H., Richards, M., Boyaval, P., Moineau, S., Romero, D.A., and Horvath, P. (2007). CRISPR provides acquired resistance against viruses in prokaryotes. Science *315*, 1709–1712.

Bastepe, M., and Ashby, B. (1999). Identification of a region of the C-terminal domain involved in short-term desensitization of the prostaglandin EP4 receptor. Br. J. Pharmacol. *126*, 365–371.

Beauvais, D.M., Ell, B.J., McWhorter, A.R., and Rapraeger, A.C. (2009). Syndecan-1 regulates αvβ3 and αvβ5 integrin activation during angiogenesis and is blocked by synstatin, a novel peptide inhibitor. J. Exp. Med. *206*, 691–705.

Beckers, J., Clark, A., Wünsch, K., Hrabé De Angelis, M., and Gossler, A. (1999). Expression of the mouse Delta1 gene during organogenesis and fetal development. Mech. Dev. *84*, 165–168.

Berger, M., Bergers, G., Arnold, B., Hämmerling, G.J., and Ganss, R. (2005). Regulator of G-protein signaling-5 induction in pericytes coincides with active vessel remodeling during neovascularization. Blood *105*, 1094–1101.

Bergers, G., and Song, S. (2005). The role of pericytes in blood-vessel formation and maintenance. Neuro-Oncol. *7*, 452–464.

Bergers, G., Song, S., Meyer-Morse, N., Bergsland, E., and Hanahan, D. (2003). Benefits of targeting both pericytes and endothelial cells in the tumor vasculature with kinase inhibitors. J. Clin. Invest. *111*, 1287–1295.

Bergwerff, M., Verberne, M.E., DeRuiter, M.C., Poelmann, R.E., and Gittenberger-de-Groot, A.C. (1998). Neural crest cell contribution to the developing circulatory system. Circ. Res. *82*, 221–231.

Bernatchez, P.N., Soker, S., and Sirois, M.G. (1999). Vascular endothelial growth factor effect on endothelial cell proliferation, migration, and platelet-activating factor synthesis is Flk-1-dependent. J. Biol. Chem. *274*, 31047–31054.

Betsholtz, C. (2004). Insight into the physiological functions of PDGF through genetic studies in mice. Cytokine Growth Factor Rev. *15*, 215–228.

Betsholtz, C., Karlsson, L., and Lindahl, P. (2001). Developmental roles of platelet-derived growth factors. BioEssays News Rev. Mol. Cell. Dev. Biol. *23*, 494–507.

Birbrair, A., Zhang, T., Wang, Z.-M., Messi, M.L., Mintz, A., and Delbono, O. (2014). Pericytes: multitasking cells in the regeneration of injured, diseased, and aged skeletal muscle. Front. Aging Neurosci. *6*.

Bischoff, A., Czyborra, P., Fetscher, C., Meyer zu Heringdorf, D., Jakobs, K.H., and Michel, M.C. (2000). Sphingosine-1-phosphate and sphingosylphosphorylcholine constrict renal and mesenteric microvessels in vitro. Br. J. Pharmacol. *130*, 1871–1877.

Blaho, V.A., and Hla, T. (2011). Regulation of mammalian physiology, development, and disease by the sphingosine 1-phosphate and lysophosphatidic acid receptors. Chem. Rev. *111*, 6299–6320.

Blaho, V.A., and Hla, T. (2014). An update on the biology of sphingosine 1-phosphate receptors. J. Lipid Res. *55*, 1596–1608.

Blood, D.C. (1988). Baillière's Comprehensive Veterinary Dictionary (London: Baillère Tindall).

Bondjers, C., Kalén, M., Hellström, M., Scheidl, S.J., Abramsson, A., Renner, O., Lindahl, P., Cho, H., Kehrl, J., and Betsholtz, C. (2003). Transcription profiling of platelet-derived growth factor-B-deficient mouse embryos identifies RGS5 as a novel marker for pericytes and vascular smooth muscle cells. Am. J. Pathol. *162*, 721–729.

Bondjers, C., He, L., Takemoto, M., Norlin, J., Asker, N., Hellström, M., Lindahl, P., and Betsholtz, C. (2006). Microarray analysis of blood microvessels from PDGF-B and PDGF-Rbeta mutant mice identifies novel markers for brain pericytes. FASEB J. Off. Publ. Fed. Am. Soc. Exp. Biol. *20*, 1703–1705.

Bonvalet, J.P., Pradelles, P., and Farman, N. (1987). Segmental synthesis and actions of prostaglandins along the nephron. Am. J. Physiol. *253*, F377-387.

Bos, C.L., Richel, D.J., Ritsema, T., Peppelenbosch, M.P., and Versteeg, H.H. (2004). Prostanoids and prostanoid receptors in signal transduction. Int. J. Biochem. Cell Biol. *36*, 1187–1205.

Bose, A., Barik, S., Banerjee, S., Ghosh, T., Mallick, A., Bhattacharyya Majumdar, S., Goswami, K.K., Bhuniya, A., Banerjee, S., Baral, R., et al. (2013). Tumor-derived vascular pericytes anergize Th cells. J. Immunol. *191*, 971–981.

Bouchard, B.A., Shatos, M.A., and Tracy, P.B. (1997). Human brain pericytes differentially regulate expression of procoagulant enzyme complexes comprising the extrinsic pathway of blood coagulation. Arterioscler. Thromb. Vasc. Biol. *17*, 1–9.

Bresnick, A.R. (1999). Molecular mechanisms of nonmuscle myosin-II regulation. Curr. Opin. Cell Biol. *11*, 26–33.

Breyer, R.M., Bagdassarian, C.K., Myers, S.A., and Breyer, M.D. (2001). Prostanoid receptors: subtypes and signaling. Annu. Rev. Pharmacol. Toxicol. *41*, 661–690.

Brinkmann, V., Billich, A., Baumruker, T., Heining, P., Schmouder, R., Francis, G., Aradhye, S., and Burtin, P. (2010). Fingolimod (FTY720): discovery and development of an oral drug to treat multiple sclerosis. Nat. Rev. Drug Discov. *9*, 883–897.

Capecchi, M.R. (1989). Altering the genome by homologous recombination. Science *244*, 1288–1292.

Capecchi, M.R. (2001). Generating mice with targeted mutations. Nat. Med. *7*, 1086–1090.

Capecchi, M.R. (2005). Gene targeting in mice: functional analysis of the mammalian genome for the twenty-first century. Nat. Rev. Genet. *6*, 507–512.

Capetanaki, Y., Milner, D.J., and Weitzer, G. (1997). Desmin in muscle formation and maintenance: knockouts and consequences. Cell Struct. Funct. *22*, 103–116.

Carmeliet, P. (2003). Angiogenesis in health and disease. Nat. Med. *9*, 653–660.

Carmeliet, P. (2005). Angiogenesis in life, disease and medicine. Nature *438*, 932–936.

Carmeliet, P., Ferreira, V., Breier, G., Pollefeyt, S., Kieckens, L., Gertsenstein, M., Fahrig, M., Vandenhoeck, A., Harpal, K., Eberhardt, C., et al. (1996). Abnormal blood vessel development and lethality in embryos lacking a single VEGF allele. Nature *380*, 435–439.

Chan, J.P., Hu, Z., and Sieburth, D. (2012). Recruitment of sphingosine kinase to presynaptic terminals by a conserved muscarinic signaling pathway promotes neurotransmitter release. Genes Dev. *26*, 1070–1085.

Chang, Y., She, Z.-G., Sakimura, K., Roberts, A., Kucharova, K., Rowitch, D.H., and Stallcup, W.B. (2012). Ablation of NG2 proteoglycan leads to deficits in brown fat function and to adult onset obesity. PLOS ONE *7*, e30637.

Chan-Ling, T., Page, M.P., Gardiner, T., Baxter, L., Rosinova, E., and Hughes, S. (2004). Desmin ensheathment ratio as an indicator of vessel stability. Am. J. Pathol. *165*, 1301–1313.

Chappell, J.C., Taylor, S.M., Ferrara, N., and Bautch, V.L. (2009). Local guidance of emerging vessel sprouts requires soluble Flt-1. Dev. Cell *17*, 377–386.

Chen, Q., Zhang, H., Liu, Y., Adams, S., Eilken, H., Stehling, M., Corada, M., Dejana, E., Zhou, B., and Adams, R.H. (2016). Endothelial cells are progenitors of cardiac pericytes and vascular smooth muscle cells. Nat. Commun. *7*, 12422.

Chen, Y.-T., Chang, F.-C., Wu, C.-F., Chou, Y.-H., Hsu, H.-L., Chiang, W.-C., Shen, J., Chen, Y.-M., Wu, K.-D., Tsai, T.-J., et al. (2011). Platelet-derived growth factor receptor signaling activates pericyte-

myofibroblast transition in obstructive and post-ischemic kidney fibrosis. Kidney Int. *80*, 1170–1181.

Cheng, X., Wan, Y., Xu, Y., Zhou, Q., Wang, Y., and Zhu, H. (2015). Melatonin alleviates myosin light chain kinase expression and activity via the mitogen-activated protein kinase pathway during atherosclerosis in rabbits. Mol. Med. Rep. *11*, 99–104.

Cho, H., Kozasa, T., Bondjers, C., Betsholtz, C., and Kehrl, J.H. (2003). Pericyte-specific expression of Rgs5: implications for PDGF and EDG receptor signaling during vascular maturation. FASEB J. Off. Publ. Fed. Am. Soc. Exp. Biol. *17*, 440–442.

Cho, S.W., Kim, S., Kim, Y., Kweon, J., Kim, H.S., Bae, S., and Kim, J.-S. (2014). Analysis of off-target effects of CRISPR/Cas-derived RNA-guided endonucleases and nickases. Genome Res. *24*, 132–141.

Christian, S., Ahorn, H., Koehler, A., Eisenhaber, F., Rodi, H.P., Garin-Chesa, P., Park, J.E., Rettig, W.J., and Lenter, M.C. (2001). Molecular cloning and characterization of endosialin, a C-type lectin-like cell surface receptor of tumor endothelium. J. Biol. Chem. *276*, 7408–7414.

Christian, S., Winkler, R., Helfrich, I., Boos, A.M., Besemfelder, E., Schadendorf, D., and Augustin, H.G. (2008). Endosialin (Tem1) is a marker of tumor-associated myofibroblasts and tumor vessel-associated mural cells. Am. J. Pathol. *172*, 486–494.

Christoffersen, C., Obinata, H., Kumaraswamy, S.B., Galvani, S., Ahnström, J., Sevvana, M., Egerer-Sieber, C., Muller, Y.A., Hla, T., Nielsen, L.B., et al. (2011). Endothelium-protective sphingosine-1-phosphate provided by HDL-associated apolipoprotein M. Proc. Natl. Acad. Sci. U. S. A. *108*, 9613–9618.

Chu, V.T., Weber, T., Wefers, B., Wurst, W., Sander, S., Rajewsky, K., and Kühn, R. (2015). Increasing the efficiency of homology-directed repair for CRISPR-Cas9-induced precise gene editing in mammalian cells. Nat. Biotechnol. *33*, 543–548.

Cleaver, O., and Melton, D.A. (2003). Endothelial signaling during development. Nat. Med. *9*, 661–668.

Cohen, T., Gitay-Goren, H., Sharon, R., Shibuya, M., Halaban, R., Levi, B.Z., and Neufeld, G. (1995). VEGF121, a vascular endothelial growth factor (VEGF) isoform lacking heparin binding ability, requires cell-surface heparan sulfates for efficient binding to the VEGF receptors of human melanoma cells. J. Biol. Chem. *270*, 11322–11326.

Coleman, R.A., Smith, W.L., and Narumiya, S. (1994). International Union of Pharmacology classification of prostanoid receptors: properties, distribution, and structure of the receptors and their subtypes. Pharmacol. Rev. *46*, 205–229.

Colié, S., Van Veldhoven, P.P., Kedjouar, B., Bedia, C., Albinet, V., Sorli, S.-C., Garcia, V., Djavaheri-Mergny, M., Bauvy, C., Codogno, P., et al. (2009). Disruption of sphingosine 1-phosphate lyase confers resistance to chemotherapy and promotes oncogenesis through Bcl-2/Bcl-xL upregulation. Cancer Res. *69*, 9346–9353.

Cong, L., Ran, F.A., Cox, D., Lin, S., Barretto, R., Habib, N., Hsu, P.D., Wu, X., Jiang, W., Marraffini, L.A., et al. (2013). Multiplex genome engineering using CRISPR/Cas systems. Science *339*, 819–823.

Cooke, V.G., LeBleu, V.S., Keskin, D., Khan, Z., O'Connell, J.T., Teng, Y., Duncan, M.B., Xie, L., Maeda, G., Vong, S., et al. (2012). Pericyte depletion results in hypoxia-associated epithelial-to-mesenchymal transition and metastasis mediated by met signaling pathway. Cancer Cell *21*, 66–81.

Crisan, M., Yap, S., Casteilla, L., Chen, C.-W., Corselli, M., Park, T.S., Andriolo, G., Sun, B., Zheng, B., Zhang, L., et al. (2008a). A perivascular origin for mesenchymal stem cells in multiple human organs. Cell Stem Cell *3*, 301–313.

Crisan, M., Huard, J., Zheng, B., Sun, B., Yap, S., Logar, A., Giacobino, J.-P., Casteilla, L., and Péault, B. (2008b). Purification and culture of human blood vessel-associated progenitor cells. Curr. Protoc. Stem Cell Biol. *Chapter 2*, Unit 2B.2.1-2B.2.13.

Crisan, M., Deasy, B., Gavina, M., Zheng, B., Huard, J., Lazzari, L., and Péault, B. (2008c). Purification and long-term culture of multipotent progenitor cells affiliated with the walls of human blood vessels: myoendothelial cells and pericytes. Methods Cell Biol. *86*, 295–309.

Daneman, R., Zhou, L., Kebede, A.A., and Barres, B.A. (2010). Pericytes are required for blood-brain barrier integrity during embryogenesis. Nature *468*, 562–566.

Davis, R.J., Murdoch, C.E., Ali, M., Purbrick, S., Ravid, R., Baxter, G.S., Tilford, N., Sheldrick, R.L.G., Clark, K.L., and Coleman, R.A. (2004). EP4 prostanoid receptor-mediated vasodilatation of human middle cerebral arteries. Br. J. Pharmacol. *141*, 580–585.

De Palma, M., Venneri, M.A., Galli, R., Sergi Sergi, L., Politi, L.S., Sampaolesi, M., and Naldini, L. (2005). Tie2 identifies a hematopoietic lineage of proangiogenic monocytes required for tumor vessel formation and a mesenchymal population of pericyte progenitors. Cancer Cell *8*, 211–226.

Dejana, E. (2004). Endothelial cell–cell junctions: happy together. Nat. Rev. Mol. Cell Biol. *5*, 261–270.

Deriano, L., and Roth, D.B. (2013). Modernizing the nonhomologous end-joining repertoire: alternative and classical NHEJ share the stage. Annu. Rev. Genet. *47*, 433–455.

Dermietzel, R., and Krause, D. (1991). Molecular anatomy of the blood-brain barrier as defined by immunocytochemistry. Int. Rev. Cytol. *127*, 57–109.

DeRuiter, M.C., Poelmann, R.E., VanMunsteren, J.C., Mironov, V., Markwald, R.R., and Gittenberger-de Groot, A.C. (1997). Embryonic endothelial cells transdifferentiate into mesenchymal cells expressing smooth muscle actins in vivo and in vitro. Circ. Res. *80*, 444–451.

Desai, S., April, H., Nwaneshiudu, C., and Ashby, B. (2000). Comparison of agonist-induced internalization of the human EP2 and EP4 prostaglandin receptors: role of the carboxyl terminus in EP4 receptor sequestration. Mol. Pharmacol. *58*, 1279–1286.

Dey, I., Lejeune, M., and Chadee, K. (2006). Prostaglandin E2 receptor distribution and function in the gastrointestinal tract. Br. J. Pharmacol. *149*, 611–623.

Díaz-Flores, L., Gutiérrez, R., Varela, H., Rancel, N., and Valladares, F. (1991). Microvascular pericytes: a review of their morphological and functional characteristics. Histol. Histopathol. *6*, 269–286.

Diaz-Flores, L., Gutierrez, R., Lopez-Alonso, A., Gonzalez, R., and Varela, H. (1992). Pericytes as a supplementary source of osteoblasts in periosteal osteogenesis. Clin. Orthop. 280–286.

Díaz-Flores, L., Gutiérrez, R., Madrid, J.F., Varela, H., Valladares, F., Acosta, E., Martín-Vasallo, P., and Díaz-Flores, L. (2009). Pericytes. Morphofunction, interactions and pathology in a quiescent and activated mesenchymal cell niche. Histol. Histopathol. *24*, 909–969.

Ding, R., Darland, D.C., Parmacek, M.S., and D'Amore, P.A. (2004). Endothelial-mesenchymal interactions in vitro reveal molecular mechanisms of smooth muscle/pericyte differentiation. Stem Cells Dev. *13*, 509–520.

DiPietrantonio, H.J., and Dymecki, S.M. (2009). ZIC1 levels regulate mossy fiber neuron position and axon laterality choice in the ventral brain stem. Neuroscience *162*, 560–573.

Distler, J.H.W., Hirth, A., Kurowska-Stolarska, M., Gay, R.E., Gay, S., and Distler, O. (2003). Angiogenic and angiostatic factors in the molecular control of angiogenesis. Q. J. Nucl. Med. Off. Publ. Ital. Assoc. Nucl. Med. AIMN Int. Assoc. Radiopharmacol. IAR *47*, 149–161.

Djonov, V., Schmid, M., Tschanz, S.A., and Burri, P.H. (2000). Intussusceptive angiogenesis. Circ. Res. *86*, 286–292.

Dong, A., Seidel, C., Snell, D., Ekawardhani, S., Ahlskog, J.K.J., Baumann, M., Shen, J., Iwase, T., Tian, J., Stevens, R., et al. (2014). Antagonism of PDGF-BB suppresses subretinal neovascularization and enhances the effects of blocking VEGF-A. Angiogenesis *17*, 553–562.

Dore-Duffy, P., Katychev, A., Wang, X., and Van Buren, E. (2006). CNS microvascular pericytes exhibit multipotential stem cell activity. J. Cereb. Blood Flow Metab. Off. J. Int. Soc. Cereb. Blood Flow Metab. *26*, 613–624.

Driskell, R.R., Lichtenberger, B.M., Hoste, E., Kretzschmar, K., Simons, B.D., Charalambous, M., Ferron, S.R., Herault, Y., Pavlovic, G., Ferguson-Smith, A.C., et al. (2013). Distinct fibroblast lineages determine dermal architecture in skin development and repair. Nature *504*, 277–281.

Dudley, A.C. (2012). Tumor Endothelial Cells. Cold Spring Harb. Perspect. Med. *2*.

Dufourcq, P., Louis, H., Moreau, C., Daret, D., Boisseau, M.R., Lamazière, J.M., and Bonnet, J. (1998). Vitronectin expression and interaction with receptors in smooth muscle cells from human atheromatous plaque. Arterioscler. Thromb. Vasc. Biol. *18*, 168–176.

Dumont, D.J., Gradwohl, G., Fong, G.H., Puri, M.C., Gertsenstein, M., Auerbach, A., and Breitman, M.L. (1994). Dominant-negative and targeted null mutations in the endothelial receptor tyrosine kinase, tek, reveal a critical role in vasculogenesis of the embryo. Genes Dev. *8*, 1897–1909.

Durham, J.T., Surks, H.K., Dulmovits, B.M., and Herman, I.M. (2014). Pericyte contractility controls endothelial cell cycle progression and sprouting: insights into angiogenic switch mechanics. Am. J. Physiol. Cell Physiol. *307*, C878-892.

Egan, K.M., Lawson, J.A., Fries, S., Koller, B., Rader, D.J., Smyth, E.M., and Fitzgerald, G.A. (2004). COX-2-derived prostacyclin confers atheroprotection on female mice. Science *306*, 1954–1957.

Eibl, G., Bruemmer, D., Okada, Y., Duffy, J.P., Law, R.E., Reber, H.A., and Hines, O.J. (2003). PGE(2) is generated by specific COX-2 activity and increases VEGF production in COX-2-expressing human pancreatic cancer cells. Biochem. Biophys. Res. Commun. *306*, 887–897.

Ellis, L.M., and Hicklin, D.J. (2008). VEGF-targeted therapy: mechanisms of anti-tumour activity. Nat. Rev. Cancer *8*, 579–591.

Enge, M., Bjarnegård, M., Gerhardt, H., Gustafsson, E., Kalén, M., Asker, N., Hammes, H.-P., Shani, M., Fässler, R., and Betsholtz, C. (2002). Endothelium-specific platelet-derived growth factor-B ablation mimics diabetic retinopathy. EMBO J. *21*, 4307–4316.

Erber, R., Thurnher, A., Katsen, A.D., Groth, G., Kerger, H., Hammes, H.-P., Menger, M.D., Ullrich, A., and Vajkoczy, P. (2004). Combined inhibition of VEGF and PDGF signaling enforces tumor vessel regression by interfering with pericyte-mediated endothelial cell survival mechanisms. FASEB J. *18*, 338–340.

Etchevers, H.C., Vincent, C., Le Douarin, N.M., and Couly, G.F. (2001). The cephalic neural crest provides pericytes and smooth muscle cells to all blood vessels of the face and forebrain. Dev. Camb. Engl. *128*, 1059–1068.

Fabris, L., and Strazzabosco, M. (2011). Epithelial-mesenchymal interactions in biliary diseases. Semin. Liver Dis. *31*, 11–32.

Fabry, Z., Fitzsimmons, K.M., Herlein, J.A., Moninger, T.O., Dobbs, M.B., and Hart, M.N. (1993). Production of the cytokines interleukin 1 and 6 by murine brain microvessel endothelium and smooth muscle pericytes. J. Neuroimmunol. *47*, 23–34.

Falahi, F., Sgro, A., and Blancafort, P. (2015). Epigenome engineering in cancer: fairytale or a realistic path to the clinic? Front. Oncol. *5:22*.

Farahani, R.M., and Xaymardan, M. (2015). Platelet-derived growth factor receptor alpha as a marker of mesenchymal stem cells in development and stem cell biology. Stem Cells Int. *2015*, e362753.

Ferrara, N., Carver-Moore, K., Chen, H., Dowd, M., Lu, L., O'Shea, K.S., Powell-Braxton, L., Hillan, K.J., and Moore, M.W. (1996). Heterozygous embryonic lethality induced by targeted inactivation of the VEGF gene. Nature *380*, 439–442.

Ferrara, N., Gerber, H.-P., and LeCouter, J. (2003). The biology of VEGF and its receptors. Nat. Med. *9*, 669–676.

Ferrari-Dileo, G., Davis, E.B., and Anderson, D.R. (1992). Effects of cholinergic and adrenergic agonists on adenylate cyclase activity of retinal microvascular pericytes in culture. Invest. Ophthalmol. Vis. Sci. *33*, 42–47.

Ferrari-Dileo, G., Davis, E.B., and Anderson, D.R. (1996). Glaucoma, capillaries and pericytes. 3. Peptide hormone binding and influence on pericytes. Ophthalmol. *210*, 269–275.

Fiedler, U., Scharpfenecker, M., Koidl, S., Hegen, A., Grunow, V., Schmidt, J.M., Kriz, W., Thurston, G., and Augustin, H.G. (2004). The Tie-2 ligand angiopoietin-2 is stored in and rapidly released upon stimulation from endothelial cell Weibel-Palade bodies. Blood *103*, 4150–4156.

Fineran, P.C., and Charpentier, E. (2012). Memory of viral infections by CRISPR-Cas adaptive immune systems: acquisition of new information. Virology *434*, 202–209.

Fischer, I., Alliod, C., Martinier, N., Newcombe, J., Brana, C., and Pouly, S. (2011a). Sphingosine kinase 1 and sphingosine 1-phosphate receptor 3 are functionally upregulated on astrocytes under pro-inflammatory conditions. PLoS ONE *6*.

Fischer, S.M., Hawk, E., and Lubet, R.A. (2011b). Non-steroidal anti-inflammatory drugs and coxibs in chemoprevention: a commentary based primarily on animal studies. Cancer Prev. Res. Phila. Pa *4*, 1728–1735.

Folkman, J. (2006). Angiogenesis. Annu. Rev. Med. *57*, 1–18.

Folkman, J. (2007). Angiogenesis: an organizing principle for drug discovery? Nat. Rev. Drug Discov. *6*, 273–286.

Fraisl, P., Mazzone, M., Schmidt, T., and Carmeliet, P. (2009). Regulation of angiogenesis by oxygen and metabolism. Dev. Cell *16*, 167–179.

Fu, Y., Foden, J.A., Khayter, C., Maeder, M.L., Reyon, D., Joung, J.K., and Sander, J.D. (2013). High-frequency off-target mutagenesis induced by CRISPR-Cas nucleases in human cells. Nat. Biotechnol. *31*, 822–826.

Fujii, K., Machida, T., Iizuka, K., and Hirafuji, M. (2014). Sphingosine 1-phosphate increases an intracellular Ca2+ concentration via S1P3 receptor in cultured vascular smooth muscle cells. J. Pharm. Pharmacol. *66*, 802–810.

Fujikawa, L.S., Reay, C., and Morin, M.E. (1989). Class II antigens on retinal vascular endothelium, pericytes, macrophages, and lymphocytes of the rat. Invest. Ophthalmol. Vis. Sci. *30*, 66–73.

Fukuhara, S., Simmons, S., Kawamura, S., Inoue, A., Orba, Y., Tokudome, T., Sunden, Y., Arai, Y., Moriwaki, K., Ishida, J., et al. (2012). The sphingosine-1-phosphate transporter Spns2 expressed on endothelial cells regulates lymphocyte trafficking in mice. J. Clin. Invest. *122*, 1416–1426.

Fukushi, J., Inatani, M., Yamaguchi, Y., and Stallcup, W.B. (2003). Expression of NG2 proteoglycan during endochondral and intramembranous ossification. Dev. Dyn. Off. Publ. Am. Assoc. Anat. *228*, 143–148.

Fukushi, J., Makagiansar, I.T., and Stallcup, W.B. (2004). NG2 proteoglycan promotes endothelial cell motility and angiogenesis via engagement of galectin-3 and alpha3beta1 integrin. Mol. Biol. Cell *15*, 3580–3590.

Funa, K., and Sasahara, M. (2014). The roles of PDGF in development and during neurogenesis in the normal and diseased nervous system. J. Neuroimmune Pharmacol. *9*, 168–181.

Funahashi, Y., Shawber, C.J., Vorontchikhina, M., Sharma, A., Outtz, H.H., and Kitajewski, J. (2010). Notch regulates the angiogenic response via induction of VEGFR-1. J. Angiogenesis Res. *2*, 3.

Funk, C.D. (2001). Prostaglandins and leukotrienes: advances in eicosanoid biology. Science *294*, 1871–1875.

Gaengel, K., Niaudet, C., Hagikura, K., Laviña, B., Siemsen, B.L., Muhl, L., Hofmann, J.J., Ebarasi, L., Nyström, S., Rymo, S., et al. (2012). The sphingosine-1-phosphate receptor S1PR1 restricts sprouting angiogenesis by regulating the interplay between VE-cadherin and VEGFR2. Dev. Cell *23*, 587–599.

Gaj, T., Gersbach, C.A., and Barbas III, C.F. (2013). ZFN, TALEN, and CRISPR/Cas-based methods for genome engineering. Trends Biotechnol. *31*, 397–405.

Gardiner, P.J. (1986). Characterization of prostanoid relaxant/inhibitory receptors (psi) using a highly selective agonist, TR4979. Br. J. Pharmacol. *87*, 45–56.

Gee, M.S., Procopio, W.N., Makonnen, S., Feldman, M.D., Yeilding, N.M., and Lee, W.M.F. (2003). Tumor vessel development and maturation impose limits on the effectiveness of anti-vascular therapy. Am. J. Pathol. *162*, 183–193.

Geraldes, P., Hiraoka-Yamamoto, J., Matsumoto, M., Clermont, A., Leitges, M., Marette, A., Aiello, L.P., Kern, T.S., and King, G.L. (2009). Activation of PKC-delta and SHP-1 by hyperglycemia causes vascular cell apoptosis and diabetic retinopathy. Nat. Med. *15*, 1298–1306.

Gerhardt, H., and Betsholtz, C. (2003). Endothelial-pericyte interactions in angiogenesis. Cell Tissue Res. *314*, 15–23.

Gerhardt, H., Wolburg, H., and Redies, C. (2000). N-cadherin mediates pericytic-endothelial interaction during brain angiogenesis in the chicken. Dev. Dyn. Off. Publ. Am. Assoc. Anat. *218*, 472–479.

Gerhardt, H., Golding, M., Fruttiger, M., Ruhrberg, C., Lundkvist, A., Abramsson, A., Jeltsch, M., Mitchell, C., Alitalo, K., Shima, D., et al. (2003). VEGF guides angiogenic sprouting utilizing endothelial tip cell filopodia. J. Cell Biol. *161*, 1163–1177.

Giurdanella, G., Anfuso, C.D., Olivieri, M., Lupo, G., Caporarello, N., Eandi, C.M., Drago, F., Bucolo, C., and Salomone, S. (2015). Aflibercept, bevacizumab and ranibizumab prevent glucose-induced damage in human retinal pericytes in vitro, through a PLA2/COX-2/VEGF-A pathway. Biochem. Pharmacol. *96*, 278–287.

Goretzki, L., Burg, M.A., Grako, K.A., and Stallcup, W.B. (1999). High-affinity Binding of Basic Fibroblast Growth Factor and Platelet-derived Growth Factor-AA to the Core Protein of the NG2 Proteoglycan. J. Biol. Chem. *274*, 16831–16837.

Goumans, M.-J., Lebrin, F., and Valdimarsdottir, G. (2003). Controlling the angiogenic switch: a balance between two distinct TGF-b receptor signaling pathways. Trends Cardiovasc. Med. *13*, 301–307.

Grako, K.A., Ochiya, T., Barritt, D., Nishiyama, A., and Stallcup, W.B. (1999). PDGF (alpha)-receptor is unresponsive to PDGF-AA in aortic smooth muscle cells from the NG2 knockout mouse. J. Cell Sci. *112 (Pt 6)*, 905–915.

Gräler, M.H., Bernhardt, G., and Lipp, M. (1998). EDG6, a novel G-protein-coupled receptor related to receptors for bioactive lysophospholipids, is specifically expressed in lymphoid tissue. Genomics *53*, 164–169.

Greenberg, J.I., Shields, D.J., Barillas, S.G., Acevedo, L.M., Murphy, E., Huang, J., Scheppke, L., Stockmann, C., Johnson, R.S., Angle, N., et al. (2008). A role for VEGF as a negative regulator of pericyte function and vessel maturation. Nature *456*, 809–813.

Gruden, G., Zonca, S., Hayward, A., Thomas, S., Maestrini, S., Gnudi, L., and Viberti, G.C. (2000). Mechanical stretch-induced fibronectin and transforming growth factor-beta1 production in human mesangial cells is p38 mitogen-activated protein kinase-dependent. Diabetes *49*, 655–661.

Guan, H., Song, L., Cai, J., Huang, Y., Wu, J., Yuan, J., Li, J., and Li, M. (2011). Sphingosine kinase 1 regulates the Akt/FOXO3a/Bim pathway and contributes to apoptosis resistance in glioma cells. PLOS ONE *6*, e19946.

Gugliotta, P., Sapino, A., Macrí, L., Skalli, O., Gabbiani, G., and Bussolati, G. (1988). Specific demonstration of myoepithelial cells by anti-alpha smooth muscle actin antibody. J. Histochem. Cytochem. Off. J. Histochem. Soc. *36*, 659–663.

Gunther, E.C., von Bartheld, C.S., Goodman, L.J., Johnson, J.E., and Bothwell, M. (2000). The G-protein inhibitor, pertussis toxin, inhibits the secretion of brain-derived neurotrophic factor. Neuroscience *100*, 569–579.

Haefliger, I.O., Zschauer, A., and Anderson, D.R. (1994). Relaxation of retinal pericyte contractile tone through the nitric oxide-cyclic guanosine monophosphate pathway. Invest. Ophthalmol. Vis. Sci. *35*, 991–997.

Hall, A.P. (2006). Review of the pericyte during angiogenesis and its role in cancer and diabetic retinopathy. Toxicol. Pathol. *34*, 763–775.

Hammes, H.-P., Lin, J., Renner, O., Shani, M., Lundqvist, A., Betsholtz, C., Brownlee, M., and Deutsch, U. (2002). Pericytes and the pathogenesis of diabetic retinopathy. Diabetes *51*, 3107–3112.

Hammes, H.-P., Lin, J., Wagner, P., Feng, Y., Vom Hagen, F., Krzizok, T., Renner, O., Breier, G., Brownlee, M., and Deutsch, U. (2004). Angiopoietin-2 causes pericyte dropout in the normal retina: evidence for involvement in diabetic retinopathy. Diabetes *53*, 1104–1110.

Hamzah, J., Jugold, M., Kiessling, F., Rigby, P., Manzur, M., Marti, H.H., Rabie, T., Kaden, S., Gröne, H.-J., Hämmerling, G.J., et al. (2008). Vascular normalization in Rgs5-deficient tumours promotes immune destruction. Nature *453*, 410–414.

Hasanov, Z., Ruckdeschel, T., König, C., Mogler, C., Kapel, S.S., Korn, C., Spegg, C., Eichwald, V., Wieland, M., Appak, S., et al. (2017). Endosialin promotes atherosclerosis through phenotypic remodeling of vascular smooth muscle cells. Arterioscler. Thromb. Vasc. Biol. *3*, 495-505.

Hata, A.N., and Breyer, R.M. (2004). Pharmacology and signaling of prostaglandin receptors: multiple roles in inflammation and immune modulation. Pharmacol. Ther. *103*, 147–166.

Hauwaert, C.V. der, Savary, G., Gnemmi, V., Glowacki, F., Pottier, N., Bouillez, A., Maboudou, P., Zini, L., Leroy, X., Cauffiez, C., et al. (2013). Isolation and characterization of a primary proximal tubular epithelial cell model from human kidney by CD10/CD13 double labeling. PLOS ONE *8*, e66750.

He, L., Vanlandewijck, M., Raschperger, E., Mäe, M.A., Jung, B., Lebouvier, T., Ando, K., Hofmann, J., Keller, A., and Betsholtz, C. (2016). Analysis of the brain mural cell transcriptome. Sci. Rep. *6*, 35108.

Heldin, C.H., and Westermark, B. (1999). Mechanism of action and in vivo role of platelet-derived growth factor. Physiol. Rev. *79*, 1283–1316.

Heldin, C.H., Ostman, A., and Rönnstrand, L. (1998). Signal transduction via platelet-derived growth factor receptors. Biochim. Biophys. Acta *1378*, F79-113.

Hellström, M., Kalén, M., Lindahl, P., Abramsson, A., and Betsholtz, C. (1999). Role of PDGF-B and PDGFR-beta in recruitment of vascular smooth muscle cells and pericytes during embryonic blood vessel formation in the mouse. Dev. Camb. Engl. *126*, 3047–3055.

Hellström, M., Gerhardt, H., Kalén, M., Li, X., Eriksson, U., Wolburg, H., and Betsholtz, C. (2001). Lack of pericytes leads to endothelial hyperplasia and abnormal vascular morphogenesis. J. Cell Biol. *153*, 543–554.

Hellström, M., Phng, L.-K., Hofmann, J.J., Wallgard, E., Coultas, L., Lindblom, P., Alva, J., Nilsson, A.-K., Karlsson, L., Gaiano, N., et al. (2007). Dll4 signalling through Notch1 regulates formation of tip cells during angiogenesis. Nature *445*, 776–780.

Herbert, S.P., and Stainier, D.Y.R. (2011). Molecular control of endothelial cell behaviour during blood vessel morphogenesis. Nat. Rev. Mol. Cell Biol. *12*, 551–564.

Herman, I.M., and D'Amore, P.A. (1985). Microvascular pericytes contain muscle and nonmuscle actins. J. Cell Biol. *101*, 43–52.

Hernández, G.L., Volpert, O.V., Iñiguez, M.A., Lorenzo, E., Martínez-Martínez, S., Grau, R., Fresno, M., and Redondo, J.M. (2001). Selective inhibition of vascular endothelial growth factor-mediated angiogenesis by cyclosporin A: roles of the nuclear factor of activated T cells and cyclooxygenase 2. J. Exp. Med. *193*, 607–620.

Herrmann, H., Fouquet, B., and Franke, W.W. (1989). Expression of intermediate filament proteins during development of Xenopus laevis. II. Identification and molecular characterization of desmin. Dev. Camb. Engl. *105*, 299–307.

Hiratsuka, S., Minowa, O., Kuno, J., Noda, T., and Shibuya, M. (1998). Flt-1 lacking the tyrosine kinase domain is sufficient for normal development and angiogenesis in mice. Proc. Natl. Acad. Sci. *95*, 9349–9354.

Hirota, S., Helli, P., and Janssen, L.J. (2007). Ionic mechanisms and Ca2+ handling in airway smooth muscle. Eur. Respir. J. *30*, 114–133.

Hirschi, K.K., and D'Amore, P.A. (1996). Pericytes in the microvasculature. Cardiovasc. Res. *32*, 687–698.

Hirschi, K.K., and D'Amore, P.A. (1997). Control of angiogenesis by the pericyte: molecular mechanisms and significance. EXS *79*, 419–428.

Hirschi, K.K., Rohovsky, S.A., and D'Amore, P.A. (1998). PDGF, TGF-beta, and heterotypic cell-cell interactions mediate endothelial cell-induced recruitment of 10T1/2 cells and their differentiation to a smooth muscle fate. J. Cell Biol. *141*, 805–814.

Hizaki, H., Segi, E., Sugimoto, Y., Hirose, M., Saji, T., Ushikubi, F., Matsuoka, T., Noda, Y., Tanaka, T., Yoshida, N., et al. (1999). Abortive expansion of the cumulus and impaired fertility in mice lacking the prostaglandin E receptor subtype EP(2). Proc. Natl. Acad. Sci. U. S. A. *96*, 10501–10506.

Hla, T., and Maciag, T. (1990). An abundant transcript induced in differentiating human endothelial cells encodes a polypeptide with structural similarities to G-protein-coupled receptors. J. Biol. Chem. *265*, 9308–9313.

Hollinger, S., and Hepler, J.R. (2002). Cellular regulation of RGS proteins: modulators and integrators of G protein signaling. Pharmacol. Rev. *54*, 527–559.

Honda, T., Segi-Nishida, E., Miyachi, Y., and Narumiya, S. (2006). Prostacyclin-IP signaling and prostaglandin E2-EP2/EP4 signaling both mediate joint inflammation in mouse collagen-induced arthritis. J. Exp. Med. *203*, 325–335.

Hong, T., and Grabel, L.B. (2006). Migration of F9 parietal endoderm cells is regulated by the ERK pathway. J. Cell. Biochem. *97*, 1339–1349.

van Hooren, K.W.E.M., Spijkers, L.J.A., van Breevoort, D., Fernandez-Borja, M., Bierings, R., van Buul, J.D., Alewijnse, A.E., Peters, S.L.M., and Voorberg, J. (2014). Sphingosine-1-phosphate receptor 3 mediates sphingosine-1-phosphate induced release of weibel-palade bodies from endothelial cells. PloS One *9*, e91346.

Horvath, P., and Barrangou, R. (2010). CRISPR/Cas, the immune system of bacteria and archaea. Science *327*, 167–170.

Hsu, P., Shibata, M., and Leffler, C.W. (1993). Prostanoid synthesis in response to high CO2 in newborn pig brain microvascular endothelial cells. Am. J. Physiol. *264*, H1485-1492.

Hsu, P.D., Scott, D.A., Weinstein, J.A., Ran, F.A., Konermann, S., Agarwala, V., Li, Y., Fine, E.J., Wu, X., Shalem, O., et al. (2013). DNA targeting specificity of RNA-guided Cas9 nucleases. Nat. Biotechnol. *31*, 827–832.

Huang, M., Stolina, M., Sharma, S., Mao, J.T., Zhu, L., Miller, P.W., Wollman, J., Herschman, H., and Dubinett, S.M. (1998). Non-small cell lung cancer cyclooxygenase-2-dependent regulation of cytokine balance in lymphocytes and macrophages: up-regulation of interleukin 10 and down-regulation of interleukin 12 production. Cancer Res. *58*, 1208–1216.

Hung, C., Linn, G., Chow, Y.-H., Kobayashi, A., Mittelsteadt, K., Altemeier, W.A., Gharib, S.A., Schnapp, L.M., and Duffield, J.S. (2013). Role of lung pericytes and resident fibroblasts in the pathogenesis of pulmonary fibrosis. Am. J. Respir. Crit. Care Med. *188*, 820–830.

Hurtado-Alvarado, G., Cabañas-Morales, A.M., and Gómez-Gónzalez, B. (2014). Pericytes: brain-immune interface modulators. Front. Integr. Neurosci. *7*.

Igarashi, N., Okada, T., Hayashi, S., Fujita, T., Jahangeer, S., and Nakamura, S. (2003). Sphingosine kinase 2 is a nuclear protein and inhibits DNA synthesis. J. Biol. Chem. *278*, 46832–46839.

Im, D.S., Heise, C.E., Ancellin, N., O'Dowd, B.F., Shei, G.J., Heavens, R.P., Rigby, M.R., Hla, T., Mandala, S., McAllister, G., et al. (2000). Characterization of a novel sphingosine 1-phosphate receptor, Edg-8. J. Biol. Chem. *275*, 14281–14286.

Ishii, I., Ye, X., Friedman, B., Kawamura, S., Contos, J.J.A., Kingsbury, M.A., Yang, A.H., Zhang, G., Brown, J.H., and Chun, J. (2002). Marked perinatal lethality and cellular signaling deficits in mice null for the two sphingosine 1-phosphate (S1P) receptors, S1P(2)/LP(B2)/EDG-5 and S1P(3)/LP(B3)/EDG-3. J. Biol. Chem. *277*, 25152–25159.

Jaffer, S., Mattana, J., and Singhal, P.C. (1995). Effects of prostaglandin E2 on mesangial cell migration. Am. J. Nephrol. *15*, 300–305.

Jain, S., Chakraborty, G., Raja, R., Kale, S., and Kundu, G.C. (2008). Prostaglandin E2 regulates tumor angiogenesis in prostate cancer. Cancer Res. *68*, 7750–7759.

Jin, S.-W., and Patterson, C. (2009). The opening act: vasculogenesis and the origins of circulation. Arterioscler. Thromb. Vasc. Biol. *29*, 623–629.

Jinek, M., Chylinski, K., Fonfara, I., Hauer, M., Doudna, J.A., and Charpentier, E. (2012). A programmable dual-RNA-guided DNA endonuclease in adaptive bacterial immunity. Science *337*, 816–821.

Jing, H., Vassiliou, E., and Ganea, D. (2003). Prostaglandin E2 inhibits production of the inflammatory chemokines CCL3 and CCL4 in dendritic cells. J. Leukoc. Biol. *74*, 868–879.

Johansson, J.U., Pradhan, S., Lokteva, L.A., Woodling, N.S., Ko, N., Brown, H.D., Wang, Q., Loh, C., Cekanaviciute, E., Buckwalter, M., et al. (2013). Suppression of inflammation with conditional deletion of the prostaglandin E2 EP2 receptor in macrophages and brain microglia. J. Neurosci. Off. J. Soc. Neurosci. *33*, 16016–16032.

Johnson, K.R., Johnson, K.Y., Crellin, H.G., Ogretmen, B., Boylan, A.M., Harley, R.A., and Obeid, L.M. (2005). Immunohistochemical distribution of sphingosine kinase 1 in normal and tumor lung tissue. J. Histochem. Cytochem. Off. J. Histochem. Soc. *53*, 1159–1166.

Jones, N., Voskas, D., Master, Z., Sarao, R., Jones, J., and Dumont, D.J. (2001). Rescue of the early vascular defects in Tek/Tie2 null mice reveals an essential survival function. EMBO Rep. *2*, 438–445.

Joyce, N.C., DeCamilli, P., and Boyles, J. (1984). Pericytes, like vascular smooth muscle cells, are immunocytochemically positive for cyclic GMP-dependent protein kinase. Microvasc. Res. *28*, 206–219.

Juarez, J.G., Harun, N., Thien, M., Welschinger, R., Baraz, R., Pena, A.D., Pitson, S.M., Rettig, M., DiPersio, J.F., Bradstock, K.F., et al. (2012). Sphingosine-1-phosphate facilitates trafficking of hematopoietic stem cells and their mobilization by CXCR4 antagonists in mice. Blood *119*, 707–716.

Kabashima, K., Sakata, D., Nagamachi, M., Miyachi, Y., Inaba, K., and Narumiya, S. (2003). Prostaglandin E2-EP4 signaling initiates skin immune responses by promoting migration and maturation of Langerhans cells. Nat. Med. *9*, 744–749.

Kaipainen, A., Korhonen, J., Mustonen, T., van Hinsbergh, V.W., Fang, G.H., Dumont, D., Breitman, M., and Alitalo, K. (1995). Expression of the fms-like tyrosine kinase 4 gene becomes restricted to lymphatic endothelium during development. Proc. Natl. Acad. Sci. U. S. A. *92*, 3566–3570.

Kamiyama, M., Pozzi, A., Yang, L., DeBusk, L.M., Breyer, R.M., and Lin, P.C. (2006). EP2, a receptor for PGE2, regulates tumor angiogenesis through direct effects on endothelial cell motility and survival. Oncogene *25*, 7019–7028.

Kaneko-Kawano, T., Takasu, F., Naoki, H., Sakumura, Y., Ishii, S., Ueba, T., Eiyama, A., Okada, A., Kawano, Y., and Suzuki, K. (2012). Dynamic regulation of myosin light chain phosphorylation by Rho-kinase. PLOS ONE *7*, e39269.

Kanwar, Y.S., Wada, J., Sun, L., Xie, P., Wallner, E.I., Chen, S., Chugh, S., and Danesh, F.R. (2008). Diabetic nephropathy: mechanisms of renal disease progression. Exp. Biol. Med. *233*, 4–11.

Kashfi, K., and Rigas, B. (2005). Non-COX-2 targets and cancer: expanding the molecular target repertoire of chemoprevention. Biochem. Pharmacol. *70*, 969–986.

Katsuyama, M., Nishigaki, N., Sugimoto, Y., Morimoto, K., Negishi, M., Narumiya, S., and Ichikawa, A. (1995). The mouse prostaglandin E receptor EP2 subtype: cloning, expression, and northern blot analysis. FEBS Lett. *372*, 151–156.

Kawamori, T., Uchiya, N., Nakatsugi, S., Watanabe, K., Ohuchida, S., Yamamoto, H., Maruyama, T., Kondo, K., Sugimura, T., and Wakabayashi, K. (2001). Chemopreventive effects of ONO-8711, a

selective prostaglandin E receptor EP(1) antagonist, on breast cancer development. Carcinogenesis *22*, 2001–2004.

Keck, P.J., Hauser, S.D., Krivi, G., Sanzo, K., Warren, T., Feder, J., and Connolly, D.T. (1989). Vascular permeability factor, an endothelial cell mitogen related to PDGF. Science *246*, 1309–1312.

Kennedy, C.R., Zhang, Y., Brandon, S., Guan, Y., Coffee, K., Funk, C.D., Magnuson, M.A., Oates, J.A., Breyer, M.D., and Breyer, R.M. (1999). Salt-sensitive hypertension and reduced fertility in mice lacking the prostaglandin EP2 receptor. Nat. Med. *5*, 217–220.

Kennedy-Lydon, T.M., Crawford, C., Wildman, S.S.P., and Peppiatt-Wildman, C.M. (2013). Renal pericytes: regulators of medullary blood flow. Acta Physiol. Oxf. Engl. *207*, 212–225.

Keul, P., Lucke, S., von Wnuck Lipinski, K., Bode, C., Gräler, M., Heusch, G., and Levkau, B. (2011). Sphingosine-1-phosphate receptor 3 promotes recruitment of monocyte/macrophages in inflammation and atherosclerosis. Circ. Res. *108*, 314–323.

Kida, S., Steart, P.V., Zhang, E.T., and Weller, R.O. (1993). Perivascular cells act as scavengers in the cerebral perivascular spaces and remain distinct from pericytes, microglia and macrophages. Acta Neuropathol. (Berl.) *85*, 646–652.

Kienast, Y., von Baumgarten, L., Fuhrmann, M., Klinkert, W.E.F., Goldbrunner, R., Herms, J., and Winkler, F. (2010). Real-time imaging reveals the single steps of brain metastasis formation. Nat. Med. *16*, 116–122.

Kim, M., Allen, B., Korhonen, E.A., Nitschké, M., Yang, H.W., Baluk, P., Saharinen, P., Alitalo, K., Daly, C., Thurston, G., et al. (2016). Opposing actions of angiopoietin-2 on Tie2 signaling and FOXO1 activation. J. Clin. Invest. *126*, 3511–3525.

Kluk, M.J., and Hla, T. (2001). Role of the sphingosine 1-phosphate receptor EDG-1 in vascular smooth muscle cell proliferation and migration. Circ. Res. *89*, 496–502.

Koch, S., and Claesson-Welsh, L. (2012). Signal transduction by vascular endothelial growth factor receptors. Cold Spring Harb. Perspect. Med. *2*.

Koch, S., Tugues, S., Li, X., Gualandi, L., and Claesson-Welsh, L. (2011). Signal transduction by vascular endothelial growth factor receptors. Biochem. J. *437*, 169–183.

Kohno, M., Momoi, M., Oo, M.L., Paik, J.-H., Lee, Y.-M., Venkataraman, K., Ai, Y., Ristimaki, A.P., Fyrst, H., Sano, H., et al. (2006). Intracellular role for sphingosine kinase 1 in intestinal adenoma cell proliferation. Mol. Cell. Biol. *26*, 7211–7223.

Konger, R.L., Billings, S.D., Prall, N.C., Katona, T.M., DaSilva, S.C., Kennedy, C.R.J., Badve, S., Perkins, S.M., and LaCelle, P.T. (2009). The EP1 subtype of prostaglandin E2 receptor: role in keratinocyte differentiation and expression in non-melanoma skin cancer. Prostaglandins Leukot. Essent. Fatty Acids *81*, 279–290.

Kono, M., Mi, Y., Liu, Y., Sasaki, T., Allende, M.L., Wu, Y.-P., Yamashita, T., and Proia, R.L. (2004). The sphingosine-1-phosphate receptors S1P1, S1P2, and S1P3 function coordinately during embryonic angiogenesis. J. Biol. Chem. *279*, 29367–29373.

Korhonen, E.A., Lampinen, A., Giri, H., Anisimov, A., Kim, M., Allen, B., Fang, S., D'Amico, G., Sipilä, T.J., Lohela, M., et al. (2016). Tie1 controls angiopoietin function in vascular remodeling and inflammation. J. Clin. Invest. *126*, 3495–3510.

Krall, A.S., Xu, S., Graeber, T.G., Braas, D., and Christofk, H.R. (2016). Asparagine promotes cancer cell proliferation through use as an amino acid exchange factor. Nat. Commun. *7*, 11457.

Kristensson, K., and Olsson, Y. (1973). Accumulation of protein tracers in pericytes of the central nervous system following systemic injection in immature mice. Acta Neurol. Scand. *49*, 189–194.

Kunikata, T., Yamane, H., Segi, E., Matsuoka, T., Sugimoto, Y., Tanaka, S., Tanaka, H., Nagai, H., Ichikawa, A., and Narumiya, S. (2005). Suppression of allergic inflammation by the prostaglandin E receptor subtype EP3. Nat. Immunol. *6*, 524–531.

Laties, A.M., Rapoport, S.I., and McGlinn, A. (1979). Hypertensive breakdown of cerebral but not of retinal blood vessels in rhesus monkey. Arch. Ophthalmol. *97*, 1511–1514.

Lax, S., Hou, T.Z., Jenkinson, E., Salmon, M., MacFadyen, J.R., Isacke, C.M., Anderson, G., Cunningham, A.F., and Buckley, C.D. (2007). CD248/Endosialin is dynamically expressed on a subset of stromal cells during lymphoid tissue development, splenic remodeling and repair. FEBS Lett. *581*, 3550–3556.

Le Stunff, H., Giussani, P., Maceyka, M., Lépine, S., Milstien, S., and Spiegel, S. (2007). Recycling of sphingosine is regulated by the concerted actions of sphingosine-1-phosphate phosphohydrolase 1 and sphingosine kinase 2. J. Biol. Chem. *282*, 34372–34380.

Lee, A.Y., and Lloyd, K.C.K. (2014). Conditional targeting of Ispd using paired Cas9 nickase and a single DNA template in mice. FEBS Open Bio *4*, 637–642.

Lee, M.J., Evans, M., and Hla, T. (1996). The inducible G protein-coupled receptor edg-1 signals via the G(i)/mitogen-activated protein kinase pathway. J. Biol. Chem. *271*, 11272–11279.

Lee, M.J., Thangada, S., Claffey, K.P., Ancellin, N., Liu, C.H., Kluk, M., Volpi, M., Sha'afi, R.I., and Hla, T. (1999). Vascular endothelial cell adherens junction assembly and morphogenesis induced by sphingosine-1-phosphate. Cell *99*, 301–312.

Lee, T.S., Hu, K.Q., Chao, T., and King, G.L. (1989). Characterization of endothelin receptors and effects of endothelin on diacylglycerol and protein kinase C in retinal capillary pericytes. Diabetes *38*, 1643–1646.

Leslie, J.D., Ariza-McNaughton, L., Bermange, A.L., McAdow, R., Johnson, S.L., and Lewis, J. (2007). Endothelial signalling by the Notch ligand Delta-like 4 restricts angiogenesis. Dev. Camb. Engl. *134*, 839–844.

Levéen, P., Pekny, M., Gebre-Medhin, S., Swolin, B., Larsson, E., and Betsholtz, C. (1994). Mice deficient for PDGF B show renal, cardiovascular, and hematological abnormalities. Genes Dev. *8*, 1875–1887.

Li, D.Y., Sorensen, L.K., Brooke, B.S., Urness, L.D., Davis, E.C., Taylor, D.G., Boak, B.B., and Wendel, D.P. (1999). Defective angiogenesis in mice lacking endoglin. Science *284*, 1534–1537.

Li, J., Guan, H.-Y., Gong, L.-Y., Song, L.-B., Zhang, N., Wu, J., Yuan, J., Zheng, Y.-J., Huang, Z.-S., and Li, M. (2008). Clinical significance of sphingosine kinase-1 expression in human astrocytomas progression and overall patient survival. Clin. Cancer Res. *14*, 6996–7003.

Li, W., Yu, C.-P., Xia, J., Zhang, L., Weng, G.-X., Zheng, H., Kong, Q., Hu, L., Zeng, M.-S., Zeng, Y., et al. (2009). Sphingosine kinase 1 is associated with gastric cancer progression and poor survival of patients. Clin. Cancer Res. Off. J. Am. Assoc. Cancer Res. *15*, 1393–1399.

Lin, C., Li, H., Hao, M., Xiong, D., Luo, Y., Huang, C., Yuan, Q., Zhang, J., and Xia, N. (2016). Increasing the efficiency of CRISPR/Cas9-mediated precise genome editing of HSV-1 Virus in human cells. Sci. Rep. *6*, 34531.

Lindahl, P., Johansson, B.R., Levéen, P., and Betsholtz, C. (1997). Pericyte loss and microaneurysm formation in PDGF-B-deficient mice. Science *277*, 242–245.

Lindblom, P., Gerhardt, H., Liebner, S., Abramsson, A., Enge, M., Hellstrom, M., Backstrom, G., Fredriksson, S., Landegren, U., Nystrom, H.C., et al. (2003). Endothelial PDGF-B retention is required for proper investment of pericytes in the microvessel wall. Genes Dev. *17*, 1835–1840.

Liu, X., Yue, S., Li, C., Yang, L., You, H., and Li, L. (2011). Essential roles of sphingosine 1-phosphate receptor types 1 and 3 in human hepatic stellate cells motility and activation. J. Cell. Physiol. *226*, 2370–2377.

Liu, Y., Wada, R., Yamashita, T., Mi, Y., Deng, C.X., Hobson, J.P., Rosenfeldt, H.M., Nava, V.E., Chae, S.S., Lee, M.J., et al. (2000). Edg-1, the G protein-coupled receptor for sphingosine-1-phosphate, is essential for vascular maturation. J. Clin. Invest. *106*, 951–961.

Liu, Y., Deng, B., Zhao, Y., Xie, S., and Nie, R. (2013). Differentiated markers in undifferentiated cells: expression of smooth muscle contractile proteins in multipotent bone marrow mesenchymal stem cells. Dev. Growth Differ. *55*, 591–605.

Livak, K.J., and Schmittgen, T.D. (2001). Analysis of relative gene expression data using real-time quantitative PCR and the 2(-Delta Delta C(T)) Method. Methods San Diego Calif *25*, 402–408.

Lobov, I.B., Renard, R.A., Papadopoulos, N., Gale, N.W., Thurston, G., Yancopoulos, G.D., and Wiegand, S.J. (2007). Delta-like ligand 4 (Dll4) is induced by VEGF as a negative regulator of angiogenic sprouting. Proc. Natl. Acad. Sci. U. S. A. *104*, 3219–3224.

Ma, Y., Chen, W., Zhang, X., Yu, L., Dong, W., Pan, S., Gao, S., Huang, X., and Zhang, L. (2016). Increasing the efficiency of CRISPR/Cas9-mediated precise genome editing in rats by inhibiting NHEJ and using Cas9 protein. RNA Biol. *13*, 605–612.

Maceyka, M., Harikumar, K.B., Milstien, S., and Spiegel, S. (2012). Sphingosine-1-phosphate signaling and its role in disease. Trends Cell Biol. *22*, 50–60.

MacFadyen, J., Savage, K., Wienke, D., and Isacke, C.M. (2007). Endosialin is expressed on stromal fibroblasts and CNS pericytes in mouse embryos and is downregulated during development. Gene Expr. Patterns GEP *7*, 363–369.

Mali, P., Yang, L., Esvelt, K.M., Aach, J., Guell, M., DiCarlo, J.E., Norville, J.E., and Church, G.M. (2013). RNA-guided human genome engineering via Cas9. Science *339*, 823–826.

Mancuso, M.R., Davis, R., Norberg, S.M., O'Brien, S., Sennino, B., Nakahara, T., Yao, V.J., Inai, T., Brooks, P., Freimark, B., et al. (2006). Rapid vascular regrowth in tumors after reversal of VEGF inhibition. J. Clin. Invest. *116*, 2610–2621.

Mandarino, L.J., Sundarraj, N., Finlayson, J., and Hassell, H.R. (1993). Regulation of fibronectin and laminin synthesis by retinal capillary endothelial cells and pericytes in vitro. Exp. Eye Res. *57*, 609–621.

Marchetti, C., and Piacentini, C. (1990). [Light microscopy and electron microscopy study of the lymphatic capillaries of human dental pulp]. Bull. Group. Int. Rech. Sci. Stomatol. Odontol. *33*, 19–23.

Maruyama, T., Dougan, S.K., Truttmann, M., Bilate, A.M., Ingram, J.R., and Ploegh, H.L. (2015). Inhibition of non-homologous end joining increases the efficiency of CRISPR/Cas9-mediated precise genome editing. Nat. Biotechnol. *33*, 538–542.

Massberg, S., Schaerli, P., Knezevic-Maramica, I., Köllnberger, M., Tubo, N., Moseman, E.A., Huff, I.V., Junt, T., Wagers, A.J., Mazo, I.B., et al. (2007). Immunosurveillance by hematopoietic progenitor cells trafficking through blood, lymph, and peripheral tissues. Cell *131*, 994–1008.

Mato, M., Ookawara, S., Sakamoto, A., Aikawa, E., Ogawa, T., Mitsuhashi, U., Masuzawa, T., Suzuki, H., Honda, M., Yazaki, Y., et al. (1996). Involvement of specific macrophage-lineage cells surrounding arterioles in barrier and scavenger function in brain cortex. Proc. Natl. Acad. Sci. U. S. A. *93*, 3269–3274.

Matsuoka, T., Hirata, M., Tanaka, H., Takahashi, Y., Murata, T., Kabashima, K., Sugimoto, Y., Kobayashi, T., Ushikubi, F., Aze, Y., et al. (2000). Prostaglandin D2 as a mediator of allergic asthma. Science *287*, 2013–2017.

Maxwell, D.S., and Kruger, L. (1965). Small blood vessels and the origin of phagocytes in the rat cerebral cortex following heavy particle irradiation. Exp. Neurol. *12*, 33–54.

McVerry, B.J., Peng, X., Hassoun, P.M., Sammani, S., Simon, B.A., and Garcia, J.G.N. (2004). Sphingosine 1-phosphate reduces vascular leak in murine and canine models of acute lung injury. Am. J. Respir. Crit. Care Med. *170*, 987–993.

Mendelson, K., Evans, T., and Hla, T. (2014). Sphingosine 1-phosphate signalling. Dev. Camb. Engl. *141*, 5–9.

Merelli, B., Massi, D., Cattaneo, L., and Mandalà, M. (2014). Targeting the PD1/PD-L1 axis in melanoma: biological rationale, clinical challenges and opportunities. Crit. Rev. Oncol. Hematol. *89*, 140–165.

Milne, S.A., Perchick, G.B., Boddy, S.C., and Jabbour, H.N. (2001). Expression, localization, and signaling of PGE2 and EP2/EP4 receptors in human nonpregnant endometrium across the menstrual cycle. J. Clin. Endocrinol. Metab. *86*, 4453–4459.

Milner, D.J., Mavroidis, M., Weisleder, N., and Capetanaki, Y. (2000). Desmin cytoskeleton linked to muscle mitochondrial distribution and respiratory function. J. Cell Biol. *150*, 1283–1298.

Mina-Osorio, P., Winnicka, B., O'Conor, C., Grant, C.L., Vogel, L.K., Rodriguez-Pinto, D., Holmes, K.V., Ortega, E., and Shapiro, L.H. (2008). CD13 is a novel mediator of monocytic/endothelial cell adhesion. J. Leukoc. Biol. *84*, 448–459.

Mitterberger, M.C., Lechner, S., Mattesich, M., Kaiser, A., Probst, D., Wenger, N., Pierer, G., and Zwerschke, W. (2012). DLK1(PREF1) is a negative regulator of adipogenesis in $CD105^{+}/CD90^{+}/CD34^{+}/CD31^{-}/FABP4^{-}$ adipose-derived stromal cells from subcutaneous abdominal fat pats of adult women. Stem Cell Res. *9*, 35–48.

Miyaoka, Y., Berman, J.R., Cooper, S.B., Mayerl, S.J., Chan, A.H., Zhang, B., Karlin-Neumann, G.A., and Conklin, B.R. (2016). Systematic quantification of HDR and NHEJ reveals effects of locus, nuclease, and cell type on genome-editing. Sci. Rep. *6*.

Mizugishi, K., Yamashita, T., Olivera, A., Miller, G.F., Spiegel, S., and Proia, R.L. (2005). Essential role for sphingosine kinases in neural and vascular development. Mol. Cell. Biol. *25*, 11113–11121.

Mogler, C., Wieland, M., König, C., Hu, J., Runge, A., Korn, C., Besemfelder, E., Breitkopf-Heinlein, K., Komljenovic, D., Dooley, S., et al. (2015). Hepatic stellate cell-expressed endosialin balances fibrogenesis and hepatocyte proliferation during liver damage. EMBO Mol. Med. *7*, 332–338.

Morikawa, S., Baluk, P., Kaidoh, T., Haskell, A., Jain, R.K., and McDonald, D.M. (2002). Abnormalities in pericytes on blood vessels and endothelial sprouts in tumors. Am. J. Pathol. *160*, 985–1000.

Moriyama, T., Higashi, T., Togashi, K., Iida, T., Segi, E., Sugimoto, Y., Tominaga, T., Narumiya, S., and Tominaga, M. (2005). Sensitization of TRPV1 by EP1 and IP reveals peripheral nociceptive mechanism of prostaglandins. Mol. Pain *1*, 3.

Mousseau, Y., Mollard, S., Richard, L., Nizou, A., Faucher-Durand, K., Cook-Moreau, J., Qiu, H., Baaj, Y., Funalot, B., Fourcade, L., et al. (2012a). Fingolimod inhibits PDGF-B-induced migration of vascular smooth muscle cell by down-regulating the S1PR1/S1PR3 pathway. Biochimie *94*, 2523–2531.

Mousseau, Y., Mollard, S., Faucher-Durand, K., Richard, L., Nizou, A., Cook-Moreau, J., Baaj, Y., Qiu, H., Plainard, X., Fourcade, L., et al. (2012b). Fingolimod potentiates the effects of sunitinib malate in a rat breast cancer model. Breast Cancer Res. Treat. *134*, 31–40.

Müller, S.M., Stolt, C.C., Terszowski, G., Blum, C., Amagai, T., Kessaris, N., Iannarelli, P., Richardson, W.D., Wegner, M., and Rodewald, H.-R. (2008). Neural crest origin of perivascular mesenchyme in the adult thymus. J. Immunol. Baltim. Md 1950 *180*, 5344–5351.

Murakami, A., Takasugi, H., Ohnuma, S., Koide, Y., Sakurai, A., Takeda, S., Hasegawa, T., Sasamori, J., Konno, T., Hayashi, K., et al. (2010). Sphingosine 1-phosphate (S1P) regulates vascular contraction via S1P3 receptor: investigation based on a new S1P3 receptor antagonist. Mol. Pharmacol. *77*, 704–713.

Murfee, W.L., Skalak, T.C., and Peirce, S.M. (2005). Differential arterial/venous expression of NG2 proteoglycan in perivascular cells along microvessels: identifying a venule-specific phenotype. Microcirculation *12*, 151–160.

Mutoh, M., Watanabe, K., Kitamura, T., Shoji, Y., Takahashi, M., Kawamori, T., Tani, K., Kobayashi, M., Maruyama, T., Kobayashi, K., et al. (2002). Involvement of prostaglandin E receptor subtype EP(4) in colon carcinogenesis. Cancer Res. *62*, 28–32.

Nakanishi, M., and Rosenberg, D.W. (2013). Multifaceted roles of PGE2 in inflammation and cancer. Semin. Immunopathol. *35*, 123–137.

Nakano, M., Atobe, Y., Goris, R.C., Yazama, F., Ono, M., Sawada, H., Kadota, T., Funakoshi, K., and Kishida, R. (2000). Ultrastructure of the capillary pericytes and the expression of smooth muscle alpha-actin and desmin in the snake infrared sensory organs. Anat. Rec. *260*, 299–307.

Narumiya, S., Sugimoto, Y., and Ushikubi, F. (1999). Prostanoid receptors: structures, properties, and functions. Physiol. Rev. *79*, 1193–1226.

Nataraj, C., Thomas, D.W., Tilley, S.L., Nguyen, M., Mannon, R., Koller, B.H., and Coffman, T.M. (2001). Receptors for prostaglandin E2 that regulate cellular immune responses in the mouse. J. Clin. Invest. *108*, 1229–1235.

Navarro, R., Compte, M., Álvarez-Vallina, L., and Sanz, L. (2016). Immune regulation by pericytes: modulating innate and adaptive immunity. Front. Immunol. *7*.

Nehls, V., and Drenckhahn, D. (1991). Heterogeneity of microvascular pericytes for smooth muscle type alpha-actin. J. Cell Biol. *113*, 147–154.

Nehls, V., Denzer, K., and Drenckhahn, D. (1992). Pericyte involvement in capillary sprouting during angiogenesis in situ. Cell Tissue Res. *270*, 469–474.

Neufeld, G., Kessler, O., and Herzog, Y. (2002). The interaction of Neuropilin-1 and Neuropilin-2 with tyrosine-kinase receptors for VEGF. Adv. Exp. Med. Biol. *515*, 81–90.

Neufeld, S., Planas-Paz, L., and Lammert, E. (2014). Blood and lymphatic vascular tube formation in mouse. Semin. Cell Dev. Biol. *31*, 115–123.

Nisancioglu, M.H., Mahoney, W.M., Kimmel, D.D., Schwartz, S.M., Betsholtz, C., and Genové, G. (2008). Generation and Characterization of rgs5 Mutant Mice. Mol. Cell. Biol. *28*, 2324–2331.

Nisancioglu, M.H., Betsholtz, C., and Genové, G. (2010). The absence of pericytes does not increase the sensitivity of tumor vasculature to vascular endothelial growth factor-A blockade. Cancer Res. *70*, 5109–5115.

Norel, X., de Montpreville, V., and Brink, C. (2004). Vasoconstriction induced by activation of EP1 and EP3 receptors in human lung: effects of ONO-AE-248, ONO-DI-004, ONO-8711 or ONO-8713. Prostaglandins Other Lipid Mediat. *74*, 101–112.

Nussbaum, C., Bannenberg, S., Keul, P., Gräler, M.H., Gonçalves-de-Albuquerque, C.F., Korhonen, H., Lipinski, K. von W., Heusch, G., Neto, H.C. de C.F., Rohwedder, I., et al. (2015). Sphingosine-1-phosphate receptor 3 promotes leukocyte rolling by mobilizing endothelial P-selectin. Nat. Commun. *6*, 6416.

Ohmori, T., Yatomi, Y., Osada, M., Kazama, F., Takafuta, T., Ikeda, H., and Ozaki, Y. (2003). Sphingosine 1-phosphate induces contraction of coronary artery smooth muscle cells via S1P2. Cardiovasc. Res. *58*, 170–177.

Okamoto, H., Takuwa, N., Yokomizo, T., Sugimoto, N., Sakurada, S., Shigematsu, H., and Takuwa, Y. (2000). Inhibitory regulation of rac activation, membrane ruffling, and cell migration by the G Protein-coupled sphingosine-1-phosphate receptor EDG5 but not EDG1 or EDG3. Mol. Cell. Biol. *20*, 9247–9261.

Okazaki, H., Ishizaka, N., Sakurai, T., Kurokawa, K., Goto, K., Kumada, M., and Takuwa, Y. (1993). Molecular cloning of a novel putative G protein-coupled receptor expressed in the cardiovascular system. Biochem. Biophys. Res. Commun. *190*, 1104–1109.

Olivera, A. (2008). Unraveling the complexities of sphingosine-1-phosphate function: The mast cell model. Prostaglandins Other Lipid Mediat. *86*, 1–11.

Olivera, A., and Rivera, J. (2011). An emerging role for the lipid mediator sphingosine-1-phosphate in mast cell effector function and allergic disease. Adv. Exp. Med. Biol. *716*, 123–142.

Olivera, A., Allende, M.L., and Proia, R.L. (2013). Shaping the landscape: Metabolic regulation of S1P gradients. Biochim. Biophys. Acta *1831*, 193–202.

Onimaru, M., Yonemitsu, Y., Fujii, T., Tanii, M., Nakano, T., Nakagawa, K., Kohno, R., Hasegawa, M., Nishikawa, S., and Sueishi, K. (2009). VEGF-C regulates lymphangiogenesis and capillary stability by regulation of PDGF-B. Am. J. Physiol. Heart Circ. Physiol. *297*, H1685-1696.

Ostman, A., Andersson, M., Betsholtz, C., Westermark, B., and Heldin, C.H. (1991). Identification of a cell retention signal in the B-chain of platelet-derived growth factor and in the long splice version of the A-chain. Cell Regul. *2*, 503–512.

Ozerdem, U., and Stallcup, W.B. (2004). Pathological angiogenesis is reduced by targeting pericytes via the NG2 proteoglycan. Angiogenesis *7*, 269–276.

Ozerdem, U., Grako, K.A., Dahlin-Huppe, K., Monosov, E., and Stallcup, W.B. (2001). NG2 proteoglycan is expressed exclusively by mural cells during vascular morphogenesis. Dev. Dyn. *222*, 218–227.

Ozerdem, U., Monosov, E., and Stallcup, W.B. (2002). NG2 proteoglycan expression by pericytes in pathological microvasculature. Microvasc. Res. *63*, 129–134.

Paik, J.H., Chae Ss, null, Lee, M.J., Thangada, S., and Hla, T. (2001). Sphingosine 1-phosphate-induced endothelial cell migration requires the expression of EDG-1 and EDG-3 receptors and Rho-dependent activation of alpha vbeta3- and beta1-containing integrins. J. Biol. Chem. *276*, 11830–11837.

Pappu, R., Schwab, S.R., Cornelissen, I., Pereira, J.P., Regard, J.B., Xu, Y., Camerer, E., Zheng, Y.-W., Huang, Y., Cyster, J.G., et al. (2007). Promotion of lymphocyte egress into blood and lymph by distinct sources of sphingosine-1-phosphate. Science *316*, 295–298.

Patterson, C., Perrella, M.A., Endege, W.O., Yoshizumi, M., Lee, M.E., and Haber, E. (1996). Downregulation of vascular endothelial growth factor receptors by tumor necrosis factor-alpha in cultured human vascular endothelial cells. J. Clin. Invest. *98*, 490–496.

dela Paz, N.G., Walshe, T.E., Leach, L.L., Saint-Geniez, M., and D'Amore, P.A. (2012). Role of shear-stress-induced VEGF expression in endothelial cell survival. J. Cell Sci. *125*, 831–843.

Peng, X., Hassoun, P.M., Sammani, S., McVerry, B.J., Burne, M.J., Rabb, H., Pearse, D., Tuder, R.M., and Garcia, J.G.N. (2004). Protective effects of sphingosine 1-phosphate in murine endotoxin-induced inflammatory lung injury. Am. J. Respir. Crit. Care Med. *169*, 1245–1251.

Phng, L.-K., and Gerhardt, H. (2009). Angiogenesis: a team effort coordinated by Notch. Dev. Cell *16*, 196–208.

Pieper, C., Pieloch, P., and Galla, H.-J. (2013). Pericytes support neutrophil transmigration via interleukin-8 across a porcine co-culture model of the blood-brain barrier. Brain Res. *1524*, 1–11.

Pitson, S.M., Moretti, P.A.B., Zebol, J.R., Lynn, H.E., Xia, P., Vadas, M.A., and Wattenberg, B.W. (2003). Activation of sphingosine kinase 1 by ERK1/2-mediated phosphorylation. EMBO J. *22*, 5491–5500.

Potente, M., and Mäkinen, T. (2017). Vascular heterogeneity and specialization in development and disease. Nat. Rev. Mol. Cell Biol.

Potente, M., Gerhardt, H., and Carmeliet, P. (2011). Basic and therapeutic aspects of angiogenesis. Cell *146*, 873–887.

Proebstl, D., Voisin, M.-B., Woodfin, A., Whiteford, J., D'Acquisto, F., Jones, G.E., Rowe, D., and Nourshargh, S. (2012). Pericytes support neutrophil subendothelial cell crawling and breaching of venular walls in vivo. J. Exp. Med. *209*, 1219–1234.

Proia, R.L., and Hla, T. (2015). Emerging biology of sphingosine-1-phosphate: its role in pathogenesis and therapy. J. Clin. Invest. *125*, 1379–1387.

Pyne, N.J., and Pyne, S. (2010). Sphingosine 1-phosphate and cancer. Nat. Rev. Cancer *10*, 489–503.

Que, J., Wilm, B., Hasegawa, H., Wang, F., Bader, D., and Hogan, B.L.M. (2008). Mesothelium contributes to vascular smooth muscle and mesenchyme during lung development. Proc. Natl. Acad. Sci. *105*, 16626–16630.

Rajantie, I., Ilmonen, M., Alminaite, A., Ozerdem, U., Alitalo, K., and Salven, P. (2004). Adult bone marrow-derived cells recruited during angiogenesis comprise precursors for periendothelial vascular mural cells. Blood *104*, 2084–2086.

Regard, J.B., Sato, I.T., and Coughlin, S.R. (2008). Anatomical profiling of G protein-coupled receptor expression. Cell *135*, 561–571.

Rettig, W.J., Garin-Chesa, P., Healey, J.H., Su, S.L., Jaffe, E.A., and Old, L.J. (1992). Identification of endosialin, a cell surface glycoprotein of vascular endothelial cells in human cancer. Proc. Natl. Acad. Sci. U. S. A. *89*, 10832–10836.

Ricciotti, E., and FitzGerald, G.A. (2011). Prostaglandins and inflammation. Arterioscler. Thromb. Vasc. Biol. *31*, 986–1000.

Risau, W. (1997). Mechanisms of angiogenesis. Nature *386*, 671–674.

Roca, C., and Adams, R.H. (2007). Regulation of vascular morphogenesis by Notch signaling. Genes Dev. *21*, 2511–2524.

Rodriguez-Baeza, A., Reina-De La Torre, F., Ortega-Sanchez, M., and Sahuquillo-Barris, J. (1998). Perivascular structures in corrosion casts of the human central nervous system: a confocal laser and scanning electron microscope study. Anat. Rec. *252*, 176–184.

Rønnov-Jessen, L., and Petersen, O.W. (1996). A function for filamentous alpha-smooth muscle actin: retardation of motility in fibroblasts. J. Cell Biol. *134*, 67–80.

Rosenberg, L., Palmer, J.R., Zauber, A.G., Warshauer, M.E., Stolley, P.D., and Shapiro, S. (1991). A hypothesis: nonsteroidal anti-inflammatory drugs reduce the incidence of large-bowel cancer. J. Natl. Cancer Inst. *83*, 355–358.

Roth, L., Prahst, C., Ruckdeschel, T., Savant, S., Weström, S., Fantin, A., Riedel, M., Héroult, M., Ruhrberg, C., and Augustin, H.G. (2016). Neuropilin-1 mediates vascular permeability independently of vascular endothelial growth factor receptor-2 activation. Sci. Signal. *9*, ra42.

Rouget, C. (1873). Memoire sur le developpement, la structures et les proprietes des capillaires sanguins et lymphatiques. Archs Physiol Norm Pathol *5*, 603–633.

Rupp, C., Dolznig, H., Puri, C., Sommergruber, W., Kerjaschki, D., Rettig, W.J., and Garin-Chesa, P. (2006). Mouse endosialin, a C-type lectin-like cell surface receptor: expression during embryonic development and induction in experimental cancer neoangiogenesis. Cancer Immun. *6*, 10.

Rybinski, K., Imtiyaz, H.Z., Mittica, B., Drozdowski, B., Fulmer, J., Furuuchi, K., Fernando, S., Henry, M., Chao, Q., Kline, B., et al. (2015). Targeting endosialin/CD248 through antibody-mediated internalization results in impaired pericyte maturation and dysfunctional tumor microvasculature. Oncotarget *6*, 25429–25440.

Ryu, Y., Takuwa, N., Sugimoto, N., Sakurada, S., Usui, S., Okamoto, H., Matsui, O., and Takuwa, Y. (2002). Sphingosine-1-phosphate, a platelet-derived lysophospholipid mediator, negatively regulates cellular Rac activity and cell migration in vascular smooth muscle cells. Circ. Res. *90*, 325–332.

Sakurai, T., Suzuki, K., Yoshie, M., Hashimoto, K., Tachikawa, E., and Tamura, K. (2011). Stimulation of tube formation mediated through the prostaglandin EP2 receptor in rat luteal endothelial cells. J. Endocrinol. *209*, 33–43.

Salazar-Peláez, L.M., Abraham, T., Herrera, A.M., Correa, M.A., Ortega, J.E., Paré, P.D., and Seow, C.Y. (2015). Vitronectin expression in the airways of subjects with asthma and chronic obstructive pulmonary disease. PloS One *10*, e0119717.

Sato, Y., and Rifkin, D.B. (1989). Inhibition of endothelial cell movement by pericytes and smooth muscle cells: activation of a latent transforming growth factor-beta 1-like molecule by plasmin during co-culture. J. Cell Biol. *109*, 309–315.

Sato, M., Suzuki, S., and Senoo, H. (2003). Hepatic stellate cells: unique characteristics in cell biology and phenotype. Cell Struct. Funct. *28*, 105–112.

Sato, M., Ohtsuka, M., Watanabe, S., and Gurumurthy, C.B. (2016). Nucleic acids delivery methods for genome editing in zygotes and embryos: the old, the new, and the old-new. Biol. Direct *11*.

Sato, T.N., Tozawa, Y., Deutsch, U., Wolburg-Buchholz, K., Fujiwara, Y., Gendron-Maguire, M., Gridley, T., Wolburg, H., Risau, W., and Qin, Y. (1995). Distinct roles of the receptor tyrosine kinases Tie-1 and Tie-2 in blood vessel formation. Nature *376*, 70–74.

Savant, S., La Porta, S., Budnik, A., Busch, K., Hu, J., Tisch, N., Korn, C., Valls, A.F., Benest, A.V., Terhardt, D., et al. (2015). The orphan receptor Tie1 controls angiogenesis and vascular remodeling by differentially regulating Tie2 in tip and stalk cells. Cell Rep. *12*, 1761–1773.

Schildmeyer, L.A., Braun, R., Taffet, G., Debiasi, M., Burns, A.E., Bradley, A., and Schwartz, R.J. (2000). Impaired vascular contractility and blood pressure homeostasis in the smooth muscle alpha-actin null mouse. FASEB J. *14*, 2213–2220.

Schlingemann, R.O., Rietveld, F.J., de Waal, R.M., Ferrone, S., and Ruiter, D.J. (1990). Expression of the high molecular weight melanoma-associated antigen by pericytes during angiogenesis in tumors and in healing wounds. Am. J. Pathol. *136*, 1393–1405.

Schlingemann, R.O., Rietveld, F.J., Kwaspen, F., van de Kerkhof, P.C., de Waal, R.M., and Ruiter, D.J. (1991). Differential expression of markers for endothelial cells, pericytes, and basal lamina in the microvasculature of tumors and granulation tissue. Am. J. Pathol. *138*, 1335–1347.

Schmitt-Gräff, A., Krüger, S., Bochard, F., Gabbiani, G., and Denk, H. (1991). Modulation of alpha smooth muscle actin and desmin expression in perisinusoidal cells of normal and diseased human livers. Am. J. Pathol. *138*, 1233–1242.

Schrimpf, C., and Duffield, J.S. (2011). Mechanisms of fibrosis: the role of the pericyte. Curr. Opin. Nephrol. Hypertens. *20*, 297–305.

Schuster, V.L. (1998). Molecular mechanisms of prostaglandin transport. Annu. Rev. Physiol. *60*, 221–242.

Segi, E., Sugimoto, Y., Yamasaki, A., Aze, Y., Oida, H., Nishimura, T., Murata, T., Matsuoka, T., Ushikubi, F., Hirose, M., et al. (1998). Patent ductus arteriosus and neonatal death in prostaglandin receptor EP4-deficient mice. Biochem. Biophys. Res. Commun. *246*, 7–12.

Senger, D.R., Galli, S.J., Dvorak, A.M., Perruzzi, C.A., Harvey, V.S., and Dvorak, H.F. (1983). Tumor cells secrete a vascular permeability factor that promotes accumulation of ascites fluid. Science *219*, 983–985.

Senior, J., Marshall, K., Sangha, R., Baxter, G.S., and Clayton, J.K. (1991). In vitro characterization of prostanoid EP-receptors in the non-pregnant human myometrium. Br. J. Pharmacol. *102*, 747–753.

Sennino, B., Falcón, B.L., McCauley, D., Le, T., McCauley, T., Kurz, J.C., Haskell, A., Epstein, D.M., and McDonald, D.M. (2007). Sequential loss of tumor vessel pericytes and endothelial cells after inhibition of platelet-derived growth factor B by selective aptamer AX102. Cancer Res. *67*, 7358–7367.

Seno, H., Oshima, M., Ishikawa, T., Oshima, H., Takaku, K., Chiba, T., Narumiya, S., and Taketo, M.M. (2002). Cyclooxygenase 2- and prostaglandin E(2) receptor EP(2)-dependent angiogenesis in Apc(Delta716) mouse intestinal polyps. Cancer Res. *62*, 506–511.

Shen, B., Zhang, W., Zhang, J., Zhou, J., Wang, J., Chen, L., Wang, L., Hodgkins, A., Iyer, V., Huang, X., et al. (2014). Efficient genome modification by CRISPR-Cas9 nickase with minimal off-target effects. Nat. Methods *11*, 399–402.

Shepro, D., and Morel, N.M. (1993). Pericyte physiology. FASEB J. *7*, 1031–1038.

Shimizu, T., De Wispelaere, A., Winkler, M., D'Souza, T., Caylor, J., Chen, L., Dastvan, F., Deou, J., Cho, A., Larena-Avellaneda, A., et al. (2012). Sphingosine-1-phosphate receptor 3 promotes neointimal hyperplasia in mouse iliac-femoral arteries. Arterioscler. Thromb. Vasc. Biol. *32*, 955–961.

Shoji, Y., Takahashi, M., Takasuka, N., Niho, N., Kitamura, T., Sato, H., Maruyama, T., Sugimoto, Y., Narumiya, S., Sugimura, T., et al. (2005). Prostaglandin E receptor EP3 deficiency modifies tumor outcome in mouse two-stage skin carcinogenesis. Carcinogenesis *26*, 2116–2122.

da Silva Meirelles, L., Caplan, A.I., and Nardi, N.B. (2008). In search of the in vivo identity of mesenchymal stem cells. Stem Cells Dayt. Ohio *26*, 2287–2299.

Simons, M., Gordon, E., and Claesson-Welsh, L. (2016). Mechanisms and regulation of endothelial VEGF receptor signalling. Nat. Rev. Mol. Cell Biol. *17*, 611–625.

Sims, D.E. (2000). Diversity within pericytes. Clin. Exp. Pharmacol. Physiol. *27*, 842–846.

Sims, D.E., and Westfall, J.A. (1983). Analysis of relationships between pericytes and gas exchange capillaries in neonatal and mature bovine lungs. Microvasc. Res. *25*, 333–342.

Singh, P., Schimenti, J.C., and Bolcun-Filas, E. (2015). A mouse geneticist's practical guide to CRISPR applications. Genetics *199*, 1–15.

Singleton, P.A., Dudek, S.M., Chiang, E.T., and Garcia, J.G.N. (2005). Regulation of sphingosine 1-phosphate-induced endothelial cytoskeletal rearrangement and barrier enhancement by S1P1 receptor, PI3 kinase, Tiam1/Rac1, and α-actinin. FASEB J. *19*, 1646–1656.

Skalli, O., Pelte, M.F., Peclet, M.C., Gabbiani, G., Gugliotta, P., Bussolati, G., Ravazzola, M., and Orci, L. (1989). Alpha-smooth muscle actin, a differentiation marker of smooth muscle cells, is present in microfilamentous bundles of pericytes. J. Histochem. Cytochem. Off. J. Histochem. Soc. *37*, 315–321.

Skoura, A., Michaud, J., Im, D.-S., Thangada, S., Xiong, Y., Smith, J.D., and Hla, T. (2011). Sphingosine-1-phosphate receptor-2 function in myeloid cells regulates vascular inflammation and atherosclerosis. Arterioscler. Thromb. Vasc. Biol. *31*, 81–85.

Smid, S.D., and Svensson, K.M. (2009). Inhibition of cyclooxygenase-2 and EP1 receptor antagonism reduces human colonic longitudinal muscle contractility in vitro. Prostaglandins Other Lipid Mediat. *88*, 117–121.

Smith, W.L. (1992). Prostanoid biosynthesis and mechanisms of action. Am. J. Physiol. *263*, F181-191.

Smith, W.L., DeWitt, D.L., and Garavito, R.M. (2000). Cyclooxygenases: structural, cellular, and molecular biology. Annu. Rev. Biochem. *69*, 145–182.

Song, S., Ewald, A.J., Stallcup, W., Werb, Z., and Bergers, G. (2005). PDGFRβ+ perivascular progenitor cells in tumours regulate pericyte differentiation and vascular survival. Nat. Cell Biol. *7*, 870–879.

Sonoshita, M., Takaku, K., Sasaki, N., Sugimoto, Y., Ushikubi, F., Narumiya, S., Oshima, M., and Taketo, M.M. (2001). Acceleration of intestinal polyposis through prostaglandin receptor EP2 in Apc(Delta 716) knockout mice. Nat. Med. *7*, 1048–1051.

Soriano, P. (1994). Abnormal kidney development and hematological disorders in PDGF beta-receptor mutant mice. Genes Dev. *8*, 1888–1896.

Spiegel, S., and Milstien, S. (2003). Sphingosine-1-phosphate: an enigmatic signalling lipid. Nat. Rev. Mol. Cell Biol. *4*, 397–407.

St Croix, B., Rago, C., Velculescu, V., Traverso, G., Romans, K.E., Montgomery, E., Lal, A., Riggins, G.J., Lengauer, C., Vogelstein, B., et al. (2000). Genes expressed in human tumor endothelium. Science *289*, 1197–1202.

Stark, K., Eckart, A., Haidari, S., Tirniceriu, A., Lorenz, M., von Brühl, M.-L., Gärtner, F., Khandoga, A.G., Legate, K.R., Pless, R., et al. (2013). Capillary and arteriolar pericytes attract innate leukocytes exiting through venules and "instruct" them with pattern-recognition and motility programs. Nat. Immunol. *14*, 41–51.

Stedman, T.L. (1995). Stedman's Medical Dictionary (Baltimore: Williams & Wilkins).

Stratmann, A., Risau, W., and Plate, K.H. (1998). Cell type-specific expression of angiopoietin-1 and angiopoietin-2 suggests a role in glioblastoma angiogenesis. Am. J. Pathol. *153*, 1459–1466.

Stricker, S. (Salomon), Arnold, J., and Royal College of Physicians of Edinburgh (1872). Handbuch der Lehre von den Geweben des Menschen und der Thiere (Leipzig : W. Engelmann).

Stroka, K.M., and Aranda-Espinoza, H. (2011). Endothelial cell substrate stiffness influences neutrophil transmigration via myosin light chain kinase-dependent cell contraction. Blood *118*, 1632–1640.

Subramanian, A., Tamayo, P., Mootha, V.K., Mukherjee, S., Ebert, B.L., Gillette, M.A., Paulovich, A., Pomeroy, S.L., Golub, T.R., Lander, E.S., et al. (2005). Gene set enrichment analysis: A knowledge-based approach for interpreting genome-wide expression profiles. Proc. Natl. Acad. Sci. *102*, 15545–15550.

Suchting, S., Freitas, C., le Noble, F., Benedito, R., Bréant, C., Duarte, A., and Eichmann, A. (2007). The Notch ligand Delta-like 4 negatively regulates endothelial tip cell formation and vessel branching. Proc. Natl. Acad. Sci. U. S. A. *104*, 3225–3230.

Sun, X., Singleton, P.A., Letsiou, E., Zhao, J., Belvitch, P., Sammani, S., Chiang, E.T., Moreno-Vinasco, L., Wade, M.S., Zhou, T., et al. (2012a). Sphingosine-1-phosphate receptor-3 is a novel biomarker in acute lung injury. Am. J. Respir. Cell Mol. Biol. *47*, 628–636.

Sun, Z., Li, X., Massena, S., Kutschera, S., Padhan, N., Gualandi, L., Sundvold-Gjerstad, V., Gustafsson, K., Choy, W.W., Zang, G., et al. (2012b). VEGFR2 induces c-Src signaling and vascular permeability in vivo via the adaptor protein TSAd. J. Exp. Med. *209*, 1363–1377.

Suri, C., Jones, P.F., Patan, S., Bartunkova, S., Maisonpierre, P.C., Davis, S., Sato, T.N., and Yancopoulos, G.D. (1996). Requisite role of angiopoietin-1, a ligand for the TIE2 receptor, during embryonic angiogenesis. Cell *87*, 1171–1180.

Surks, H.K., Richards, C.T., and Mendelsohn, M.E. (2003). Myosin phosphatase-Rho interacting protein. A new member of the myosin phosphatase complex that directly binds RhoA. J. Biol. Chem. *278*, 51484–51493.

Swift, M.R., and Weinstein, B.M. (2009). Arterial–venous specification during development. Circ. Res. *104*, 576–588.

Tachibana, K., Jones, N., Dumont, D.J., Puri, M.C., and Bernstein, A. (2005). Selective role of a distinct tyrosine residue on Tie2 in heart development and early hematopoiesis. Mol. Cell. Biol. *25*, 4693–4702.

Takabe, K., Kim, R.H., Allegood, J.C., Mitra, P., Ramachandran, S., Nagahashi, M., Harikumar, K.B., Hait, N.C., Milstien, S., and Spiegel, S. (2010). Estradiol induces export of sphingosine 1-phosphate from breast cancer cells via ABCC1 and ABCG2. J. Biol. Chem. *285*, 10477–10486.

Tanaka, K., Furuyashiki, T., Kitaoka, S., Senzai, Y., Imoto, Y., Segi-Nishida, E., Deguchi, Y., Breyer, R.M., Breyer, M.D., and Narumiya, S. (2012). Prostaglandin E2-mediated attenuation of mesocortical dopaminergic pathway is critical for susceptibility to repeated social defeat stress in mice. J. Neurosci. Off. J. Soc. Neurosci. *32*, 4319–4329.

Tanaka, M., Okabe, M., Suzuki, K., Kamiya, Y., Tsukahara, Y., Saito, S., and Miyajima, A. (2009). Mouse hepatoblasts at distinct developmental stages are characterized by expression of EpCAM

and DLK1: Drastic change of EpCAM expression during liver development. Mech. Dev. *126*, 665–676.

Tanaka, S.S., Yamaguchi, Y.L., Tsoi, B., Lickert, H., and Tam, P.P.L. (2005). IFITM/Mil/Fragilis family proteins IFITM1 and IFITM3 play distinct roles in mouse primordial germ cell homing and repulsion. Dev. Cell *9*, 745–756.

Tanski, W.J., Nicholl, S.M., Kim, D., Fegley, A.J., Roztocil, E., and Davies, M.G. (2005). Sphingosine-1-phosphate-induced smooth muscle cell migration involves the mammalian target of rapamycin. J. Vasc. Surg. *41*, 91–98.

Tao, R., Hoover, H.E., Zhang, J., Honbo, N., Alano, C.C., and Karliner, J.S. (2009). Cardiomyocyte S1P1 receptor–mediated extracellular signal–related kinase signaling and desensitization. J. Cardiovasc. Pharmacol. *53*, 486–494.

Teichert, M., Milde, L., Holm, A., Staniczek, L., Gengenbacher, N., Savant, S., Ruckdeschel, T., Hasanov, Z., Srivastava, K., Hu, J., et al. (2017). Pericyte-expressed Tie2 controls angiogenesis and vessel maturation. Nat.Commun. in press.

Thomas, W.E. (1999). Brain macrophages: on the role of pericytes and perivascular cells. Brain Res. Brain Res. Rev. *31*, 42–57.

Thomas, M., and Augustin, H.G. (2009). The role of the Angiopoietins in vascular morphogenesis. Angiogenesis *12*, 125–137.

Thudichum, J.L.W. (John L.W., and Royal College of Physicians of London (1884). A treatise on the chemical constitution of the brain : based throughout upon original researches (London : Bailliere, Tindall, and Cox).

Tidhar, A., Reichenstein, M., Cohen, D., Faerman, A., Copeland, N.G., Gilbert, D.J., Jenkins, N.A., and Shani, M. (2001). A novel transgenic marker for migrating limb muscle precursors and for vascular smooth muscle cells. Dev. Dyn. Off. Publ. Am. Assoc. Anat. *220*, 60–73.

Tilton, R.G., Kilo, C., Williamson, J.R., and Murch, D.W. (1979). Differences in pericyte contractile function in rat cardiac and skeletal muscle microvasculatures. Microvasc. Res. *18*, 336–352.

Tomkowicz, B., Rybinski, K., Sebeck, D., Sass, P., Nicolaides, N.C., Grasso, L., and Zhou, Y. (2010). Endosialin/TEM-1/CD248 regulates pericyte proliferation through PDGF receptor signaling. Cancer Biol. Ther. *9*, 908–915.

Tosaka, M., Okajima, F., Hashiba, Y., Saito, N., Nagano, T., Watanabe, T., Kimura, T., and Sasaki, T. (2001). Sphingosine 1-phosphate contracts canine basilar arteries in vitro and in vivo: possible role in pathogenesis of cerebral vasospasm. Stroke *32*, 2913–2919.

Trebino, C.E., Stock, J.L., Gibbons, C.P., Naiman, B.M., Wachtmann, T.S., Umland, J.P., Pandher, K., Lapointe, J.-M., Saha, S., Roach, M.L., et al. (2003). Impaired inflammatory and pain responses in mice lacking an inducible prostaglandin E synthase. Proc. Natl. Acad. Sci. U. S. A. *100*, 9044–9049.

Tsujii, M., Kawano, S., Tsuji, S., Sawaoka, H., Hori, M., and DuBois, R.N. (1998). Cyclooxygenase regulates angiogenesis induced by colon cancer cells. Cell *93*, 705–716.

Turner, J.R., Angle, J.M., Black, E.D., Joyal, J.L., Sacks, D.B., and Madara, J.L. (1999). PKC-dependent regulation of transepithelial resistance: roles of MLC and MLC kinase. Am. J. Physiol. *277*, C554-562.

Uemura, N., Okamoto, S., Yamamoto, S., Matsumura, N., Yamaguchi, S., Yamakido, M., Taniyama, K., Sasaki, N., and Schlemper, R.J. (2001). Helicobacter pylori infection and the development of gastric cancer. N. Engl. J. Med. *345*, 784–789.

Ueno, A., Matsumoto, H., Naraba, H., Ikeda, Y., Ushikubi, F., Matsuoka, T., Narumiya, S., Sugimoto, Y., Ichikawa, A., and Oh-ishi, S. (2001). Major roles of prostanoid receptors IP and EP3 in endotoxin-induced enhancement of pain perception. Biochem. Pharmacol. *62*, 157–160.

Ushikubi, F., Segi, E., Sugimoto, Y., Murata, T., Matsuoka, T., Kobayashi, T., Hizaki, H., Tuboi, K., Katsuyama, M., Ichikawa, A., et al. (1998). Impaired febrile response in mice lacking the prostaglandin E receptor subtype EP3. Nature *395*, 281–284.

Valton, J., Dupuy, A., Daboussi, F., Thomas, S., Maréchal, A., Macmaster, R., Melliand, K., Juillerat, A., and Duchateau, P. (2012). Overcoming transcription activator-like effector (TALE) DNA binding domain sensitivity to cytosine methylation. J. Biol. Chem. *287*, 38427–38432.

Venkataraman, K., Lee, Y.-M., Michaud, J., Thangada, S., Ai, Y., Bonkovsky, H.L., Parikh, N.S., Habrukowich, C., and Hla, T. (2008). Vascular endothelium as a contributor of plasma sphingosine 1-phosphate. Circ. Res. *102*, 669–676.

Verbeek, M.M., Otte-Höller, I., Wesseling, P., Ruiter, D.J., and de Waal, R.M. (1994). Induction of alpha-smooth muscle actin expression in cultured human brain pericytes by transforming growth factor-beta 1. Am. J. Pathol. *144*, 372–382.

Verhoeven, D., and Buyssens, N. (1988). Desmin-positive stellate cells associated with angiogenesis in a tumour and non-tumour system. Virchows Arch. B Cell Pathol. Incl. Mol. Pathol. *54*, 263–272.

Villa, N., Walker, L., Lindsell, C.E., Gasson, J., Iruela-Arispe, M.L., and Weinmaster, G. (2001). Vascular expression of Notch pathway receptors and ligands is restricted to arterial vessels. Mech. Dev. *108*, 161–164.

Virgintino, D., Girolamo, F., Errede, M., Capobianco, C., Robertson, D., Stallcup, W.B., Perris, R., and Roncali, L. (2007). An intimate interplay between precocious, migrating pericytes and endothelial cells governs human fetal brain angiogenesis. Angiogenesis *10*, 35–45.

Viski, C., König, C., Kijewska, M., Mogler, C., Isacke, C.M., and Augustin, H.G. (2016). Endosialin-expressing pericytes promote metastatic dissemination. Cancer Res. *76*, 5313–5325.

Wacker, A., and Gerhardt, H. (2011). Endothelial development taking shape. Curr. Opin. Cell Biol. *23*, 676–685.

Waeber, C., Blondeau, N., and Salomone, S. (2004). Vascular sphingosine-1-phosphate S1P1 and S1P3 receptors. Drug News Perspect. *17*, 365–382.

Wakui, S., Yokoo, K., Muto, T., Suzuki, Y., Takahashi, H., Furusato, M., Hano, H., Endou, H., and Kanai, Y. (2006). Localization of Ang-1, -2, Tie-2, and VEGF expression at endothelial-pericyte interdigitation in rat angiogenesis. Lab. Investig. J. Tech. Methods Pathol. *86*, 1172–1184.

Walch, L., de Montpreville, V., Brink, C., and Norel, X. (2001). Prostanoid EP1- and TP-receptors involved in the contraction of human pulmonary veins. Br. J. Pharmacol. *134*, 1671–1678.

Wamhoff, B.R., Lynch, K.R., Macdonald, T.L., and Owens, G.K. (2008). Sphingosine-1-phosphate receptor subtypes differentially regulate smooth muscle cell phenotype. Arterioscler. Thromb. Vasc. Biol. *28*, 1454–1461.

Wang, D., and DuBois, R.N. (2006). Prostaglandins and cancer. Gut *55*, 115–122.

Wang, X., and Klein, R.D. (2007). Prostaglandin E2 induces vascular endothelial growth factor secretion in prostate cancer cells through EP2 receptor-mediated cAMP pathway. Mol. Carcinog. *46*, 912–923.

Wang, X.S., and Lau, H.Y.A. (2006). Prostaglandin E potentiates the immunologically stimulated histamine release from human peripheral blood-derived mast cells through EP1/EP3 receptors. Allergy *61*, 503–506.

Wang, C., Mao, J., Redfield, S., Mo, Y., Lage, J.M., and Zhou, X. (2014). Systemic distribution, subcellular localization and differential expression of sphingosine-1-phosphate receptors in benign and malignant human tissues. Exp. Mol. Pathol. *97*, 259–265.

Wang, H., Yang, H., Shivalila, C.S., Dawlaty, M.M., Cheng, A.W., Zhang, F., and Jaenisch, R. (2013). One-step generation of mice carrying mutations in multiple genes by CRISPR/Cas-mediated genome engineering. Cell *153*, 910–918.

Wang, S., Cao, C., Chen, Z., Bankaitis, V., Tzima, E., Sheibani, N., and Burridge, K. (2012). Pericytes regulate vascular basement membrane remodeling and govern neutrophil extravasation during inflammation. PloS One *7*, e45499.

Ware, L.B., and Matthay, M.A. (2000). The acute respiratory distress syndrome. N. Engl. J. Med. *342*, 1334–1349.

Watabe, A., Sugimoto, Y., Honda, A., Irie, A., Namba, T., Negishi, M., Ito, S., Narumiya, S., and Ichikawa, A. (1993). Cloning and expression of cDNA for a mouse EP1 subtype of prostaglandin E receptor. J. Biol. Chem. *268*, 20175–20178.

Watanabe, K., Kawamori, T., Nakatsugi, S., Ohta, T., Ohuchida, S., Yamamoto, H., Maruyama, T., Kondo, K., Ushikubi, F., Narumiya, S., et al. (1999). Role of the prostaglandin E receptor subtype EP1 in colon carcinogenesis. Cancer Res. *59*, 5093–5096.

Weibel, E.R. (1974). On pericytes, particularly their existence on lung capillaries. Microvasc. Res. *8*, 218–235.

Welti, J.C., Powles, T., Foo, S., Gourlaouen, M., Preece, N., Foster, J., Frentzas, S., Bird, D., Sharpe, K., van Weverwijk, A., et al. (2012). Contrasting effects of sunitinib within in vivo models of metastasis. Angiogenesis *15*, 623–641.

Wiedenheft, B., Sternberg, S.H., and Doudna, J.A. (2012). RNA-guided genetic silencing systems in bacteria and archaea. Nature *482*, 331–338.

Wilm, B., Ipenberg, A., Hastie, N.D., Burch, J.B.E., and Bader, D.M. (2005). The serosal mesothelium is a major source of smooth muscle cells of the gut vasculature. Dev. Camb. Engl. *132*, 5317–5328.

Windh, R.T., Lee, M.-J., Hla, T., An, S., Barr, A.J., and Manning, D.R. (1999). Differential coupling of the sphingosine 1-phosphate receptors Edg-1, Edg-3, and H218/Edg-5 to the Gi, Gq, and G12 families of heterotrimeric G proteins. J. Biol. Chem. *274*, 27351–27358.

Winkler, E.A., Bell, R.D., and Zlokovic, B.V. (2010). Pericyte-specific expression of PDGF beta receptor in mouse models with normal and deficient PDGF beta receptor signaling. Mol. Neurodegener. *5*, 32.

Wu, J., Iwata, F., Grass, J.A., Osborne, C.S., Elnitski, L., Fraser, P., Ohneda, O., Yamamoto, M., and Bresnick, E.H. (2005). Molecular determinants of NOTCH4 transcription in vascular endothelium. Mol. Cell. Biol. *25*, 1458–1474.

Xiong, Y., and Hla, T. (2014). S1P Control of endothelial integrity. Curr. Top. Microbiol. Immunol. *378*, 85–105.

Xiong, B., Sun, T.-J., Hu, W.-D., Cheng, F.-L., Mao, M., and Zhou, Y.-F. (2005). Expression of cyclooxygenase-2 in colorectal cancer and its clinical significance. World J. Gastroenterol. WJG *11*, 1105–1108.

Xiong, Y., Yang, P., Proia, R.L., and Hla, T. (2014). Erythrocyte-derived sphingosine 1-phosphate is essential for vascular development. J. Clin. Invest. *124*, 4823–4828.

Yamaguchi, F., Tokuda, M., Hatase, O., and Brenner, S. (1996). Molecular cloning of the novel human G protein-coupled receptor (GPCR) gene mapped on chromosome 9. Biochem. Biophys. Res. Commun. *227*, 608–614.

Yamashita, J., Itoh, H., Hirashima, M., Ogawa, M., Nishikawa, S., Yurugi, T., Naito, M., Nakao, K., and Nishikawa, S.-I. (2000). Flk1-positive cells derived from embryonic stem cells serve as vascular progenitors. Nature *408*, 92–96.

Yang, H., Zhang, J., Breyer, R.M., and Chen, C. (2009). Altered hippocampal long-term synaptic plasticity in mice deficient in the PGE2 EP2 receptor. J. Neurochem. *108*, 295–304.

Yang, L., Yamagata, N., Yadav, R., Brandon, S., Courtney, R.L., Morrow, J.D., Shyr, Y., Boothby, M., Joyce, S., Carbone, D.P., et al. (2003). Cancer-associated immunodeficiency and dendritic cell abnormalities mediated by the prostaglandin EP2 receptor. J. Clin. Invest. *111*, 727–735.

Yao, C., Sakata, D., Esaki, Y., Li, Y., Matsuoka, T., Kuroiwa, K., Sugimoto, Y., and Narumiya, S. (2009). Prostaglandin E2-EP4 signaling promotes immune inflammation through Th1 cell differentiation and Th17 cell expansion. Nat. Med. *15*, 633–640.

Yau, L., and Zahradka, P. (2003). PGE2 stimulates vascular smooth muscle cell proliferation via the EP2 receptor. Mol. Cell. Endocrinol. *203*, 77–90.

Yoshida, K., Oida, H., Kobayashi, T., Maruyama, T., Tanaka, M., Katayama, T., Yamaguchi, K., Segi, E., Tsuboyama, T., Matsushita, M., et al. (2002). Stimulation of bone formation and prevention of bone loss by prostaglandin E EP4 receptor activation. Proc. Natl. Acad. Sci. U. S. A. *99*, 4580–4585.

You, W.-K., Yotsumoto, F., Sakimura, K., Adams, R.H., and Stallcup, W.B. (2014). NG2 proteoglycan promotes tumor vascularization via integrin-dependent effects on pericyte function. Angiogenesis *17*, 61–76.

Zeisberg, E.M., Tarnavski, O., Zeisberg, M., Dorfman, A.L., McMullen, J.R., Gustafsson, E., Chandraker, A., Yuan, X., Pu, W.T., Roberts, A.B., et al. (2007). Endothelial-to-mesenchymal transition contributes to cardiac fibrosis. Nat. Med. *13*, 952–961.

Zeisberg, E.M., Potenta, S.E., Sugimoto, H., Zeisberg, M., and Kalluri, R. (2008). Fibroblasts in kidney fibrosis emerge via endothelial-to-mesenchymal transition. J. Am. Soc. Nephrol. JASN *19*, 2282–2287.

Zeng, Y. (2017). Endothelial glycocalyx as a critical signalling platform integrating the extracellular haemodynamic forces and chemical signalling. J. Cell. Mol. Med.

Zeng, Y., Adamson, R.H., Curry, F.-R.E., and Tarbell, J.M. (2014). Sphingosine-1-phosphate protects endothelial glycocalyx by inhibiting syndecan-1 shedding. Am. J. Physiol. Heart Circ. Physiol. *306*, H363-372.

Zhang, Z., and DuBois, R.N. (2000). Par-4, a proapoptotic gene, is regulated by NSAIDs in human colon carcinoma cells. Gastroenterology *118*, 1012–1017.

Zhang, L., Yu, J., Park, B.H., Kinzler, K.W., and Vogelstein, B. (2000). Role of BAX in the apoptotic response to anticancer agents. Science *290*, 989–992.

Zhang, L., Yang, N., Park, J.-W., Katsaros, D., Fracchioli, S., Cao, G., O'Brien-Jenkins, A., Randall, T.C., Rubin, S.C., and Coukos, G. (2003). Tumor-derived vascular endothelial growth factor up-regulates angiopoietin-2 in host endothelium and destabilizes host vasculature, supporting angiogenesis in ovarian cancer. Cancer Res. *63*, 3403–3412.

Zhou, J., and Saba, J.D. (1998). Identification of the first mammalian sphingosine phosphate lyase gene and its functional expression in yeast. Biochem. Biophys. Res. Commun. *242*, 502–507.

Zhou, M., He, H.-J., Tanaka, O., Suzuki, R., Sekiguchi, M., Yasuoka, Y., Kawahara, K., Itoh, H., and Abe, H. (2008). Localization of the sulphonylurea receptor subunits, SUR2A and SUR2B, in rat renal tubular epithelium. Tohoku J. Exp. Med. *214*, 247–256.

Zhu, L., Su, Q., Jie, X., Liu, A., Wang, H., He, B., and Jiang, H. (2016). NG2 expression in microglial cells affects the expression of neurotrophic and proinflammatory factors by regulating FAK phosphorylation. Sci. Rep. *6*, 27983.

Zhu, X., Bergles, D.E., and Nishiyama, A. (2008). NG2 cells generate both oligodendrocytes and gray matter astrocytes. Dev. Camb. Engl. *135*, 145–157.